Universidad Autónoma de Madrid
Programa de Doctorado en Bioquímica,
Biología Molecular, Biomedicina y Biotecnología

COMPUTATIONAL APPROACHES TO DRUG DESIGN AND TREATMENT OPTIMIZATION IN GENETIC DISEASES

Victoria Lucía Doldán Martelli

Madrid, 2017

Universidad Autónoma de Madrid. Facultad de Ciencias
Departamento de Biología Molecular

Computational approaches to drug design and treatment optimization in genetic diseases

Autora:

Victoria Lucía Doldán Martelli
Licenciada en Biología

Directores:

Dr. David Míguez Gómez
Dra. Cristina Murga Montesinos

Departamento de Biología Molecular y Departamento de Física de la Materia Condensada

Agradecimientos

Me gustaría agradecer en primer lugar a mi director de tesis, siempre dispuesto a echar una mano en todo lo posible, en haberme dedicado todo este tiempo y esfuerzo necesarios para crear esta tesis. También agradecer al resto del laboratorio, Mario, Nuria, Pau y mis antiguas compañeras, Paula y Adriana, por el apoyo mostrado y la paciencia en tiempos más difíciles. Gracias a la Dra. Cristina Murga por el tiempo dedicado y sus aportaciones al desarrollo de esta tesis. No puedo olvidarme de agradecer el tiempo y conocimiento que me han aportado el Dr. Raúl Guantes, el doctorando Juan D. Colunga y el Dr. Javier Estrada, y agradecer también a todo el Instituto Nicolás Cabrera, a Manuela Moreno, que siempre ha estado ahí para solucionar cualquier inconveniencia. Esta tesis no habría sido posible sin la ayuda de colaboradores como el Dr. Jordi García Ojalvo y la doctoranda Rosa Martínez Corral de la Universidad Pompeu Fabra, que han sido una guía e inspiración en esta última parte de la tesis. Agradecer de corazón al profesor Julio Sáez Rodríguez por darme la maravillosa oportunidad de formar parte de su laboratorio en el EBI-EMBL, por encauzar los esfuerzos del equipo en una brillante publicación y dejarme ser parte de ella. No puedo olvidarme además de todos mis compañeros de estancia, en particular el Dr. Thomas Cokelaer y la Dra. Federica Eduati, por darme un punto de vista completamente diferente de la Biología Computacional y aportarme nuevas herramientas que han facilitado el progreso de mi labor como doctoranda.

Este trabajo ha sido financiado por la Universidad Autónoma de Madrid a través de la ayuda FPI-UAM y por el Ministerio de Educación, Cultura y Deporte a través de una beca de Formación de Profesorado Universitario. Además, el proyecto ha sido financiado por el Plan Nacional.

Abstract

Quantitative Systems Pharmacology has the potential to change the way we approach Biomedical research and to ensure more robustly design studies to reduce the failure rate in the clinical phases of drug development. This thesis is focused on the study of different therapeutic ligands and drugs from a computational perspective in order to design, optimize and improve drug treatments.

First, the thesis explores different ligand-receptor models to understand the mechanisms of action of asymmetric ligands such as the growth hormone (GH) and the erythropoietin (EPO) which binds their receptors sequentially to form a 1:2 ligand receptor active complex configuration. The final model is able to explain the singular signaling dynamics of these systems. Furthermore, the model unveils the regulatory role of each of the two different ligand binding sites, which can help to optimize the design of agonist and antagonist molecules in order to develop more efficient treatments against GH- and EPO-related diseases.

The next publication of this thesis presents the first mathematical model to test and optimize selective chimeric drugs, using as a case of study a chimera composed of the epidermal growth factor (EGF) linked to different mutants of interferon (IFN), with selective potential toward tumoral cells over-expressing the EGF receptor. This model quantitatively reproduces all the experimental results, illustrating how chimeras using mutants of IFN with reduced affinity exhibit enhanced selectivity against cell over-expressing EGF receptor.

Then, a more complex theoretical framework based on the previos model was designed in order to study the behavior of chimeric combinatorial therapies in cell populations, predicting that drug combination of selective drugs is synergistic in terms of their selective potential. This study provides a way to gain optimal selective potential at reduced doses compared to the same drugs when applied individually.

The last contribution of the thesis presents the first global analysis of how the network nonlin-

earities can influence the cellular response to a given drug treatment. Here it was created a high-throughput framework to study the response to molecular inhibition of three-node generic signaling pathways with different regulatory motifs. Most of the analyzed networks show that the initial state of activation of the nodes strongly influences the outcome of the treatment. The network architecture can induce multiple dose-response curves where the drug efficiency increases or decreases depending on the initial state of activation of the proteins of the pathway. Several novel modes of bistability and hysteresis were characterized, illustrating how this dependence of the drug effect on the initial state of the network may affect the reproducibility of drug studies and clinical trials.

La Farmacología Cuantitiva de Sistemas tiene el potencial de cambiar nuestro el enfoque de la Investigación Biomédica y asegurar un diseño de los estudios más robusto, para así poder reducir la tasa de fracaso en las fases clínicas de desarrollo de fármacos. Esta tesis doctoral se centra en el estudio de diferentes fármacos y ligandos terapéuticos desde un punto de vista computacional, con el objetivo de diseñar, optimizar y mejorar los tratamientos farmacológicos.

Inicialmente, la tesis explora distintos ejemplos de ligando-receptor para comprender los mecanismos de acción de moléculas como la hormona del crecimiento (GH) y la eritropoyetina (EPO), que se unen a sus receptores de manera secuencial para formar un complejo activo de configuración 1:2 de ligando-receptor. El modelo matemático final es capaz de explicar la singular dinámica de señalización de estos sistemas. Además, el modelo revela el papel regulador de los distintos sitios de unión de los ligandos, lo cual puede ayudar a la optimización del diseño de moléculas agonistas y antagonistas para poder desarrollar tratamientos más eficientes de enfermedades relacionadas con GH y EPO.

La siguiente aportación presenta una herramienta matemática para evaluar y optimizar fármacos quiméricos selectivos (quimeras), utilizando como modelo a un compuesto resultado de la fusión del factor epidérmico del crecimiento (EGF) y diferentes mutantes del interferón (IFN), con selectividad hacia células tumorales que sobre-expresan el receptor de EGF. Este modelo matemático reproduce cuantitativamente los resultados experimentales de la misma quimera, e ilustra cómo las quimeras cuya subunidad citotóxica (el interferón) posee una mutación que la hace menos afín a su receptor, poseen mayor selectividad hacia las células tumorales, que sobre-expresan el receptor de EGF.

A continuación se diseñó una plataforma teórica basada en el modelo matemático anterior para así poder estudiar el comportamiento de las quimeras en terapias combinatorias aplicadas a poblaciones celulares. Los resultados predicen que la combinación de quimeras es sinérgica en términos de selectividad, aportando así una manera de aumentar su selectividad, reduciendo al mismo tiempo la cantidad de dosis, en comparación con las mismas quimeras aplicadas individualmente.

La última contribución de esta tesis doctoral presenta el primer análisis global de cómo las no-linealidades en las redes de señalización pueden influenciar la respuesta celular a tratamientos farmacológicos. Para ello, se estableció una plataforma teórica donde estudiar la respuesta a la inhibición molecular en redes de señalización genéricas de tres nodos con diferentes interacciones no lineales (autorregulación, bucles de retroalimentación, etc.). La mayor parte de las

redes analizadas muestran que el estado inicial de activación de los nodos implicados en la red afecta enormemente a la respuesta al tratamiento. La arquitectura de la red puede inducir múltiples curvas de dosis-respuesta, donde la eficacia del fármaco puede incrementarse o reducirse dependiendo del estado inicial de activación de las proteínas de la ruta de señalización. Por último, se caracterizaron nuevos tipos de biestabilidad e histéresis en la respuesta a la señal, lo cual ilustra cómo esa dependencia entre el estado inicial del sistema y el efecto de la droga podría estar afectando a la reproducibilidad de los estudios farmacológicos y ensayos clínicos.

Contents

1 Introduction

1.1 Quantitative Systems Pharmacology

The progress in basic biomedical research is driven by major advances in biotechnology techniques and increasing R&D budgets. Nonetheless, the pharmaceutical industry faces unprecedented challenges in discovering new drugs and moving them into the clinic: the current drug development cost is rising rapidly (the average cost of bringing a drug to market is $1.5 billion, over 10 times higher than the cost in the 1970s) while the number of truly innovative drugs approved has decreased significantly in the last ten years [1]; only 10% of drug development programs successfully make it to market.

The clinical phases of development (especially Phase II and III), where the dosage, safety and efficacy of the drug are assessed, have the greatest impact on the overall cost of drug development [2]. This mainly derives from high failure rates at these stages, considering that the success rates are 20-30% for Phase II and 30-50% for Phase III.

The emerging discipline of Quantitative Systems Pharmacology (QSP) has the potential to change the way we approach biomedical research and to reverse the continued decline of R&D productivity by shifting compound attrition from late clinical development to earlier stages, ensuring more robustly designed studies and improving confidence in the compound.

QSP is defined as an approach to translational medicine that combines computational and experimental methods to elucidate, validate and apply new pharmacological concepts to the development and use of small molecule and biological drugs [3]. QSP provides an integrated systems-level approach to determine mechanism of action of new and existing drugs in preclinical and animal models and in patients, enabling the prediction of efficacy and safety of those compounds at all stages of drug discovery and development. This emerging discipline has drawn an increasing awareness and focus in recent years.

The field of QSP has its origin in inherently quantitative disciplines like classical pharmacology

and physiology. Classical Pharmacology had two basic pillars — the study and quantification of drug behavior in the body comprising *pharmacokinetics* and *pharmacodynamics* (what the body does to the drug and what the drug does to the body, respectively) and the "receptor hypothesis", the idea that drug action is mediated through binding to specific target molecules or *receptive substances*. In Classical Pharmacology, drug discovery relied on *phenotypic screening*, that is, the identification of compounds that cause a desirable change in phenotype. This approach does not require a prior understanding of the molecular mechanism of drug action and even after the activity and efficacy of the drug are determined. Nonetheless, the classical approach has resulted in many successful drugs.

Beginning in the 1980s, advances in molecular biology and genomics led to phenotypic screens largely replaced by *target-based screening* [4], which measures the effect of compounds on a purified target protein via *in vitro* assays.

The idea of merging the disciplines of Pharmacology and Systems Biology is conceptually compelling because they share an interest in precise, mathematical relationships between perturbations — such as drug dose and exposure, but also genotypic and environmental variation – and physiological consequences in terms of drug action.

The discipline of Systems Biology has important historical roots in physiology. Claude Bernard is considered the first systems biologist [5]. He established the homeostatic basis of modern physiological science with his concept of the systems principle of control of the internal environment (*le milieu intérieur*) in 1865. It is much less well known that Bernard also predicted the development of mathematical biology when he wrote 'this application of mathematics to natural phenomena is the aim of all science, because the expression of the laws of phenomena should always be mathematical' [6]. More historical origins of Systems Biology can be found in Hodgkin & Huxley's ground-breaking mathematical reconstruction of the nerve impulse [7] or Noble's first mathematical model of the working heart [8]. Systems Biology flourished in the second half of the twentieth century due to the spectacular growth of molecular biology and gained a huge interest in the last 10 years, as biology enters into the challenging "post-genomic era". While an understanding of genes and proteins continues to be important, the focus is now on explaining the structure and dynamics of biological systems, complementing reductionist molecular biology by integrative approaches [9]. Systems biology combines mathematical modeling and quantitative experimental data as a way of generating formal representations of biological processes and revealing emergent properties which cannot be inferred by the study of individual components.

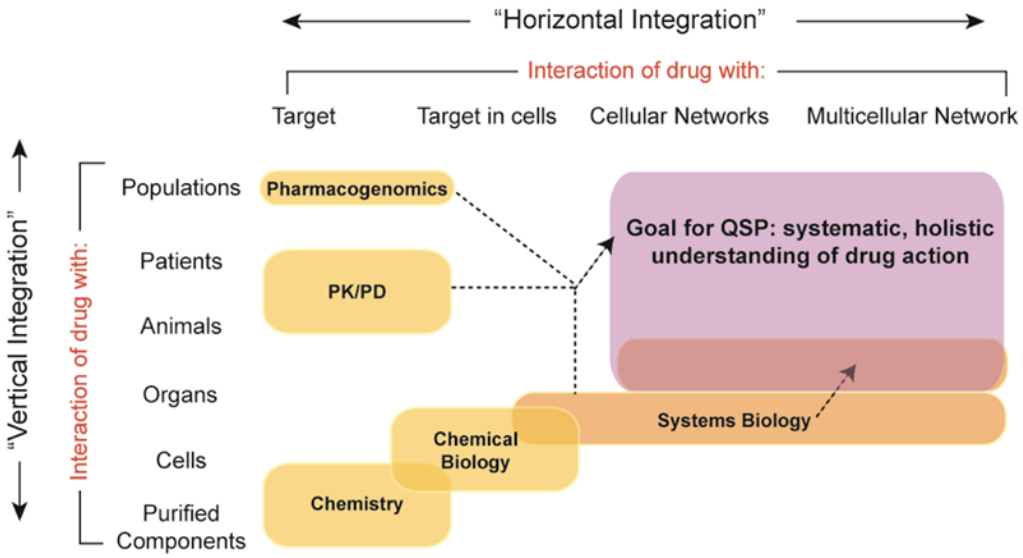

Figure 1: Representation of the horizontal and vertical integrative approaches in the fields of Systems Biology and Pharmacology. Quantitative Systems Pharmacology aims to provide a network-level insight to the Classical Pharmacology field, in order to determine the mechanisms of action of new and existing drugs in cell cultures, animal models and patients. Figure adapted from [3].

Quantitative Systems Pharmacology is the application of systems biology principles to the Pharmacology field. While Systems Biology is more *horizontally integrated*, studying multiple receptors, signaling networks, metabolic pathways or cell types at the same time, Systems Pharmacology adds *vertical integration* by integrating data from multiple spatial and temporal scales, moving from molecules to cells, tissues and organisms (see Fig. 1) [10, 11].

In this thesis the author uses QSP approach in order to understand drug response in three different directions:

- To determine the full mechanisms of action of different ligands and drugs on diverse disease states and increase the effectiveness of selective drugs (sections 3.1 and 3.2 in 'Results').
- To predict and analyze effective combination therapies (section 3.3 in 'Results').
- To underline the effect of the architecture of signaling pathways and the initial conditions of a system in the response to drug inhibitory treatments (section 3.4 in 'Results').

1.2 Signaling pathways

In order to adapt to their environment, cells have to sense and respond to external stimuli. The process by which a cell converts this extracellular stimuli to a specific response is called *signal transduction*. A typical signal transduction event involves the binding of a signaling molecule, or *ligand*, to a specific cellular protein called *receptor* that initiates a response in the target cell.

Receptors

In most cases, receptors are transmembrane proteins on the target cell surface. When they bind an extracellular signal molecule, they become activated and generate a cascade of intracellular signals that alter the behavior of the cell. In other cases, the receptors are inside the target cell, and the signal molecule has to enter the cell to activate them [12].

Cell-surface receptors can be classified as: ion-channel-linked receptors, involved in rapid synaptic signaling between electrically excitable cells, G-protein-linked receptors, which regulate the activity of a separate plasma-membrane-bound target protein, and enzyme-linked receptors.

In this thesis, the author focuses on two families of receptors inside the enzyme-linked receptor group: the tyrosine-kinase-associated receptors and the receptors tyrosine kinases (RTKs).
Tyrosine-kinase-associated receptors are cell-surface receptors which depend on tyrosine phosphorylation for their activity but they lack a tyrosine kinase domain. These receptors associate with cytoplasmatic tyrosine kinases, like the JAnus Kinase or JAK, which phosphorylates and activates a set of latent gene regulatory proteins called STATs (signal transducers and activators of transcription). STATs move into the nucleus and stimulate the transcription of specific genes. This cascade is called the Jak-STAT signaling pathway.

Cytokine receptors are the the largest and most diverse class of tyrosine-kinase-associated receptors and respond to ligand binding and stimulation by forming oligomeric active assemblages. More than 30 cytokines and hormones activate the Jak-STAT pathway by binding to cytokine receptors (see bellow).

On the other hand, the receptor tyrosine kinases (RTKs) have intrinsic catalytic activity and they are able to phosphorylate specific tyrosines on a small set of intracellular signaling proteins. After the binding of a ligand, RTKs form oligomers; even some monomeric ligands, such as the epidermal growth factor (EGF), bind to two receptors simultaneously and cross-link them directly. The oligomerization induces the cytosolic kinase domains (also called *tails*) to rearrange and cross-phosphorylate each other on multiple tyrosines, a process referred to as autophosphorylation. This

event contributes to the RTK activation by increasing the kinase activity of the tails and by creating high-affinity docking sites for the binding of a number of intracellular signaling proteins.

RTKs phosphorylation has been particularly well studied as a signaling mechanism involved in the control of animal cell growth and differentiation. This family includes the receptors for most growth factors: epidermal growth factor (EGF), hepatocyte growth factor (HGF), insulin or the macrophage-colony-stimulating factor (M-CSF). In particular, the EGF receptor (EGFR), a very important piece of this thesis, is commonly over-expressed on the surface of many types of tumor cells, such as squamous carcinoma [13], breast cancer [14], and human epithelial cancers [15], being a extremely relevant therapeutic target for cancer treatment.

Signal molecules

Cells in higher animals communicate by means of hundreds of kinds of signal molecules. These include proteins, small peptides, amino acids, nucleotides, steroids, retinoids, fatty acid derivatives, and even dissolved gases such as nitric oxide and carbon monoxide.

Most ligands are unable to cross the cell membrane, so they bind to cell surface receptors. Classical examples of these soluble ligands include growth factors (which control cell growth, differentiation and survival in their target cells), neurotransmitters (the messengers that mediate signals transmission across a chemical synapse) or peptide hormones (for instance, insulin or cytokines). In contrast, some signaling molecules are small and lipid-soluble, thus cross the plasma membrane to bind receptors inside the target cell, either in the cytosol or in the nucleus. Steroid hormones are the typical small hydrophobic signaling molecules, but also the thyroid hormone, vitamin D3, and retinoic acid are intracellular signaling proteins [16].

The research presented herein is focused on the ligand-receptor system of the cytokines EPO (erythropoietin) and GH (growth hormone) (in 'Results', section 3.1), and also on the use of the interferon IFN$\alpha 2a$ as one of the components of a chimeric selective cancer treatment (see section 1.4 and 'Results', sections 3.2 and 3.3). Interferons are cytokines secreted by leukocytes cells in response to viral infection, inducing in the neighboring cells an increase in their resistance to viral infection or having an anti-proliferative effect. In 1986, interferons IFN$\alpha 2a$ and IFN$\alpha 2b$ were the first recombinant cytokines to be FDA approved for the treatment of a malignancy (hairy cell leukemia) and at the moment, it is used as treatment of many other types of cancer diseases [17], hepatitis B and C [18] and multiple esclerosis.

The erythropoietin (EPO) is a glycoprotein hormone synthesized and secreted by cells in the kidney into the bloodstream after a lack of oxygen or a shortage of erythrocytes, which stimu-

lates erythrocyte precursor cells to survive, proliferate, and differentiate, ultimately increasing the production of erythrocytes. Recombinant EPO is approved for clinical use of iron deficiency and anemia resulting from chronic kidney disease and chemotherapy, and has a neuroprotective role for immature central neural system [19].

The growth hormone (GH) is secreted by endocrine cells into the bloodstream and participates in the regulation of many physiological processes, promoting growth and controlling metabolism. Growth hormone therapy is used to treat Turner's syndrome, Prader-Willi syndrome, chronic kidney disease hGH deficiency or insufficiency and preterm infants development [20].

EPO and GH are similar in structure, with two independent binding sites with asymmetrical affinities toward the receptor. This important feature will be addressed in the ligand-receptor modeling systems presented in this thesis.

Signal Transduction Pathways and Networks

Receptor activation by ligand-receptor interaction modifies the behavior of a chain of several interacting intracellular proteins. This cascade of biochemical reactions induced by receptor activation is called signal transduction pathway (or signaling pathway). The key players of these signaling pathways are the kinases and phosphatases, which act as key regulators of cell function by catalyzing (facilitating) the addition of a negatively charged phosphate group to proteins. These signaling cascades ultimately lead to induction of gene transcription and translation into specific proteins. Cell signaling pathways interact with one another generating complex networks of protein interactions ('signaling networks'). The crosstalk between pathways starts at the level of receptors (e.g. growth factor receptors interact with multiple pathways like the mitogen-activated protein kinase (MAPK) pathway [21], the Phosphatidylinositol-4,5-bisphosphate 3-kinase (PI3K) pathway and the phospholipase-C pathway [22]).

These highly complex networks are extremely hard to analyze in the context of the classical Molecular Biology approach and claim for a more quantitative perspective. From a drug development perspective, those non-linear interactions (auto-regulations, feedback loops, etc.) between circuit components endow signaling networks with emergent properties that modify the effects of drug action and need to be taken into account. In section 1.3, the author will address signaling network emergent behaviors.

1.3 Emergent Properties of Signaling Pathways

Many biological processes are irreversible and this is not a trivial property since the basic biochemical reactions are all reversible. For example, the differentiated state of cells is stable and cells remain differentiated for years after the stimulus triggering their differentiation disappeared. How will the reversible activation of cell signaling pathways possibly give rise to irreversible changes in cell fate, despite the short lifetime of the involved molecules and the stimulus?

Forty years ago, Monod and Jacob tried to addressed that question in a highly influential paper [23], claiming that the wiring of the signal transduction systems was responsible for the cell cycle irreversibility. Furthermore, they depicted specific signaling topologies capable of remembering a transient differentiation stimulus after it was removed. Mimicking electronic engineering principles, the visionary idea that signaling networks could remember and process signal information, was supported by many subsequent studies, and it is one of the basic concepts of systems biology field. One of the highest achievements of Molecular Cell Biology in the 1980-2000 period was to identify components of the biological networks and their basic interactions with each other. But biological systems cannot be fully understood just by knowing their parts and interconnections. Nowadays, the real challenge of molecular systems biology is to understand, predict, and intervene in the decision-making of the cell based on these interactions between proteins, genes or metabolites.

For that purpose, we should first identify the basic information-processing modules —*network motifs* [24] — in protein regulatory networks and characterize their functional significance in signal processing and cell response. This type of characterization uses many concepts and analytical tools from Nonlinear Dynamics like *stability, feedback loop, autoregulation or bifurcation diagram* [25].

Network motifs are patterns of activatory or inhibitory interactions between a small number of genes, proteins or mRNAs, usually with identifiable information-processing functions in real regulatory and signaling networks [26]. Network motifs appear at different levels of complexity (from bacteria and yeast to plants and animals) and present a wide range of functional roles in signal processing and cell response like adaptation, ultrasensitivity, homeostasis or bistability. A network motif is represented as a diagram of nodes — the species involved in the motif — interacting with each other via the arrows, which can be positive or negative. Fig. 2a shows some examples of network motifs, based on the excellent review of Dr. Alon [24].

Some of the most simple and ubiquitous motifs in regulatory networks are the autoregulatory

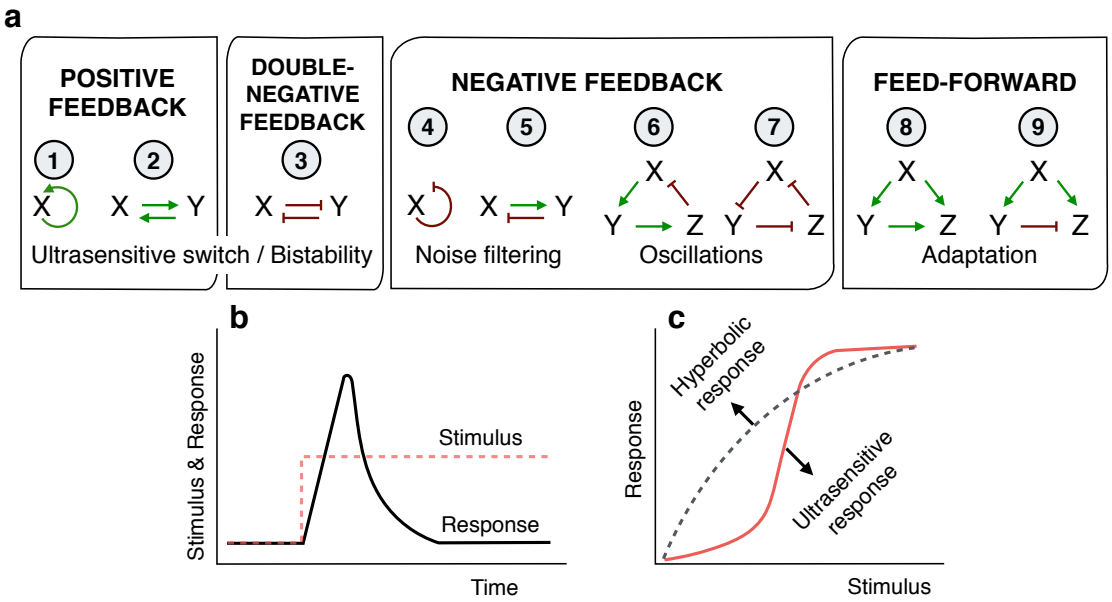

Figure 2: Network motifs and signal processing behaviors (a) Abbreviated list of two- and three-component network motifs. (b) Typical stimulus input dynamics for a system with perfect adaptation. While the change in the input is sustained over time (dashed red curve), the system responds to the input (black curve) but it recovers its prestimulated level after a while. (c) Dose-response characteristic curves for a hyperbolic response (dashed grey curve) and a ultrasensitive response (dashed red curve) with its typical sigmoidal shape: the response raises with stimulus in a steep manner, before saturation.

circuits which can involve direct (a protein autoactivating itself) or indirect (with intervening links) feedback loops that can be positive or negative. Examples of positive feedback loop (PFBL) motifs are shown in Fig. 2a(1,2), often observed in systems that exhibit ultransensitive switch behavior or bistability.

Another network motif that, under the right conditions, can exhibit bistabilty, is the double-negative feedback loop, which consists of two nodes repressing or inhibiting each other [27]. Each of the circuits with *memory abilities* of the previously cited work of Monod and Jacob [23] were variations of a double-negative feedback circuit (see Fig. 2a(3)).

Negative feedback loops are functionally associated with systems that show strong noise resistance to perturbations [28] (Figs.2a(4-7)). Furthermore, three-node feedback loops (Fig. 2a(6,7)) associate with sustained oscillatory systems under constrained conditions. The *repressilator*, a synthetic gene network built by Elowitz & Leibler, demonstrated the capacity of a simple negative FBL to generate sustained oscillations in single cells [29].

Another network architecture, which is highly enriched in bacterial transcriptional circuits, is the

feedforward loop (FFL), in which a single upstream node fans out to regulate two distinct downstream pathway branches of different lengths, but then these branches converge on an integrating node further downstream (see Fig. 2a(8,9)). Incoherent feedforward loops (Fig. 2a(9)) are associated with perfect adaptation in signal transduction networks (see 'sniffers' in [30]) and with signal integration in developmental biology (stripe-forming patterns [31]). In general, feedforward loops (Figs. 2a(8,9)) present noise-suppressive characteristics [32].

At this point, the author will give a more detailed description of some of the functional roles of network motifs: adaptation, ultrasensitivity and bistability. Adaptation refers to the system's ability to respond to a change in input stimulus and then return to its pre-stimulated output level, even when the change in input persists in time ([33], see Fig. 2b). This behavior is typical of chemotactic systems, which respond to an abrupt change in attractants or repellents, but then adapt to a constant level of the signal. It is present in different organisms like bacteria [34] or neutrophils [35]. The maintenance of homeostasis in the presence of perturbations is another example of adapted response (e.g. the calcium homeostasis in mammals [36]).

Ultrasensitivity defines a situation where a small increase in the input concentration causes a significant change in the output, in a "switch-like" manner [37]. Fig. 2c represents a hyperbolic and an ultrasensitive response as a function of the stimulus. Ultrasensitive responses resemble like those of cooperative enzymes, but they are not necessarily produced by cooperativity. Many mechanisms apart from positive feedback loops (Fig. 2a(1,2)) can generate ultrasensitive responses such as zero-order ultrasensitivity processes, multistep mechanisms, stoichiometric inhibitors. An exhaustive review of ultrasensitivity can be found in [38]). Ultrasensitivity is present in a wide range of biological processes like cell cycle regulation [39–41] or metabolic states [42].

Ultrasensitivity is a basic building block of many other emergent behaviors shown by signaling networks. It allows the effective transmission of signals down a signal transduction pathway and contributes to the generation of bistability when combined together into positive feedback loops and also oscillations when combined together into negative feedback loops [38].

The concept of bistability is addressed in the forth contribution of the thesis (see 'Results' section 3.4) and is crucial to understand behaviors such as decision-making processes in cell cycle progression, cellular differentiation or apoptosis. A system is bistable when the same input state can lead to two different, stable outputs. A simple example of a bistable system is the ultrasensitive positive feedback, which is an autoregulatory system (Fig. 2a(1)) where a cooperative feedback loop: X is phosphorylated to X active (X^*) by the stimulus S, but it can also autoactivate itself by

autophosphorylation in a cooperative manner (i.e. we need n molecules of X^* to activate X via autophosphorylation). Now, the strength of the positive feedback increases more than linearly with X^*, leading to an ultrasensitive feedback loop (more information about the system can be found in [43]). A diagram of the system can be found in Fig. {fig:adapt1a.

The change in X^* concentration is given by:

$$\frac{dX^*}{dt} = \left(k_f\,[S] + \frac{k_a \cdot [X^*]^n}{[X^*]^n + K_{MM}^a}\right) \cdot (1 - [X^*]) - k_r \cdot [X^*] \tag{1.1}$$

where k_f is the forward rate constant ($M^{-1}sec^{-1}$), k_r is the reverse rate constant (in sec^{-1}), k_a is the autophosphorylation rate constant ($M^{-1}sec^{-1}$) and n is the Hill coefficient (degree of cooperativity; here n>1).

Now, we decompose $\frac{dX^*}{dt}$ into a rate of production PR and a rate of removal RR of X^*:

$$\begin{aligned} PR &= \left(k_f\,[S] + \frac{k_a \cdot [X^*]^n}{[X^*]^n + K_{MM}^{fb}}\right) \cdot (1 - [X^*]) \\ RR &= k_r \cdot [X^*] \end{aligned} \tag{1.2}$$

The intersection of both rates corresponds to $\frac{dX^*}{dt} = 0$. In Fig. 3b, we plot both production and removal rates as a function of X^*. The steady states of the system correspond to the intersection of both curves (black circles). That graphical representation is called the *rate-balance plot*, which provides an intuitive method to determine the stability characteristics of a network.

The feedback curve is sigmoidal which allows both rate curves to intersect in three different steady states: two stables and one unstable, the latter corresponding to the the threshold concentration. If the system is on the left side of the threshold, it will settle into the off-state, but if it is on the right of the threshold, it will stay on the on-state. The concentration threshold is an unstable steady state since any perturbation will send the system either to the on-state or to the off-state [43].

Fig. 3c shows the bifurcation diagram of the system, which plots the steady-state response (stable and unstable) as a function of signal strength. Again, solid circles are the stable steady-state points while empty circles are the unstable steady-state points. S_{crit} is the critic S concentration where stable and unstable branches coalescence [25].

The presence of nonlinearities in a given signaling network can induce bistability or adaptation and these behaviors may have a strong impact on the physiological response of cells to drug treatments. The effect of a drug in a specific target will not necessarily correlate with its concentration

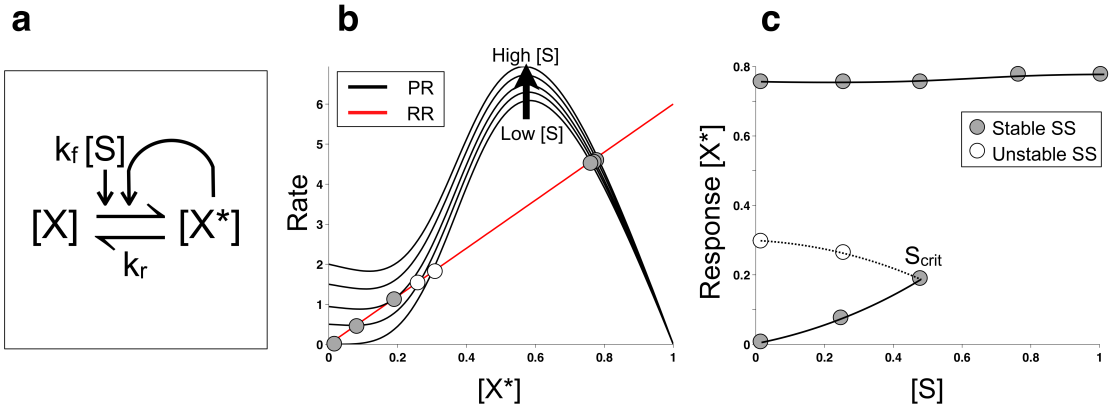

Figure 3: Ultrasensitive positive feedback system. (a) Diagram showing X phosphorylation by S (and its corresponding forward rate constant k_f) and X cooperative autorregulation. k_r is the reverse rate constant of X^* dephosphorylation. (b) Rate-balance plot for PR (rate of production) and RR rate of removal of X^*. Solid circles = stable steady-state points. Empty circles = unstable steady-state points. PR varies for different $[S]$. (c) Bifurcation diagram for X^* showing the stable branch (black curves) and the unstable branch (dashed curves). S_{crit} is the critical point where both branches colapse (also called bifurcation point) .

when the target is embedded in a network presenting nonlinear interactions, and the application of an inhibitory treatment may have unexpected results. Therefore, it is highly relevant to understand the architecture of the targeted network and its emergent properties in order to design reliable drug treatments. All these features must be considered in early phases of drug development and demand, as we have previously pointed out in section 1.1, for those quantitative and computational approaches offered by Quantitative Systems Pharmacology field. A more detailed analysis on the impact of nonlinearities on targeted therapies will be addressed in 'Results' section 3.4.

1.4 Deregulation of Signaling Pathways in Cancer and Targeted Therapy

Coordinated regulation of cellular processes allows cells to maintain homeostatic balance and make decisions as to whether to divide, differentiate, or die. Oncogenic mutations disturb the normal behavior of those signaling pathways involved in cell fate, triggering the transformation of cells from healthy to tumoral. These mutations confer cells with six capabilities or "hallmarks" (described by Hanahan & Weinberg, [44]) which enable their malignant behavior: sustained proliferative signaling, insensitivity to growth suppressors, resistance cell death, replicative immortality, induction of angiogenesis, and tissue invasion and metastasis (see Fig. 4).

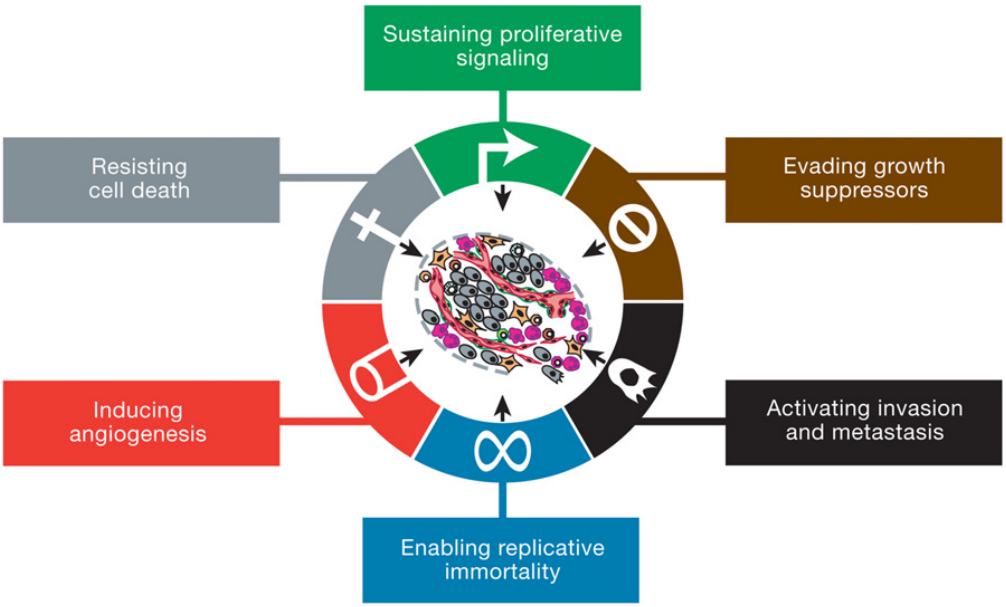

Figure 4: The Hallmarks of Cancer. This illustration encompasses the six hallmark capabilities originally proposed in Hanahan and Weinberg perspective. The past decade has witnessed remarkable progress toward understanding the mechanistic underpinnings of each hallmark. Adapted from [44]

This thesis is focused on studying therapies that target the ability of cancer cells to sustain chronic proliferation, which constitutes an essential trait for cancer development. Healthy cells have meticulous control over the production and release of growth-promoting signals that orchestrate cell growth-and-division cycles, ensuring homeostasis of cell number and thus maintenance of normal tissue architecture and function. A deregulation of key signaling cascades results in uncontrolled proliferation in an autonomous way. These signals are mainly growth factors that typically bind receptors tyrosine kinase (RTKs), which transmit signals via the signaling pathways involved in cell fate (see section 1.2). Cancer cells can acquire sustained proliferation in different ways:

- Autocrine or paracrine proliferative stimulation: Tumoral cells may produce growth factors, to which they can respond by expressing their corresponding receptors; they can also send signals to stimulate normal cells (paracrine signaling).
- Receptor overexpression: Mutations can elevate the levels of cell surface receptors, rendering such cells hyperresponsive to growth factor ligands.
- Receptor structural alterations, giving rise to ligand-independent activation.

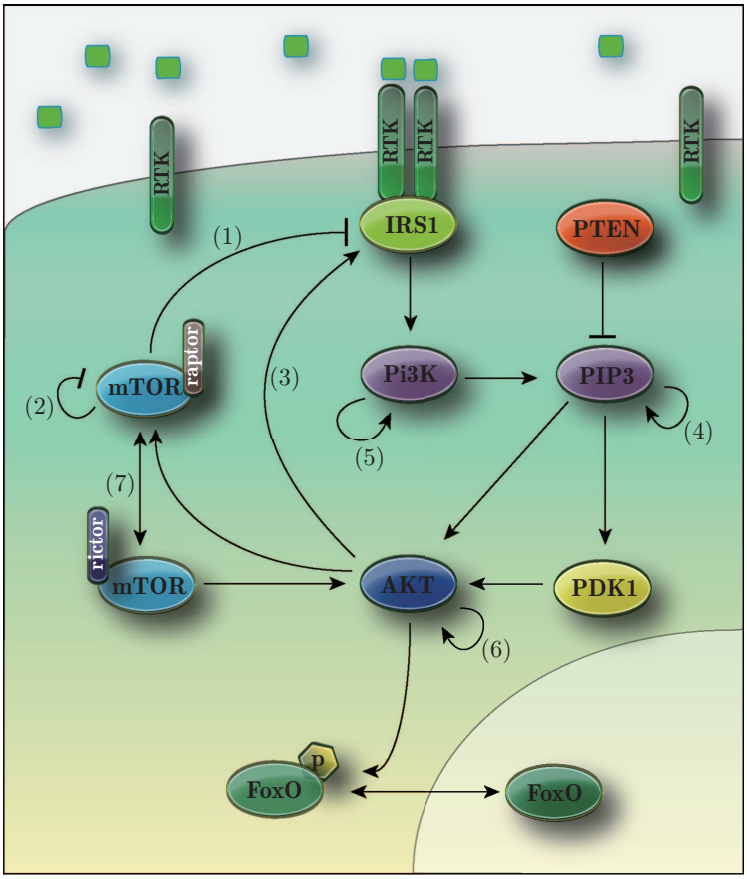

Figure 5: Nonlinear interactions of the PI3K-Akt pathway. Simplified diagram of the signaling pathway, including positive and negative feedback loops related to this network. Figure adapted from [45].

- Constitutive activation of components of signaling pathways downstream RTKs, making cells independent of growth factor stimulation.

The PI3K-Akt Pathway

An important example of nonlinear pathway highly involved in cancer initiation and progression is the PI3K-Akt pathway. DNA sequencing analyses of cancer cell genomes have shown mutations that predict constitutive activation of signaling circuits usually triggered by activated growth factor receptors, like the PI3K-Akt pathway (see Fig. 5 based on [46]). At the core of the pathway it stands the serine/theonine kinase Akt (Protein kinase B), a central regulator of cell proliferation, differentiation, migration, survival and metabolism [47]. Akt is activated by a variety of stimuli, through growth factor receptors, in phosphatidylinositol 3-kinase (PI3K)-dependent manner. PI3K-dependent Akt activation is counterbalanced by PTEN (Phosphatase and Tensin Homolog), a tumor suppressor phosphatase [48], which appears mutated in many human cancers.

A vast set of tumor tissues shows mutations in PI3K (Phosphatidylinositol-4,5-bisphosphate 3-kinase), which lead to the hyperactivation of the PI3K signaling circuitry, including Akt [49]. Furthermore, numerous studies confirm that the blockage of Akt signaling results in apoptosis and growth inhibition of tumor cells. Several members of the PI3K-Akt pathway are kinases, considered one of the most 'druggable' classes of intracellular targets. Therefore, the PI3K-Akt pathway is extremely attractive as a target for cancer therapeutic strategies and constitutes an ideal landscape for the development of small molecule inhibitors.

The PI3K-Akt pathway presents a high number of nonlinear interactions that can potentially affect the way cells respond to drugs targeting this network. Insulin signaling is regulated by feedback inhibition of the expression of IRS1 (insulin receptor substrate 1) (Fig. 5(1)): the activation of the PI3K-Akt pathway leads to the formation of the complex mTOR (mechanistic target of rapamycin)-Raptor complex that phosphorylates S6K1, which finally induces IRS1 degradation by phosphorylation [50]. In cancer cells, the cross-talk between the PI3K-Akt pathway and the mitogen-activated protein kinase (MAPK) pathway creates a negative feedback loop between mTOR-Raptor and the MAPK pathway activation in a PI3K-dependent manner Fig. 5(2) [46]. The activation of Akt in response to insulin promotes the phosphorylation of IRS1 on serine residue in turn generating a positive-feedback loop for insulin action [51](Fig. 5(3)). A positive feedback loop has been observed in PIP3 (Phosphatidylinositol (3,4,5)-trisphosphate) in cell polarity during eukaryotic chemotaxis [52] (Fig. 5(4)). In human breast carcinoma cells, PI3K presented a positive feedback in a cross-talk interaction with the ErbB2 receptor and hyaluronan [53] (Fig. 5(5)). In some cancers, Akt presents a positive regulation through the fatty acid synthase (FAS) (Fig. 5(6)) [54]. Lastly, the equilibrium between mTOR-rictor and mTOR-raptor, one positively regulating Akt and the other negatively regulating Akt (mTOR-rictor and mTOR-raptor, respectively) might play an important role in the response to treatments targeting one of these complexes (see Fig. 5(7)) [45].

Cancer Targeted Therapy

Kinases have emerged as one of the most intensively pursued targets in current pharmacological research and the largest target group for anticancer therapy [55], due to their critical roles in cellular signaling.

Small-molecule kinase inhibitors (SMKIs) have experienced an outstanding success in the last 10-15 years, powered by tremendous progress in both academic and industrial settings; 31 SMKIs have already been approved by the US Food and Drug Administration (FDA) and several other kinase inhibitors are enrolled in clinical trials at different phases [56] — an exceptional achievement

in the history of pharmaceutical research —.

SMKIs are englobed in the so-called targeted therapy, which is one the major procedures for cancer treatment, along with hormonal therapy or cytotoxic chemotherapy. Targeted cancer therapy is defined as a drug or another substance which acts by: (1) Blocking the action of specific molecules (involved in growth, progression, and spread of tumors), (2) helping the immune system to kill malignant cells or (3) delivering toxic substances directly to damaged cells. Targeted therapies are less likely to harm healthy cells than cytotoxic chemotherapy, ideally presenting less side effects. In this thesis, the author focuses on two different targeted therapy agents: the already addressed small molecule inhibitors and selective chimeric ligands.

Chimeric ligands (abbreviated: 'chimeras') are built by the fusion of a *targeting element* that discerns between undamaged and damaged cells, and an *activity element* that repairs or triggers apoptotic signals only in cells targeted by the targeting element.

The most extensive family of chimeras are *immunotoxins*: Cytotoxic agents comprising a modified toxin linked to a targeting domain derived from an antibody, a growth factor, a carbohydrate antigen, or a tumor-associated antigen [57]. Examples of immunotoxins with good clinical performance are Ontak, [58], LMB-2 [59] or IL13-PE [60]. Another family of chimeric proteins combines an antiproliferative agent such as TRAIL (TNF-related apoptosis-inducing ligand), with an antibody fragment as a cell surface tumor marker. Type-1 interferons have also been fused with tumor-specific ligands, for instance, in antiCD20-interferon (antiCD20-IFN)[61] or IFN$\alpha 2a$-asparagine-glycine-arginine peptide [17]. IFN$\alpha 2a$ has also been combined with the epidermal growth factor (EGF) to target EGF receptors (EGFR)-overexpressing cells. Chimeric ligands follow a sequential mechanism of action where the first binding event creates a local concentration of drug, which facilitates the interaction of the free subunit with its corresponding receptor, triggering the cytotoxic response.

In the second publication (see 'Results', section 3.2), the author presents a mathematical framework to design and optimize synthetic chimeric ligands using IFN$\alpha 2a$-EGF as a model. This mathematical model was also applied in the third manuscript 3.3 to combined chimeric ligands in cell populations.

Drug combination therapies (also known as polytherapies) are successfully used to treat many diseases like cancer [62, 63] or HIV's [64]. When two or more drugs are applied simultaneously, the interaction between them (i.e., when two drugs alter each other pharmacological effect) results in a complex and multi-scale problem [65]. Drug interactions are classified into additive, synergistic or

antagonistic. When drugs do not interact with each other, or are mutually exclusive by competing for the same target, they are considered as additive [66] (i.e., the effect of the combination is equal to the sum of their individual effects). Antagonism occurs when one of the drugs mitigates or counteracts the action of the other, i.e, the combination is always less effective than the single agents at the same concentration. Finally, synergism occurs when the combination of both drugs is more effective than each agent separately at the same total concentration, i.e., one of the agents enhances the actions of the other [67]. This can occur either via direct interaction, i.e, one drug increases the bioavailability of the other, or indirectly, i.e, the two drugs cooperate on targets on the same or different pathways involved in the same process. Thus, the total concentration of drug administered to achieve a certain effect is reduced, which also potentially reduces side effects, drug resistance and undesired off-target interactions.

The next section is an introduction to mathematical modeling of ligand-receptor biochemical systems and signaling network interactions.

1.5 Mathematical Modeling in Biochemical Reactions

Models are simplified representations of — our assumptions of — reality [68]. They can be informal (in which the symbols are mental, verbal, or pictorial) or formal, in which the symbols are mathematical. The election of the model should be determined by the questions being asked and the available data. Because of the quantitative and non-linear nature of the biological systems we are studying and the questions stated in this thesis, we will focus on formal — mathematical — models.

Mathematical models allow us to simulate systems, generate predictions and test hypotheses *in silico* prior to the bench work. Furthermore, models have to evolve with our knowledge and iterate with experimental data: new experiments can suggest model modifications and model predictions can guide new experimental designs [3]. In this thesis, a mathematical modeling approach is used to elucidate the mechanism of action of different signaling molecules and synthetic selective drugs and help to get a more accurate prediction of the effect of drug treatments applied to deregulated signaling pathways. In order to study those biological systems, the author uses a mathematical deterministic framework based on ordinary differential equations (ODEs) following the law of mass action. The initial formulation of the law of mass action derives from the research performed by Guldberg and Waage in 1864 [69]. Suppose we have a system where two chemicals, A and B, react upon collision with each other to form product C with a rate constant k:

$$A + B \xrightarrow{\mathrm{k}} C \tag{1.3}$$

According to the mass-action principle, the rate of this reaction (formation of C) is proportional to the product of the concentrations of the reactants (A and B): $dC = k \cdot [A] \cdot [B]$, where k is the constant of proportionality or rate constant for the reaction. For thermodynamic reasons, all chemical reactions are reversible, so eq. 1.3 should be rewritten as:

$$A + B \underset{\mathrm{k_r}}{\overset{\mathrm{k_f}}{\rightleftarrows}} C \tag{1.4}$$

where k_f and k_r are the forward and reverse rate constants of reaction, respectively. The double arrow symbol indicates that the reaction is reversible. The law of mass action states that when the reaction reaches the equilibrium, the concentrations of the chemicals involved bear a constant relationship to each other, which is described by an equilibrium constant:

$$\frac{k_r}{k_f} \equiv K_{eq} = \frac{[A]_{eq} \cdot [B]_{eq}}{[C]_{eq}} \tag{1.5}$$

While the first presented publication ('Results', section 3.1) uses mass action to develop a theoretical approach which describes the specific ligand-receptors systems like the growth hormone and the EPO interactions with their corresponding receptors, in the second publication we created a chimeric ligand-receptor model based on the monovalent ligand-receptor interaction model [70] which also applies the principles of mass-action kinetics. The third publication of this thesis ('Results', section 3.3) extends the chimeric ligand-receptor model to a heterogeneous cell population exhibiting phenotypic variability and heritability. The last contribution of this thesis ('Results', section 3.4) creates a theoretical framework to model biochemical interactions of small signaling networks and to predict the effect of inhibitory treatments depending on the topology of those interactions.

Most of the biochemical reactions in a signal transduction pathway are performed by enzymes. Enzymes are catalysts, generally proteins, that help convert other molecules called substrates into products, but they themselves are not changed by the reaction. To account for how enzymes behave, the most prevalent model in biochemistry is the Michaelis-Menten rate law [71].

A model to explain the deviation from the law of mass action was first proposed by Michaelis and Menten [72]. In their reaction scheme, the enzyme E converts the substrate S into the product P through a two-step process. First E combines with S to form a complex SE which then breaks down into the product P releasing E in the process:

$$S + E \underset{\mathrm{k_r}}{\overset{\mathrm{k_f}}{\rightleftarrows}} SE \overset{\mathrm{k_{cat}}}{\rightarrow} P + E \tag{1.6}$$

Formation of SE is characterized by a forward rate constant (k_f; units of $M^{-1}sec^{-1}$), a reverse rate constant ((k_r; in sec^{-1}), and a catalytic rate constant (k_{cat}; in sec^{-1}). As reaction rates are typically measured under conditions where P is continually removed, which prevents the reverse reaction ($P \rightarrow SE$) from occurring, thus we can consider that catalytic step as irreversible. There are two ways to analyze this equation: the *equilibrium approximation* and the *quasi-steady-state approximation*; both methods give similar results. The *equilibrium approximation* was proposed by Leonor Michaelis and Maud Menten in 1913, where they performed a "time-scale separation" assuming that the formation of the complex SE was a faster process than the formation of product P. In the typical *in vitro* situation in which substrate is in substantial excess over enzyme, this time-scale separation seems intuitively reasonable. By assuming SE to be in equilibrium with E and S, they derived an analytic approximation for the dynamics of the slower phase in which a direct link could be made between experimental data and reaction rate constants. Briggs and Haldane derived a more general formulation [73] by assuming that the rates of formation and breakdown of the intermediate complex SE are approximately equal thus $dC/dt \approx 0$. This is called the *quasi-steady state approximation*. In both approximations, the reaction velocity V (rate of P formation) takes the form:

$$V \equiv \frac{d[P]}{dt} = -\frac{d[S]}{dt} = \frac{k_{cat} \cdot [E_0] \cdot [S]}{(K_M + [S])} = \frac{V_{max} \cdot [S]}{(K_M + [S])} \tag{1.7}$$

where $V_{max} = k_{cat} \cdot [E_0]$ is the maximum reaction velocity, attained when all the enzyme is complexed with the substrate and K_M is the Michaelis constant which is the concentration of the substrate at which the reaction rate is equal to one half of the maximal velocity for the reaction V_{max}. Fig. 6a represents the reaction rate as a function of the substrate concentration. Both approaches give different mathematical meanings to K_M. In the equilibrium approximation, $K_M = \frac{k_r}{k_f}$, while in the quasi-steady state approximation $K_M = \frac{k_r + k_{cat}}{k_f}$, which is the contemporary form of the Michaelis constant.

To describe the relation between a drug and its elicit response after a specified exposure time, we use dose-response curves (Fig. 6b) where we plot the effect of the drug (drug response) for each drug concentration (dose). To measure drug efficacy, we use the half-maximal effective concentration or $EC50$ which represents the concentration of a drug that induces one half of the maximum response after drug exposure. Dose-response curves can be fitted as sigmoidal curves. A dose-response curve with a steep slope indicates that a small increment in drug concentration results in a high response increase (see section 1.3 and Fig. 2c). While the second publication in this thesis ('Results' section 3.2) studies selective drugs at the single cell, these models do not

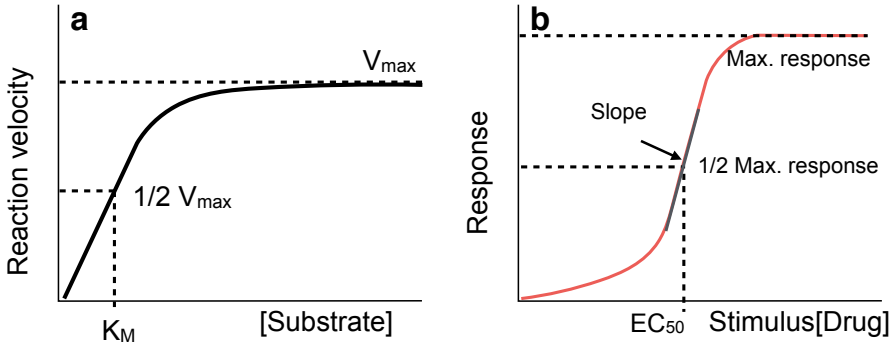

Figure 6: Michaelis-Menten approach and dose-response representation (a) Reaction velocity V versus substrate concentration : V_{max} is the maximum reaction velocity, when all the enzyme is complexed with the substrate. K_M is the Michaelis constant which is the concentration of the substrate at which the reaction rate is equal to one half of the maximal velocity for the reaction V_{max}. (b) Dose-response curve: Cell response for each drug dose. Half maximal effective concentration ($EC50$) is the drug concentration that induces one half of the maximum response (max. response) after drug exposure.

allow to explore the impact of cell-to-cell variability and phenotypic cell inheritance on drug therapies. The third publication ('Results' section 3.3) applies combinations of selective drugs to an heterogeneous population of cells. Given that the physiological response of each individual cell to the treatment depends on the concentration and efficiency of each drug, the level of expression of their corresponding receptors, and the exposure time to treatment, the authors considered a model of cells proliferating in the presence of the drug treatment, where each cell decides its fate (division, apoptosis) depending on the drug efficacy, the time of exposure to the treatment and its own phenotype. This stochastic model is the simplest scenario to simulate cell population dynamics and permits to include heritability in the expression of cell surface receptors in order to predict drug resistance mechanisms in cancer cell populations.

2 Objectives

The general objective of this thesis is to understand the mechanism of action of different therapeutic ligands and which factors may influence their effect using Quantitative Systems Pharmacology tools in order to design, optimize and improve drug treatments. The main goals of this thesis are:

- To understand the consequences of the mechanisms that regulates the active complex assembly of the growth hormone (GH) and the erythropoietin (EPO), two ligands with a particular 1:2 asymmetric and sequential ligand-receptor scheme, using mathematical models informed by experimental data, in order to test and improve drug treatment design in GH- and EPO-related diseases.

- To explore new strategies to facilitate the design of therapeutic treatments with higher selectivity at reduced drug concentrations by developing a mathematical framework informed by experimental results using the chimeric ligand composed of the epidermal growth factor (targeting element) linked to different mutants of the interferon (cytotoxic element) as a case of study, in order to test and optimize drug treatments with selective drugs.

- To generalize the previous mathematical approach for combinatorial treatments in heterogeneous cell populations in order to understand the behavior of chimeric ligands applied in combination and to study the effect of cell-to-cell variability and receptors heritability in selective drug combination treatments.

- To study the effect of the topology of signaling networks and the initial conditions of the system in the response to inhibitory treatments such as small molecule inhibitors, through the design of a high-throughput framework that explores the response to molecular inhibition of all possible three-node generic signaling pathways with different regulatory motifs and compares those responses for different initial conditions of the system.

3 Results

3.1 Theoretical Approaches to Growth Hormone Signaling

Background, Introduction and Author Contribution

The following publication continues with the line of research of 'Dynamical Modeling for Cellular Ligand-receptor Systems' started by Dr. David Míguez Gómez, head of the the Systems Biology and co-director of the author of the thesis. This research resulted in a previous publication [74], which presented a general kinetic and mechanistic model for systems with asymmetric 1:2 ligand-receptor interaction, such as the erythropoietin (EPO) and the growth hormone (GH) systems. The following publication relies on that previous article [74], giving a more exhaustive view on mathematical modeling of those specific 1:2 ligand-receptor systems.

Both EPO and GH bind to cytokine receptors (see 'Introduction', section 1.2), and respond to ligand binding and stimulation by forming dimeric active assemblages. These two ligands present interesting structural similarities, showing two binding sites with completely different affinities towards its receptor [75]. Each binding site interacts with a receptor to form the active complex in a 1:2 ligand-receptor configuration.This asymmetric 1:2 interaction scheme strongly determines the dynamics of the system, inducing interesting regulatory properties which have been extensively studied theoretically and validated with experimental data.The active complex assembly occurs sequentially: first, one binding site of the ligand interacts with a receptor to form a 1:1 complex; then, the other available binding site binds a second receptor to complete a 1:2 ligand-receptor complex [76] that can activate transcription. Because one of the binding sites of the ligand is around 10^3 times weaker than the other, this weakest interaction is often neglected, leading to a simplified 1:1 interaction scheme. However, the key properties of GH and EPO system, such as the increase in activity of the ligand homodimer and the auto-inhibition effect, are a consequence of due to this differential and sequential binding. Finally, each of the two different affinity binding sites of

the ligand have distinct roles in the regulation of the signaling, which can be characterized using mathematical tools, like those presented in this publication.

The author of this thesis has contributed to the following publication by implementing several mathematical models with increasing complexity and analyzing the dynamical properties of each model to unveil the role of each of the two different ligand binding sites in the EPO and GH signaling.The author has also participated in the elaboration of the manuscript.

The publication starts from the simplest scenario of one ligand molecule interacting reversibly with a single receptor (*1:1 interaction model*), to then describe the *1:2 symmetric interaction model*, a more realistic approximation where the ligand has two equal binding sites and binds two free receptors in a single step to form the active complex. (In this approach both ligand binding sites have the same binding and unbinding rates). The next model proposed includes the sequential binding of the symmetric ligand (*1:2 symmetric and sequential interaction scheme*) which inevitable leads to the last scenario, the *1:2 asymmetric and sequential interaction model*, where the ligand is asymmetric presenting two different binding sites that bind sequentially to their corresponding receptors to build the active complex. The *1:2 asymmetric and sequential interaction* configuration is able to explain the singular dynamic properties of EPO-EPOR and GH-GHR systems like adaptation, self-antagonism and homodimer enhanced activation.

Nova Science Publishers, Inc.
400 Oser Avenue, Suite 1600, Hauppauge, N.Y. 11788-3619, USA
Phone (631) 231-7269 * Fax (631) 231-8175
http://www.novapublishers.com

May 4, 2017

To Whom It May Concern,

We are pleased to confirm that the chapter entitled, *Theoretical Approaches to Growth Hormone Signaling*, pp. 25-46, by Victoria Doldan-Martelli and David G. Miguez was accepted for publication in the book, *Growth Hormones: Synthesis, Regulation and Health Implications,* edited by Anne Andersdtr and Jon Anderssen, ISBN: 978-1-61942-681-8. This book was published July 30th, 2012 by Nova Science Publishers, Inc. located in Hauppauge, New York, USA.

Sincerely yours,

Nadya S. Gotsiridze-Columbus
President
Nova Science Publishers, Inc.
400 Oser Avenue, Suite 1600
Hauppauge, NY 11788 USA
Tel: 631-231-7269
Fax: 631-231-8175
Email: n.columbus@novapublishers.com
Web: www.novapublishers.com

Chapter

THEORETICAL APPROACHES TO GROWTH HORMONE SIGNALING

Victoria Doldán-Martelli and David G. Míguez[*]
Departamento de Física de la Materia Condensada,
Universidad Autónoma de Madrid, Facultad de Ciencias, 28049 Madrid.

Abstract

Growth hormone is at the focus of many pharmacological interests, due to its implication in the regulation of key biological processes. Its characteristic ligand-receptor interaction scheme, in an asymmetric and sequential 1:2 configuration, induces important self-regulatory properties that determine the dynamics and strength of the signaling. Here we use a mathematical approach to unveil the consequences of the differential binding process and its relevance in the regulation of the assembly of the active complex. Several mathematical models are developed to analyze the role of each of the two different affinity binding sites of the ligand towards each of the receptors in the complex. The models allow us to study the emergence of key properties of the system due to the differential and sequential binding, such as adaptation, self-antagonism at high ligand concentrations and homodimer enhanced activation. These theoretical and computational approaches help us to optimize the design of agonist and antagonist molecules to develop more efficient treatments against growth hormone related diseases.

[*]E-mail address: david.gomez.miguez@uam.es

PACS 05.45-a, 52.35.Mw, 96.50.Fm.

Keywords: Biophysics, Mathematical Biology, Systems Biology, Theoretical Models.

1. Introduction

Cells translate extracellular information into internal responses using surface-receptors embedded in the plasma membrane. A cell surface-receptor is a highly specialized integral membrane protein that binds to a specific family of ligands, including cytokines, neurotransmitters, peptide hormones or growth factors [1]. The interaction of ligand and receptor initiates a chain of intracellular events and biochemical reactions referred as signal transduction, leading to physiological changes and regulating essential cell processes, such as differentiation, development, proliferation or apoptosis. The understanding of the regulation of cell-surface receptors and the interaction with their corresponding ligands constitutes an extremely active area of research, mainly due to their pharmacological importance as selective targets for chemotherapeutic agents. At present, receptors-based drugs represent more than 60% of medicines in the pharmacological market [2], designed to treat several diseases like autoimmune illnesses, infectious diseases or even cancer.

Growth hormone receptor (GHR) is a member of the cytokine receptor superfamily. Most of the members of this family respond to ligand binding and stimulation forming heterooligomeric active assemblages [3]. However, the GHR, along with the erythropoietin receptor (EPOR), prolactin and thrombopoietin receptor, bind to their ligands as homodimers, forming the homodimeric cytokine receptor subgroup inside the class-1 cytokine receptors family [4, 5]. Among them, GHR and EPOR have been extensively characterized, and share the same 1:2 ligand-receptor interaction scheme: the active complex is formed by a single ligand molecule flanked by two identical receptors using the two different available binding sites in the ligand [6, 7, 8]. Growth hormone receptor binds growth hormone (GH) [9], a peptide hormone that participates in the regulation of many physiological processes, promoting growth and controlling metabolism in animals and humans [10]. EPOR binds to erythropoietin (EPO), a glycoprotein which is the primary regulator of the production of circulating erythrocytes by preventing apoptosis of erythroid progenitors [11], and it is also expressed in neural stem cells, endothelial cells, and cancer cells.

EPO and GH share the spotlight of therapeutic interests. Recombinant human growth hormone (hGH) is used to treat growth disorders and metabolic dysfunctions, related or unrelated to growth hormone deficiency. For instance, hGH is used as treatment in children with chronic kidney disease [12], in patients with Crohn's disease [13], Turner syndrome or Noonan syndrome [14]. GHR is also the target of GH antagonist in acromegaly treatment. The annual market for recombinant human growth hormone was 2 billion US dollars in 2007, with sales continuing to grow [15]. Recombinant EPO, on the other hand, is at the top of protein therapeutics, with global sales of EPO in 2006 of 12 billion US dollars [16].

EPO and GH ligand molecules also share very interesting structural similarities, showing two independent binding sites with radically different affinities towards its receptor [17]. Each of the binding sites is used to interact with a receptor to form an active complex (1:2 ligand-receptor configuration). This asymmetric 1:2 interaction scheme strongly influences the dynamics of the system, inducing interesting regulatory mechanisms that have been widely analyzed theoretically and validated with experimental data. The mechanism for EPOR and GHR active complex assembly is ordered and sequential: first, the receptor forms a 1:1 complex by interacting with one of the binding sites of the ligand. Then, an additional receptor molecule binds to the other available site of the ligand, resulting in a 1:2 ligand-receptor complex [18] that can activate transcription. Since one of the binding sites of the ligand is around 10^3 times weaker than the other, the weakest interaction is often neglected and the system is simplified as a 1:1 interaction scheme. Unfortunately, many of the unique characteristics of GH signaling, such as the increase in activity of the ligand homodimer and the auto-inhibition effect, are direct consequence of the dual affinity of the ligand towards the two receptors of the complex. Furthermore, each of the binding sites has an essential role in the regulation of the signaling, which can be easily studied and characterized using simple mathematical tools.

2. Mathematical Modeling of Ligand-Receptor Systems

With the rising of systems and quantitative biology, experimental findings are more often complemented by mathematical approaches where predictions and hypotheses can be tested *in silico* prior to the bench work. In the context of ligand-receptor systems, mathematical models are developed to analyze the processes that take place after ligand stimulation, and to study the consequences

of the mechanisms that regulates the assembly of the active complex. These theoretical approaches to ligand-receptor systems constitute one of the first successfully implemented mathematical models in molecular biology [19] , due to their simple mathematical formulation and accurate characterization of the rate constants involved, both *in vitro* and *in vivo*. Among the most studied ligand-receptor systems, growth hormone stands as one of the most interesting examples to test mathematically, due to its mentioned sequential and asymmetric interaction scheme.

Models for ligand-receptor systems consist basically of simple chemical equations, where both ligand and receptor are chemical species interacting by direct binding governed by kinetic constants for their binding and unbinding rates (k_{on} and k_{off}, respectively). The strength of the signaling is often simply assumed as proportional to the amount of active complexes formed during ligand stimulation. The formation of the active complex is usually modeled as a reversible reaction, with the dissociation constant defined by $k_D = k_{off}/k_{on}$. More elaborated models include also spatial constraints such as receptor diffusion, receptor orientation, or the presence of lipid rafts. Other more complex modeling approaches, such as compartmentalized models or boolean networks are also used, although they constitute a different family of mathematical models and their analysis is far from the scope of this chapter.

Mathematical modeling is often used to validate experimental data or to predict features of an experimental system. In this chapter, we develop a simplified mathematical framework to unveil the consequences of the particular 1:2 asymmetric interaction scheme of growth hormone ligand-receptor system. We will proceed by analyzing the dynamics of increasingly complex versions of the interaction scheme, comparing them to understand the source of several specific features of the GH system: the adaptation mechanism, the self-antagonist effect at high ligand concentrations, and the enhanced efficiency of synthetic homodimers of GH ligand. For the sake of simplicity, we will only focus on the regulatory processes occurring at the membrane level, where the physical interaction between ligand and receptor takes place. The effect of intracellular regulatory processes, such as receptor expression, degradation and recycling, also impacts the dynamics of the system. Therefore, a full model including membrane ligand-receptor binding and intracellular regulatory processes can be found in [20].

Regarding the integration of the model equations, most of the mathematical models for EPOR and GHR are often computed using a classical deterministic

approach. Despite the chemical nature the model equations, the integration of the model must be done carefully, taking into account that cells usually maintain very low numbers of free GH receptors available (typically no more than a few hundred molecules) [21]. Under these conditions, the dynamics of the system will be highly dependent on stochastic fluctuations in the number of receptors and active complexes formed, so it is likely that a deterministic integration of the model equations will not reflect accurately the behavior of the system. We present here both deterministic and stochastic approaches for each of the models presented, analyzing in each case the importance of the fluctuations and comparing the outcome with the classical case. Values for the parameters used to numerically solve the model equations are listed in table 1.

Table 1. Kinetic, physical and structural parameters for GH

Parameter	Value	Reference and notes
R_T	300 molec./cell	Ref. [22, 23]
$k_{1,off}$	0.029 min^{-1}	Ref. [24]
k_{on}	0.029 $min^{-1}nM^{-1}$	Ref. [24]
$K_{1,D}$	1 nM	Ref. [17]
$k_{2,off}$	29 min^{-1}	Ref. [17]
$K_{2,D}$	920 nM	Ref. [17]
$k_{3,in}$	0.06 min^{-1}	Ref. [24]
$Q_{R,0}$	10 $nMmin^{-1}$	Ref. [22, 23]
k_{rec}	0.036 min^{-1}	Ref. [24]
k_{deg}	0.024 min^{-1}	Ref. [24]
$k_{R,in}$	0.01 min^{-1}	Ref. [25]
V	4×10^{-10} L/cell	Ref. [25]
L_0	0.2 nM	Ref. [17]
r	8.5 μm	for Hela cells. Ref. [26]
D	0.084 $\mu m^2/s$	Ref. [27]
h	7.27×10^{-3} μm	Ref. [28]
a	3×10^{-3} μm	Ref. [28]

3. 1:1 Interaction Model

The simplest scenario to capture mathematically the dynamics of ligand-receptor interaction is to consider a 1:1 interaction scheme, where one molecule of ligand interacts reversibly with a single receptor to form an active complex. The active complex then activates downstream signaling and is internalized for degradation or recycling processes. This mechanism is schematized in figure 1. This simplified scenario has been extensively used to understand the basis of ligand-receptor systems with a more complex interaction scheme, such as transferrin receptor (*TfR*), low-density lipoprotein (*LDLR*) or epidermal growth factor (*EGF*) [25]. 1:1 models have been also used to model GH and EPO receptors systems, where the formation of the active complex is simplified as a single binding event, assuming that its dynamics is mostly governed by the strong binding. In this context, the weak binding is considered as a fine-tune for the signaling, and therefore it is often neglected. Since many experimental studies have univocally shown that both binding events are required to form the active complex, these 1:1 models applied to GHR or EPOR constitute a very strong approximation to the real situation, and they miss several important characteristics which are consequence of the 1:2 interaction scheme, so they are only usefu to a certain extent. Here, we used this simple 1:1 model as a basis to develop more realistic approximations to GH system, and compare the dynamics of these simplified models with the outcome of the real 1:2 asymmetric model in the following sections. Equations for the case of 1:1 ligand-receptor interaction can be written as follows:

$$R + L \underset{k_{off}}{\overset{k_{on}}{\rightleftharpoons}} C \tag{1}$$

$$C \xrightarrow{k_{in}} S \tag{2}$$

where R represents the total number of free receptors, L is the concentration of extracellular ligand, C is the active ligand receptor complex and S represents the amount of internalized complexes, with a rate of internalization k_{in}. Experimentally, the number of molecules of freely diffusing ligand is much larger than the amount of free receptors so, for modeling purposes, L is assumed constant during the process of ligand stimulation. Numerical integration of the model equations using the values in Table. 1 is shown in Fig. 2. (using values for the binding and unbinding rates corresponding to the high affinity site, so K_D=$K_{1,D}$ in Table. 1).

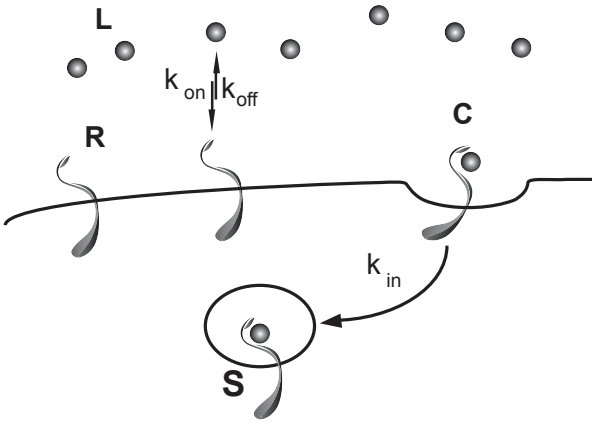

Figure 1. Scheme for the 1:1 interaction model.

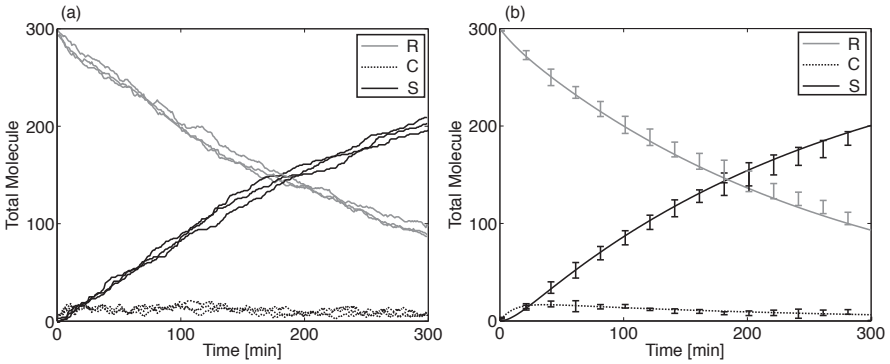

Figure 2. Numerical solution of the model corresponding to 1:1 configuration after ligand stimulation at $t = 0$. (a) Temporal evolution corresponding to three independent stochastic integrations of the model. (b) Profile of the dynamics for the deterministic model. Error bars correspond to standard deviation calculated over 50 different integrations of the stochastic model.

After ligand stimulation at $t = 0$, the number of free receptors rapidly decreases while active complexes (C) are being formed and internalized (S). The model predicts a maximum amount of active complexes C=16.5 at time t = 37

minutes and an average of $C = 6.3$ at $t = 300$ minutes. In presence of ligand, the amount of free receptors remaining at the membrane decreases due to the internalization of the active complex. The consumption of free receptors (from $R_{t=0} = 300$ to $R_{t=300} = 100$) restricts the length and strength of signaling, inducing a refractory state in the event of an increase in ligand concentration. In conclusion, this oversimplified mathematical model successfully captures several key aspects of the dynamics of GH, such as the effect of the endocytic down-regulation as a mechanism of adaptation observed after GHR stimulation [25]. Nonetheless, it does not reproduce many fundamental characteristics of the system, captured by more realistic mathematical approximations such as, for instance, the correct configuration for the active complex.

4. 1:2 Symmetric Interaction Model

The following equations reflect the fact that two free receptors R are necessary to form the active complex C.

$$2R + L \quad \underset{k_{off}}{\overset{k_{on}}{\rightleftharpoons}} \quad C \tag{3}$$

$$C \quad \xrightarrow{k_{in}} \quad S \tag{4}$$

As a first approximation to the more realistic 1:2 scheme for GH receptor, we simply assume that the formation of the complex occurs as a single step in equation 3, i.e., involving just one affinity k_{on} and one dissociation k_{off} rate constants, as shown in Fig 3. Numerical integration of these model equations can be examined in Fig. 4, where we consider the binding and unbinding rates corresponding to the high affinity site to compare the dynamics with the previous 1:1 model (K_D=$K_{1,D}$ in Table. 1).

The 1:2 configuration does not influence the dynamics of free receptors R, but the signal strength given by the amount of active complexes diminishes to about $1/2$ of the value predicted by the 1:1 model (an average maximum of $C =$ 8.3 at $t =$37 min, reduced to 3.2 at $t = 300$ minutes). This improved 1:2 model applied to GHR represents a slightly more realistic scenario, since it takes into account the correct configuration of the active complex, even if it still misses many key aspects of the system induced by the fact that the assembly of the complex requires two binding events, and therefore, it is a two-step process.

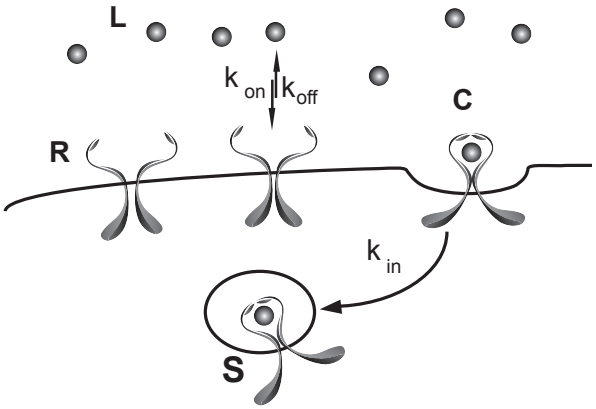

Figure 3. Scheme for the 1:2 interaction model.

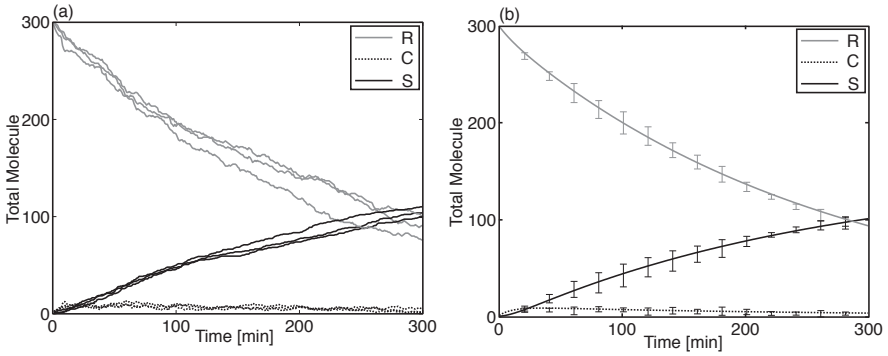

Figure 4. Numerical solution of the model corresponding to 1:2 configuration after ligand stimulation at $t = 0$ when just one binding event is considered. (a) Profile of the dynamics for three different stochastic integrations of the model. (b) Profile of the dynamics for the deterministic model. Error bars correspond to standard deviation calculated over 50 different integrations of the stochastic model.

5. 1:2 Symmetric and Sequential Interaction Model

When we consider that the active complex assembly involves two binding events, the previous equations need to be reinterpreted as a sequential process

(i.e., the ligand first binds to a free receptor and after to the second receptor of the complex). This mechanism is captured in Fig. 5 and in the following mathematical formulation.

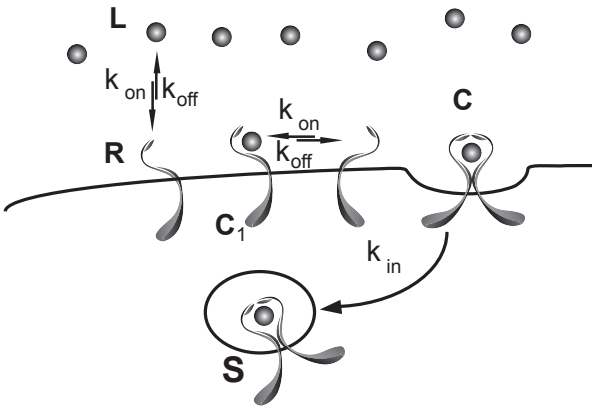

Figure 5. Scheme for the 1:2 sequential interaction model.

$$R + L \underset{k_{off}}{\overset{k_{on}}{\rightleftharpoons}} C_1 \tag{5}$$

$$R + L_1 \underset{k_{off}}{\overset{k_{on}}{\rightleftharpoons}} C \tag{6}$$

$$C \xrightarrow{k_{in}} S \tag{7}$$

The first step in the formation of active complex (eq. 5) results in an intermediate inactive complex (C_1), where the ligand is bound to the receptor using one affinity site, but still has the other site available to bind to a second receptor. This way, the formation of this intermediate complex creates a local concentration of ligand close to the cell surface (named L_1) that is available for the second receptor to form the active complex C via equation 6. This local ligand concentration L_1 is assumed to be distributed in a gasket around the cell surface and it can be calculated as a function of the Avogadro's number N_{Av}, the height of the receptor l, and the cell radius r:

$$L_1 \quad = \quad \frac{C_1}{N_{Av}V_0} = \frac{3C_1}{4\pi N_{Av}} \frac{1}{(r+l)^3 - r^3} \tag{8}$$

The sequential process induces key changes in the dynamics of the system, as we can see in the numerical solution of the equations (see Fig. 6) when compared to previous versions of the model. There is an increase in the rate of production of active complexes C via reaction 6 (a maximum of 20 actives complexes), while the number of free receptors in the membrane is rapidly reduced and it is almost completely consumed before the simulation reaches 300 minutes. At this time, almost all the initially available free receptors are in the form of internalized complexes ($S = 150$).

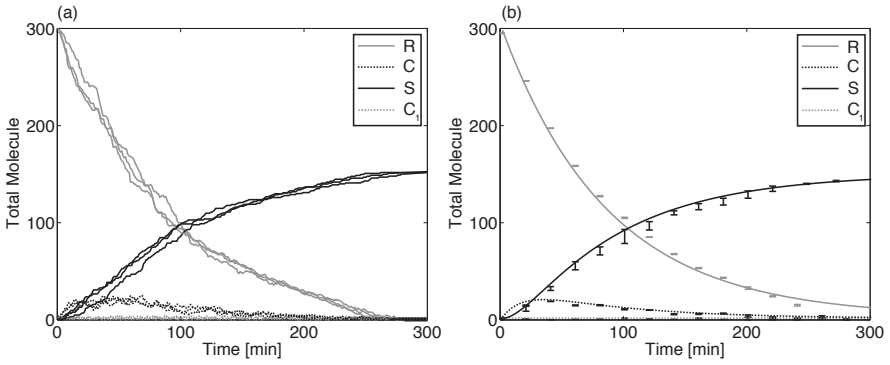

Figure 6. Numerical solution of the model corresponding to 1:2 symmetric configuration after ligand stimulation at $t = 0$ when just two sequential binding events are considered. (a) Profile of the dynamics for three different stochastic integrations of the model. (b) Profile of the dynamics for the deterministic model. Error bars correspond to standard deviation calculated over 50 different integrations of the stochastic model.

To understand the increase in the rate of formation of the active complex when the sequential binding is introduced, we compute the local ligand concentration L_1 in Fig. 7. The average local ligand concentration (black solid line) is higher than the initial ligand concentration L (gray solid line), facilitating the creation of the active complex C. This higher amount of C results in faster

internalization rate and therefore, faster consumption of receptor at the membrane.

Interestingly, the model predicts that the amount of intermediate complexes C_1 at the membrane is very low, since its rate of consumption via reaction 6 is twice the rate of its production via reaction 5 ($L_1 \approx 2L$ along the experiment, see Fig. 7). This very low values for C_1 propitiate strong stochastic fluctuations in the local concentration L_1 (dots in Fig. 7). In fact, the local concentration for this parameter values appears to be quantized in discrete values, since the source of local concentration is rapidly interacting with a free receptor to form an active complex C.

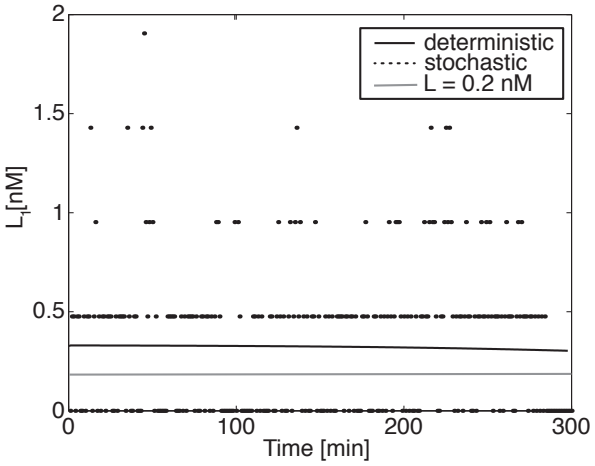

Figure 7. Plot of the local concentration L_1 corresponding to the 1:2 sequential model. Dots correspond to a single stochastic integration of the model. Black solid line corresponds to the deterministic integration. Gray solid line corresponds to the extracellular ligand L.

6. 1:2 Asymmetric and Sequential Interaction Model

Next step is to consider both binding sites of the ligand to be different in strength, as the experiments show. The asymmetric configuration of the ligand induces two very different affinities towards each of the receptors of the

active complex, with a difference in their K_D around 10^3 (see Table 1). If we assume again, that the process is sequential, each binding between a ligand and a free receptor forms an intermediate complex able to bind to a second receptor only via its free binding site. Therefore, if the first binding occurs via the strong binding site (K_1D), it forms an intermediate complex (C_1) that induces a local concentration of ligand (L_1) able to bind to a free receptor via its low affinity site (K_2D), and *vice versa*. Equations for this interaction scheme are as follows:

$$R + L \underset{k_{1,off}}{\overset{k_{on}}{\rightleftharpoons}} C_1 \tag{9}$$

$$R + L \underset{k_{2,off}}{\overset{k_{on}}{\rightleftharpoons}} C_2 \tag{10}$$

$$L_1 + R \underset{k_{2,off}}{\overset{k_{on}}{\rightleftharpoons}} C \tag{11}$$

$$L_2 + R \underset{k_{1,off}}{\overset{k_{on}}{\rightleftharpoons}} C \tag{12}$$

$$C \xrightarrow{k_{in}} S \tag{13}$$

The values for the local concentration are calculated taking into account that two different local concentrations for the ligand are originated: L_1 corresponds to the concentration of ligand bound to the receptor via the interaction site 1, so it only can interact with the free receptor via its site 2 (eq. 11). L_2 then corresponds to ligand able to use only its binding site 1, since it is using the bing site 2 to interact with the receptor (eq. 10). Expressions for each of the local concentrations are detailed bellow:

$$L_1 = \frac{C_1}{N_{Av}V_0} = \frac{3C_1}{4\pi N_{Av}} \frac{1}{(r+l)^3 - r^3} \tag{14}$$

$$L_2 = \frac{C_2}{N_{Av}V_0} = \frac{3C_2}{4\pi N_{Av}} \frac{1}{(r+l)^3 - r^3} \tag{15}$$

It is often assumed for these type of ligands with dual binding properties, that the affinity constant k_{on} is equivalent for both binding sites of the ligand (k_{on} is assumed to be dependent on structural and rotational aspects of the system), with the difference between the two dissociation rates residing in the value of the dissociation rate k_{off}. From here on, the ligand's stronger interaction will

be labeled with subindex 1, while its weaker interaction will be labeled with subindex 2. Therefore, we define:

$$K_{1,D} = k_{1,off}/k_{on} \tag{16}$$
$$K_{2,D} = k_{2,off}/k_{on} \tag{17}$$
$$K_{1,D} << K_{2,D} \tag{18}$$

The scheme for this system is shown in Fig. 8, where the two different intermediate complexes C_1 and C_2 are illustrated. The numerical solution corresponding to this system using the values for $K_{1,D}$ and $K_{2,D}$ in table 1, is represented in Fig. 8.

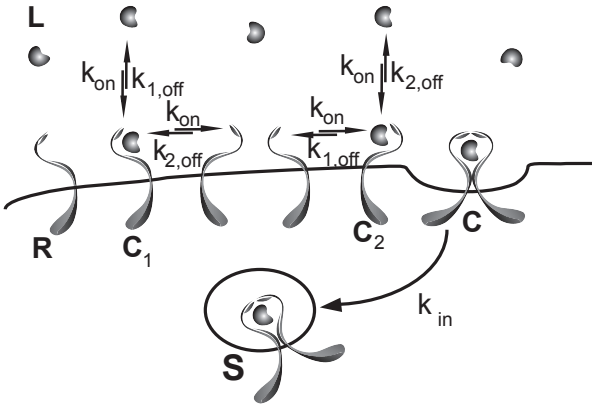

Figure 8. Scheme for the 1:2 sequential and asymmetric interaction scheme.

The numerical solution shows that the dynamics of the system are now governed by the intermediate species C_1, which represents the amount of intermediate complex C_1 waiting to interact with a free receptor to form the full active complex. This interaction occurs via equation 11 and involves the weak binding site 2. This indicates clearly that it is indeed the weaker interaction the one ultimately regulating the formation of the active complex. To analyze how, despite its very high dissociation constant, this weak reaction occurs, we need to compute the local concentration originated by the intermediate complex C_1 (shown in Fig. 10).

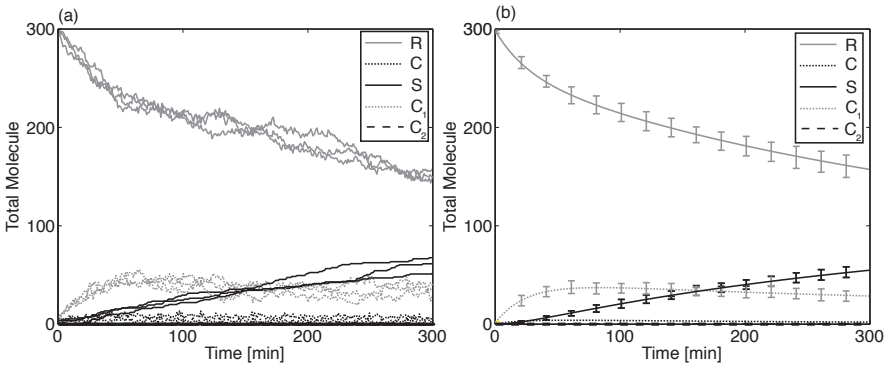

Figure 9. Numerical solution of the model corresponding to 1:2 asymmetric configuration after ligand stimulation at $t = 0$. (a) Profile of the dynamics for three different stochastic integrations of the model. (b) Profile of the dynamics for the deterministic model. Error bars correspond to standard deviation calculated over 50 different integrations of the stochastic model.

We can see that the local concentration L_1 is now 10^2 times higher than the value of the free ligand concentration L, strongly facilitating the binding via the weak interaction of equation 11. This univocally shows that the effect of the local concentration increase due to the sequential binding is essential to form the active complex. The predicted amount of active complexes is low when compared to the models previously analyzed (around 4 C complexes at t = 42 minutes and around zero active complexes at t=300 min), as a consequence of the low affinity site being 1000 times weaker than before. The intermediate complex C_2 is almost zero at all times (and its associated local concentration L_2 is also zero), which means that the low affinity interaction only occurs due to the extra increase in the local concentration of the ligand able to interact via its low affinity site (L_1).

7. Self-Antagonist Effect

One of the main characteristics of EPO and GH dynamics is the quenching of the signal at high ligand concentrations. This inhibition is often interpreted as an additional layer of regulation under conditions of very high stimulation of

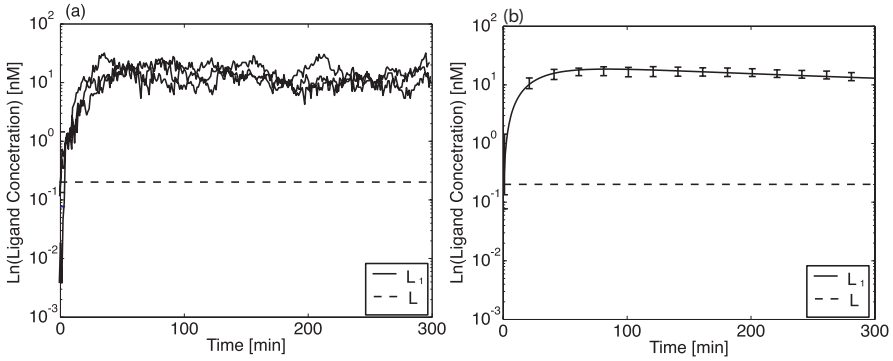

Figure 10. Plot of the local concentration L_1 corresponding to the 1:2 sequential asymmetric model (L_2 value is around zero along the experiment). (a) Three independent stochastic integrations of the model. (b) Deterministic integration of the model. Error bars correspond to standard deviation calculated over 50 different integrations of the stochastic model. Solid line corresponds to the local concentration L_1. Dashed line corresponds to the value of free ligand L.

the system, and it is a direct consequence of the interaction scheme between ligand and receptor. Figure 11 shows this effect in the 1:2 asymmetric sequential model, where we performed different numerical simulations for several values of the external ligand concentration and monitored the number of molecules at a fixed time. As we can see, increasing the ligand concentration decreases the amount of free receptors (solid gray line) while it increases the amount of intermediate complexes (dotted gray line). The weak intermediate complex C_2 remains close to zero for all concentrations used. On the contrary, the amount of active complexes and the amount of internalized complexes reaches a maximum at a certain ligand concentration and gets strongly reduced at higher ligand concentrations (from an average of $C_{max} = 7$ to $C = 2.5$ at $L = 5$ nM). This reduction occurs due to the consumption of free receptors to form inactive intermediate complexes (around 250 inactive C_1 complexes at $L = 5$ nM). These intermediate complexes find very low number of free receptors for the second ligand-receptor interaction to occur, so active complexes cannot be formed. This mechanism, known as self-antagonist effect, has been widely reported in GH [18] and EPO [29] systems, and it is a unique feature provided by the asymmetric nature of the interaction, since the previous models do not

reproduce the self-antagonist effect, as we show in figure 12 (neither S nor C gets reduced when we increase the ligand concentration).

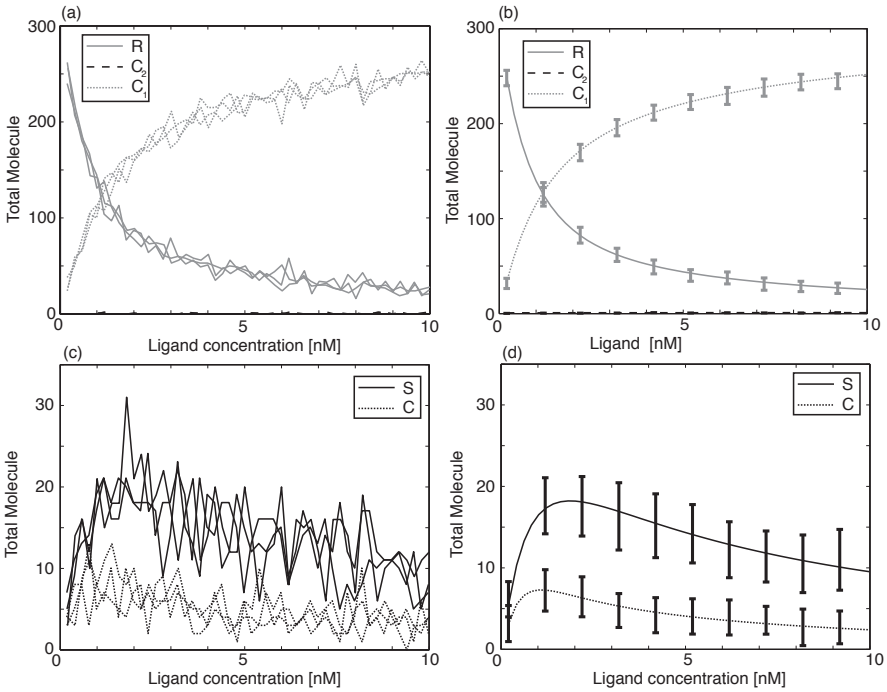

Figure 11. Effect of the increase of ligand concentration in GH signaling for the 2:1 asymmetric and sequential model. (a,c) three independent integrations of the stochastic model. (b, d) Deterministic integration of the model. Error bars correspond to the standard deviation calculated over 50 different integrations of the stochastic model. Values represented correspond to a simulation time of $t = 40$ minutes.

8. Enhanced Efficiency of GH Ligand Homodimers

It is also well described experimentally that synthetic versions of the GH ligand designed with two linked molecules of GH exhibit a strong increase in activity, when compared to the endogenous ligand stimulation. This enhanced ho-

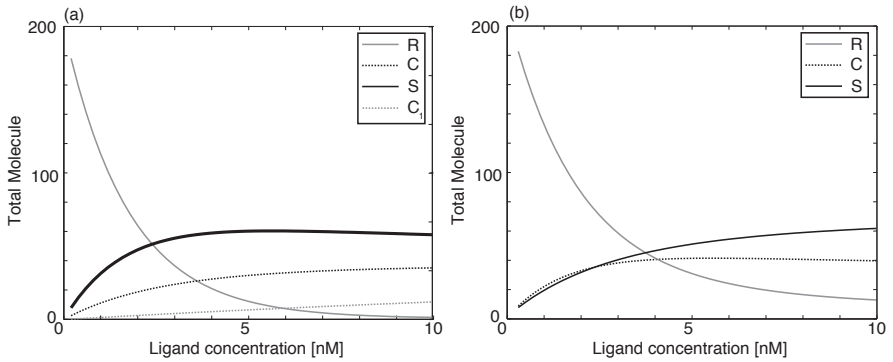

Figure 12. Effect of the increase of ligand concentration in GH signaling for the (a) symmetric sequential in section 5. and (b) symmetric 1:2 non sequential in section 4.. Values represented correspond to a simulation time of $t = 10$ minutes.

modimer ligand acts in such a way that replaces the weak binding site with an additional strong binding site, therefore, the active complex is hold together using two strong binding affinity sites ($K_{1,D} = K_{2,D} = K_D$). This homodimer ligand lacks the regulatory role of the weak binding, and the sequential asymmetric process becomes symmetric. Consequently, the system composed of ligand symmetric homodimer interacting with two receptors be modeled simply using the equations developed in section 5.. Comparison of the model outcome for symmetric (figure 6) and asymmetric (figure 9) shows that the symmetric configuration predicts much higher stimulation than the asymmetric version of the sequential model, as the experiments show [30, 31, 32, 33]. Again, this enhanced activity of synthetic GH dimers compared with ligand monomers can only be understood using models that include the asymmetric nature of the endogenous ligand.

9. Receptor Monomer Versus Receptor Dimer Hypotheses

Mathematical modeling also allows us to explore other key aspects of the receptor-ligand interaction that remain unclear. For instance, there is contro-

versy regarding the configuration of the unstimulated receptor and the effect of the ligand in the 1:2 complex [34]. Several experimental studies suggest that unstimulated receptors are monomers freely diffusing in the cell membrane. Ligand binding brings two receptors together, and the interaction between the two receptors activates downstream signaling. On the contrary, there are increasing evidences that the receptors are already pre-dimerized before ligand stimulation, and the role of the ligand is just to induce a conformational change that activates the receptor complex [35, 36, 37, 38, 39, 40].

In terms of the dynamics of the system this means that, if receptors are monomers, a ligand-receptor inactive complex has to diffuse to encounter a free receptor in the membrane to interact with. On the other hand, if receptors are already dimers, receptor diffusion across the lipid bilayer will not influence the rate of formation of the active complex C [36, 37]. To consider the effect of diffusion, the affinity rate needs to be rewritten in the form [41],

$$k'_{on} = (\frac{1}{k_{on}} + \frac{1}{k_{diff}})^{-1} \tag{19}$$

whereas an effective affinity rate constant k'_{on} is calculated as a combination of two effects: the affinity of ligand-receptor interaction k_{on}, and the effect of the collision rate between C_1 complexes and free receptors R. This k_{diff} (expressed in the appropriate units of $M^{-1}min^{-1}$) for collisions in a two-dimensional medium, is calculated based on physical considerations as follows [41]:

$$k_{diff} = \frac{2\pi D}{ln(b/a)} N_{Av} l \tag{20}$$

N_{Av} is the Avogadro's number, D and l are the diffusion coefficient and the extracellular height of the receptors, respectively. Parameter a is the diameter of the receptor. Parameter b is the average distance between free receptors in the cell, calculated for an homogeneous distribution of receptors on the cell surface of radius r as follows:

$$b = \sqrt{\frac{4r^2}{R}} \tag{21}$$

Since the number of free receptors R diminishes after ligand stimulation, the collision rate constant k_{diff} and therefore the affinity rate constant k'_{on} are time-dependent variables, and the system can change from being reaction-limited

($k_{coll} >> k_{on}$) to a diffusion-limited ($k_{coll} << k_{on}$) process along the experiment. If we compute the temporal evolution of the effective affinity constant k'_{on} (figure 13), we observe that this value experiences a 6% decrease due to the reduction of free receptors. Overall values for k_{coll} are in the range of values for k_{on}, so the diffusion in the free monomer receptor hypothesis should effectively reduce the amount of active complexes to around $1/2$ of the value, when the situation is that of unstimulated receptors as homodimers.

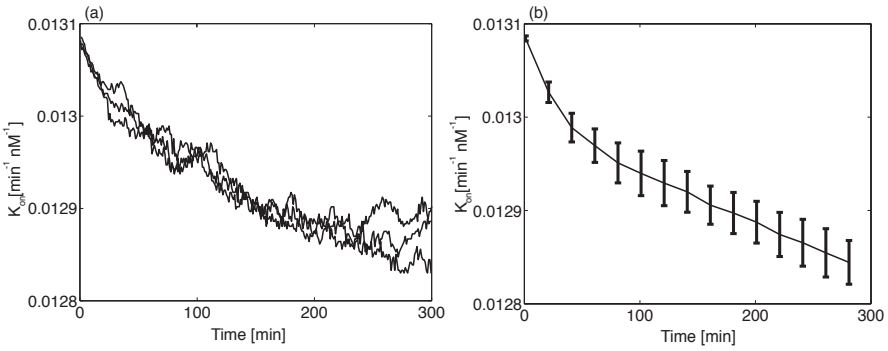

Figure 13. Plot of the effective affinity constant k'_{on} modulated by receptor diffusion. (a) there independent integrations of the stochastic model. (b) Average over 50 integrations of the stochastic model. Deterministic integration of the model. Error bars correspond to the standard deviation calculated over 50 different integrations of the stochastic model.

10. Conclusion

This chapter uses a mathematical approach to unveil the implications of the interaction scheme of GH ligand with its receptor. To do that, we explore different versions of a mathematical model where we increasingly include relevant characteristics of GH system. We start from a general model that includes few aspects of the dynamics (a simple 1:1 configuration), finishing with a more complex version which captures the key features of the system such as the self-antagonist effect and the enhanced homodimer configuration of the ligand. This approach allows us to explain the source of the key aspects of GH signaling, in-

duced by interactions at the membrane level. More complex models including the effect of intracellular processes, such as free receptor and active complex recycling, receptor degradation and downregulation of receptor production after pathway activation are studied in [20].

These type of simple kinetic models are also useful to reveal the different roles that the two binding sites of the GH ligand play during the formation of the active complex. The fact that the assembly of the complex needs to occur in a sequential manner (i.e., it needs two binding events) induces a local concentration of ligand close to the cell surface that strongly facilitates the second binding event. This is of key importance in the case of GH and EPO, where one of the bindings needed to form the 1:2 complex is too weak to occur without this increase in local concentration.

The mathematical model also reveals that this weak binding site is the one tightly controlling the signal strength and the amount of active signaling complexes. This regulatory role of the weak binding is also evident when the weak binding site in the ligand is replaced by a strong binding site. This is the situation when homodimers of the ligand (with two strong binding sites) interact with the two receptors of the complex. In this case, the theoretical model confirms the experimental data, predicting an strong increase in activity when compared to the ligand-monomer case. The strong binding site also regulates the self-antagonist effect at high ligand concentrations and the optimal ligand concentration that induces maximum activity of the complex.

The mathematical approach studied here does not consider changes in the conformation of ligand after the first binding, which will affect the dissociation constant of the second binding event, as suggested by several authors. NMR experiments that compare the crystal structure of free EPO and EPO inside the active complex show a very similar topology in the two situations [42]. Small changes in the vicinity of the binding sites have been reported, but this slight shift may be a consequence of the ligand being inside the two-receptor complex, and not due to the first binding reaction. Therefore, we can assume that the dissociation constant of both binding sites of the ligand remains unaltered after the first interaction with the receptor occurs.

Regarding the structure of unstimulated GHR as monomers or dimers, the model shows that the effect of receptor diffusion in the membrane reduces the amount of active complexes being formed. Model calculations show that the rate of collision k_{diff} is on the same order of magnitude than the affinity rate constant k_{on}, and remains more or less constant along the duration of the exper-

iment.

The addition of the effect of diffusion does not change the dynamics of the system, so the mathematical model does not allow to discriminate between both hypotheses. Nevertheless, it seems that the self-antagonist and the ligand homodimer effect are incompatible with the homodimer receptor hypothesis, unless the receptor homodimer is capable of housing a pair of ligands, resulting in a 2:2 ligand-receptor configuration. Different studies propose that the GHR extracellular domain is flexible enough to productively accommodate GH dimers [43, 31]. On the other hand, the self-antagonist effect requires that two unbound ligands fail in inducing the conformational change required to activate the complex. A third hypothesis contemplates that two GHR can weakly dimerized, undergoing conformational changes after ligand binding [34].

Altogether, our mathematical models show that the interaction scheme of the GH system strongly determines its dynamics and regulation, and the combination of the effect of the sequential binding with the asymmetric nature of the ligand dictates essential aspects of the system. These type of mathematical approaches can be also used to predict the effect of mutations that should increase or decrease differentially each of the binding sites in the signaling. A better comprehension of the details of activation of GH system will permit to develop more efficient drugs to overcome many diseases related to GH dysfunction.

11. Acknowledgments

This work has been supported by the Ministry of Science and Technology of Spain via a Ramon Y Cajal Fellowship and a Project from PLAN nacional, and a Marie Curie International Reintegration Grant from the EU 248346-NMSSBLS, as well as financial support from the CSIC-SPAIN (JAE-DOC).

References

[1] Cooper GM, Hausman RE. *The cell: a molecular approach*.4th ed. Washington, D.C.: ASM Press; 2009.

[2] Christopoulos A. Allosteric binding sites on cell-surface receptors: novel targets for drug discovery. *Nat. Rev. Drug Discov.* **2002** Mar;1:198–210.

[3] Frank SJ, O'Shea JJ. Recent advances in cytokine signal transduction: lessons from growth hormone and other cytokines. In: LeRoith D, editor. *Advances in molecular and cellular endocrinology*. vol. 3. JAI Press; 1999. p. 1–42.

[4] Watowich SS, Wu H, Socolovsky M, Klingmuller U, Constantinescu SN, Lodish HF. Cytokine receptor signal transduction and the control of hematopoietic cell development. *Annu Rev. Cell Dev. Biol*. **1996**;12:91–128.

[5] Constantinescu SN, Keren T, Socolovsky M, Nam H, Henis YI, Lodish HF. Ligand-independent oligomerization of cell-surface erythropoietin receptor is mediated by the transmembrane domain. *Proc. Natl. Acad. Sci. U.S.A*. **2001** Apr;98:4379–4384.

[6] Witthuhn BA, Quelle FW, Silvennoinen O, Yi T, Tang B, Miura O, et al. JAK2 associates with the erythropoietin receptor and is tyrosine phosphorylated and activated following stimulation with erythropoietin. *Cell*. **1993** Jul;74:227–236.

[7] Argetsinger LS, Campbell GS, Yang X, Witthuhn BA, Silvennoinen O, Ihle JN, et al. Identification of JAK2 as a growth hormone receptor-associated tyrosine kinase. *Cell*. **1993** Jul;74:237–244.

[8] Frank SJ, Gilliland G, Kraft AS, Arnold CS. Interaction of the growth hormone receptor cytoplasmic domain with the JAK2 tyrosine kinase. *Endocrinology*. **1994** Nov;135:2228–2239.

[9] Postel-Vinay MC, Finidori J. Growth hormone receptor: structure and signal transduction. *Eur. J. Endocrinol*. **1995** Dec;133:654–659.

[10] Davidson MB. Effect of growth hormone on carbohydrate and lipid metabolism. *Endocr. Rev.* **1987** May;8:115–131.

[11] Ghezzi P, Brines M. Erythropoietin as an antiapoptotic, tissue-protective cytokine. *Cell Death Differ.* **2004** Jul;11 Suppl 1:37–44.

[12] Mehls O, Wuhl E, Tonshoff B, Schaefer F, Nissel R, Haffner D. Growth hormone treatment in short children with chronic kidney disease. *Acta Paediatr.* **2008** Sep;97:1159–1164.

[13] Denson LA, Kim MO, Bezold R, Carey R, Osuntokun B, Nylund C, et al. A randomized controlled trial of growth hormone in active pediatric Crohn disease. *J. Pediatr. Gastroenterol. Nutr.* **2010** Aug;51:130–139.

[14] Kappelgaard AM, Laursen T. The benefits of growth hormone therapy in patients with Turner syndrome, Noonan syndrome and children born small for gestational age. *Growth. Horm. IGF. Res.* **2011** Dec;21:305–313.

[15] Kelly CJ, Mir FA. Economics of biological therapies. *BMJ.* **2009** 8;339:bmj.b3276.

[16] An Z. *Therapeutic Monoclonal Antibodies: From Bench to Clinic*. John Wiley & Sons; 2009.

[17] Philo JS, Aoki KH, Arakawa T, Narhi LO, Wen J. Dimerization of the extracellular domain of the erythropoietin (EPO) receptor by EPO: one high-affinity and one low-affinity interaction. *Biochemistry.* **1996** Feb;35:1681–1691.

[18] Fuh G, Cunningham BC, Fukunaga R, Nagata S, Goeddel DV, Wells JA. Rational design of potent antagonists to the human growth hormone receptor. *Science*. **1992** Jun;256:1677–1680.

[19] MONOD J, WYMAN J, CHANGEUX JP. On the nature of allosteric transitions: A plausible model. *J. Mol. Biol.* **1965** May;12:88–118.

[20] Miguez DG. *The role of asymmetric binding in ligand-receptor systems with 1:2 interaction ratio*. *Biophys. Chem.* **2010** May;148:74–81.

[21] Ridderstrale M. Signaling mechanism for the insulin-like effects of growth hormone–another example of a classical hormonal negative feedback loop. *Curr. Drug Targets Immune Endocr. Metabol. Disord.* **2005** Mar;5:79–92.

[22] Takahashi T, Chiba S, Hirano N, Yazaki Y, Hirai H. Characterization of three erythropoietin (Epo)-binding proteins in various human Epo-responsive cell lines and in cells transfected with human Epo-receptor cDNA. *Blood*. **1995** Jan;85:106–114.

[23] Sawyer ST. Introduction: the erythropoietin receptor and signal transduction. *Ann. N. Y. Acad. Sci.* **1994** Apr;718:185–190.

[24] Gross AW, Lodish HF. Cellular trafficking and degradation of erythropoietin and novel erythropoiesis stimulating protein (NESP). *J. Biol. Chem.* **2006** Jan;281:2024–2032.

[25] Shankaran H, Resat H, Wiley HS. Cell surface receptors for signal transduction and ligand transport: a design principles study. *PLoS Comput. Biol.* **2007** Jun;3:e101.

[26] Horky M, Wurzer G, Kotala V, Anton M, Vojtesek B, Vacha J, et al. Segregation of nucleolar components coincides with caspase-3 activation in cisplatin-treated HeLa cells. *J. Cell. Sci.* **2001** Feb;114:663–670.

[27] Hillman GM, Schlessinger J. Lateral diffusion of epidermal growth factor complexed to its surface receptors does not account for the thermal sensitivity of patch formation and endocytosis. *Biochemistry.* **1982** Mar;21:1667–1672.

[28] Livnah O, Stura EA, Johnson DL, Middleton SA, Mulcahy LS, Wrighton NC, et al. Functional mimicry of a protein hormone by a peptide agonist: the EPO receptor complex at 2.8 A. *Science.* **1996** Jul;273:464–471.

[29] Schneider H, Chaovapong W, Matthews DJ, Karkaria C, Cass RT, Zhan H, et al. Homodimerization of erythropoietin receptor by a bivalent monoclonal antibody triggers cell proliferation and differentiation of erythroid precursors. *Blood.* **1997** Jan;89:473–482.

[30] Qiu H, Belanger A, Yoon HW, Bunn HF. Homodimerization restores biological activity to an inactive erythropoietin mutant. *J. Biol. Chem.* **1998** May;273:11173–11176.

[31] Mockridge JW, Aston R, Morrell DJ, Holder AT. Cross-linked growth hormone dimers have enhanced biological activity. *Eur. J. Endocrinol.* **1998** Apr;138:449–459.

[32] Sytkowski AJ, Lunn ED, Davis KL, Feldman L, Siekman S. Human erythropoietin dimers with markedly enhanced in vivo activity. *Proc. Natl. Acad. Sci. U.S.A.* **1998** Feb;95:1184–1188.

[33] Sytkowski AJ, Lunn ED, Risinger MA, Davis KL. An erythropoietin fusion protein comprised of identical repeating domains exhibits enhanced biological properties. *J. Biol. Chem.* **1999** Aug;274:24773–24778.

[34] Frank SJ. Receptor dimerization in GH and erythropoietin action–it takes two to tango, but how? *Endocrinology*. **2002** Jan;143:2–10.

[35] Livnah O, Stura EA, Middleton SA, Johnson DL, Jolliffe LK, Wilson IA. Crystallographic evidence for preformed dimers of erythropoietin receptor before ligand activation. *Science*. **1999** Feb;283:987–990.

[36] Gent J, van Kerkhof P, Roza M, Bu G, Strous GJ. Ligand-independent growth hormone receptor dimerization occurs in the endoplasmic reticulum and is required for ubiquitin system-dependent endocytosis. *Proc. Natl. Acad. Sci. U.S.A.* **2002** Jul;99:9858–9863.

[37] Brown RJ, Adams JJ, Pelekanos RA, Wan Y, McKinstry WJ, Palethorpe K, et al. Model for growth hormone receptor activation based on subunit rotation within a receptor dimer. *Nat. Struct. Mol. Biol.* **2005** Sep;12:814–821.

[38] Brooks AJ, Wooh JW, Tunny KA, Waters MJ. Growth hormone receptor; mechanism of action. *The International Journal of Biochemistry & Cell Biology*. **2008**;40:1984 – 1989.

[39] Yang N, Wang X, Jiang J, Frank SJ. Role of the growth hormone (GH) receptor transmembrane domain in receptor predimerization and GH-induced activation. *Mol. Endocrinol.* **2007** Jul;21:1642–1655.

[40] Poger D, Mark AE. Turning the growth hormone receptor on: evidence that hormone binding induces subunit rotation. *Proteins*. **2010** Apr;78:1163–1174.

[41] Lauffenburger DA, Linderman J. *Models for Binding, Trafficking, and Signaling*. 4th ed. Oxford, UK: Oxford University press; 1995.

[42] Cheetham JC, Smith DM, Aoki KH, Stevenson JL, Hoeffel TJ, Syed RS, et al. NMR structure of human erythropoietin and a comparison with its receptor bound conformation. *Nat. Struct. Biol.* **1998** Oct;5:861–866.

[43] Yang N, Langenheim JF, Wang X, Jiang J, Chen WY, Frank SJ. Activation of growth hormone receptors by growth hormone and growth hormone antagonist dimers: insights into receptor triggering. *Mol. Endocrinol.* **2008** Apr;22:978–988.

3.2 A Mathematical Model for the Rational Design of Chimeric Ligands in Selective Drug Therapies

Background, Introduction and Author Contribution

This publication belongs to line of work of 'Dynamical Modeling for Cellular Ligand-receptor Systems' and explains the behavior of the synthetic chimeric ligand formed by an activity element, the interferon IFN$\alpha 2a$, a linker, and a targeting element, the epidermal growth factor (EGF).

While the EGF subunit targets cells over-expressing the EGF receptor (EGFR), the IFN$\alpha 2a$ subunit is responsible for triggering the apoptotic signal. The mechanism of action of chimeric ligands is sequential: the ligand binds its corresponding receptor via one of its subunits and this first binding event increases its local concentration, facilitating the second binding event to form the active complex. These chimeric ligands induced IFN$\alpha 2a$ signaling in an EGFR-dependent manner in HeLa cells, A431 cells and Daudi cells over-expressing EGFR [77]. The emph{chimera was patented in 2011 [78] together with a mathematical model of the binding of chimeric ligands to target cells.

The contribution of the author to this publication includes a curation of the original mathematical model for chimeric ligand design and optimization, a calibration of the model using experimental data extracted from [77] and the validation of the model solving the equations numerically on different mutants of the chimera for two cell lines with differential EGFR expression. The author performed a exhaustive literature search to obtain the experimental parameter values involved in the system.

The author of the thesis analyzed the efficiency and selectivity of those ligands in simulations comparing cells with differential EGFR expression. In order to get a measure of the chimeric anti-proliferative effect, the author calibrated the model with experimental results, using only IFN$\alpha 2a$ monomer cell toxicity assays ([77]).

The model explains aspects that determine the selective potential of the chimera and to optimize its design by testing variants with increased selectivity and efficiency. The model quantitatively fits all experimental results, showing how different versions of the chimera exhibit enhanced selectivity towards specific cell type. Furthermore, this theoretical framework permits to test the dependence of the efficiency of the chimera on receptor abundance, length of the linker between both ligand subunits, and diffusion of membrane receptors. This general model can be easily tailored to other chimeric compounds to be used as a tool to understand the experimental observations as well as

to optimize the design of potential chimeric constructs with improved selectivity.

Citation: CPT: Pharmacometrics & Systems Pharmacology (2013) 2, e26; doi:10.1038/psp.2013.2

www.nature.com/psp

ORIGINAL ARTICLE

A Mathematical Model for the Rational Design of Chimeric Ligands in Selective Drug Therapies

V Doldán-Martelli[1], R Guantes[1] and DG Míguez[1]

Chimeric drugs with selective potential toward specific cell types constitute one of the most promising forefronts of modern Pharmacology. We present a mathematical model to test and optimize these synthetic constructs, as an alternative to conventional empirical design. We take as a case study a chimeric construct composed of epidermal growth factor (EGF) linked to different mutants of interferon (IFN). Our model quantitatively reproduces all the experimental results, illustrating how chimeras using mutants of IFN with reduced affinity exhibit enhanced selectivity against cell overexpressing EGF receptor. We also investigate how chimeric selectivity can be improved based on the balance between affinity rates, receptor abundance, activity of ligand subunits, and linker length between subunits. The simplicity and generality of the model facilitate a straightforward application to other chimeric constructs, providing a quantitative systematic design and optimization of these selective drugs against certain cell-based diseases, such as Alzheimer's and cancer.
CPT: Pharmacometrics & Systems Pharmacology (2013) **2,** e26; doi:10.1038/psp.2013.2; advance online publication 13 February 2013

Next-generation therapeutic drug development integrates tools from genomics, biotechnology, molecular modeling, and computational chemistry to reduce costs and time necessary to bring new drugs to market. This redesigned drug development pipeline incorporates quantitative approaches to overcome the challenge of better, more reliable, and more efficient treatments. In the context of cancer and other cell-based diseases, the ideal "perfect" drug can be envisaged as a compound that only affects diseased cells without harming the healthy surrounding cellular environment. These types of selective drugs are chimeric in nature, composed of a targeting element that discerns between undamaged and damaged cells, and an activity element that repairs or triggers apoptotic signals only in cells targeted by the targeting element. The most extensive family of chimeras are immunotoxins: cytotoxic agents comprising a modified toxin linked to a targeting domain derived from an antibody, a growth factor, a carbohydrate antigen, or a tumor-associated antigen.[1] Examples of immunotoxins with good clinical performance are Ontak (the only agent approved to use for refractory cutaneous T-cell lymphomas by the US Food and Drug Administration),[2] LMB-2[3] BL22,[4] and IL13-PE.[5]

Another family of therapeutic chimeric proteins combines an antiproliferative agent, such as TRAIL, with an antibody fragment or a natural ligand as an specific cell surface tumor marker:[6] scFv425:sTRAIL,[7] scFvCD7:sTRAIL (specific for CD7),[8] and scFvCD19:sTRAIL (targeting CD19-positive cells).[9] Researchers also synthetized sFasL fusion proteins to target the T-cell leukemia–associated antigen CD7[10] or CD20.[11] Type-1 interferons have also been fused with tumor-specific ligands, for instance, in antiCD20-interferon (antiCD20-IFN)[12] or IFNα-2a-asparagine-glycine-arginine peptide[13] in which the asparagine-glycine-arginine peptide targets the aminopeptidase N expressed in tumor vessels. IFNα-2a has also been combined with the epidermal growth factor (EGF) to target EGF receptors (EGFR)-overexpressing cells.[14]

The sequential mechanism of action of chimeric ligands (**Figure 1**) starts by a freely diffusing chimera (**Figure 1a**) that binds via one of its subunits to its complementary membrane receptor (**Figure 1b,c**). This first binding event maintains the other free subunit of the chimera in the vicinity of the membrane, facilitating the interaction with its corresponding receptor. The efficiency of the chimeric system depends on the balance between binding and unbinding rates of both ligand–receptor interactions, concentration of receptors for the targeting and activity elements, diffusion of both receptors on the membrane, and internalization of complexes, etc.

Herein, we present a mathematical framework to design and enhance synthetic chimeric ligands. As a case study, we apply our model to different mutants of a IFNα-2a-EGF chimera developed in ref. 14, in which the EGF subunit targets cells overexpressing EGFR and the IFN subunit triggers apoptotic signals. These chimeras induced IFNα signaling in an EGFR-dependent manner in HeLa, and A431 cells, as well as in Daudi cells engineered to overexpress EGFR into the Daudi cell line (300× higher than the parental cell line). The Daudi cell line comes from a human Burkitt lymphoma and is susceptible to IFNα antiproliferative activity. Antiproliferative assays comparing Daudi and Daudi-EGFR cells showed that the inhibition of cell proliferation by chimeric proteins depended on the presence of EGFR on the cell surface.

The model allows us to understand the key aspects that determine the selective potential of the chimera and to optimize its design by testing variants with increased selectivity and efficiency. Our model quantitatively fits all experimental results, showing how different versions of the chimera exhibit enhanced selectivity (measured as the differential IFN activity of the chimera in Daudi-EGFR compared with Daudi cells). The

[1]Departamento de Física de la Materia Condensada and Instituto Nicolás Cabrera, and IFIMAC Universidad Autónoma de Madrid, Facultad de Ciencias, Madrid, Spain. Correspondence: DG Míguez (david.gomez.miguez@uam.es)
Received 21 November 2012; accepted 3 January 2013; advance online publication 13 February 2013. doi:10.1038/psp.2013.2

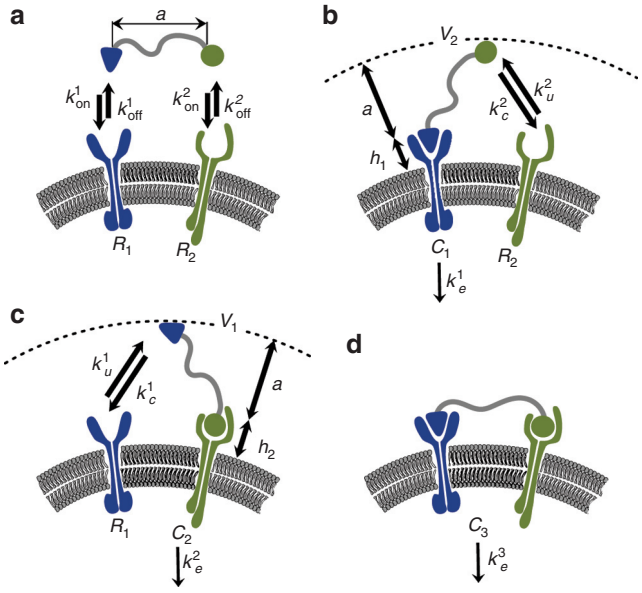

Figure 1 Scheme of the chimeric ligand/receptor interaction. (**a**) The chimeric ligand is formed by two subunits (blue and green) connected by a protein linker of length "*a*." Each subunit of the free ligand can bind to its corresponding receptor forming intermediate complexes (**b**) C_1 and (**c**) C_2. V_i is the effective reaction volume where the free ligand subunit is distributed (**b–c**) and h_i corresponds to the height of receptor R_i (i = 1, 2) above cell surface. (**d**) Once both subunits of the ligand are bound to their corresponding receptors, complex C_3 is formed, which gets internalized following the endocytotic constant k^3_e.

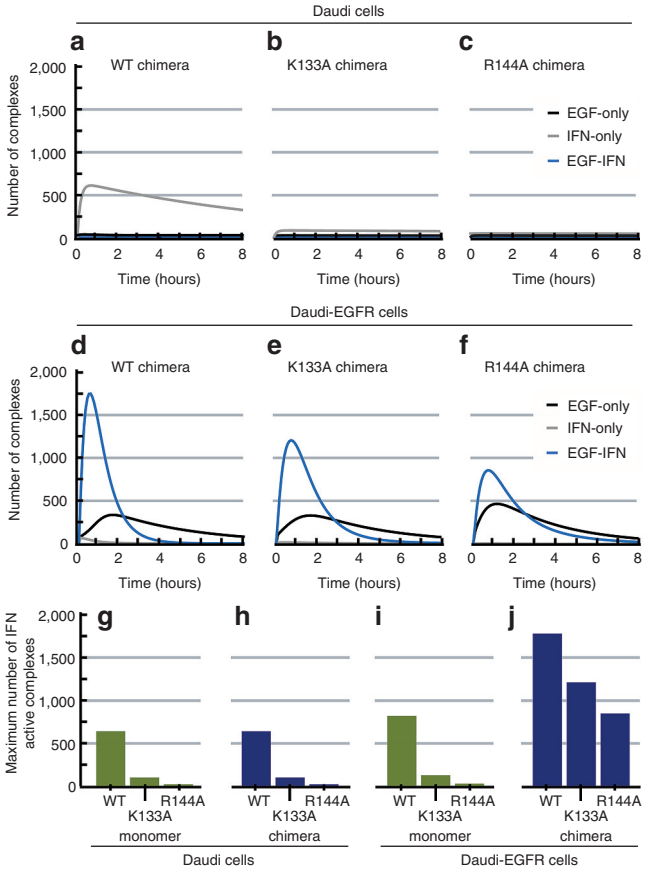

Figure 2 The model predicts higher interferon (IFN) activation in EGFR overexpressing cells. Dynamics of formation of IFN complexes at L = 1 nmol/l in (**a–c**) Daudi and (**d–f**) Daudi-EGFR cells during 8 h. Black line corresponds to EGF complexes only bound via the EGF subunit (C_1 variable in our model). Gray line corresponds to IFN complexes only bound via the IFN subunit (C_2 variable). Blue line corresponds to complexes bound via both subunits of the chimera (C_3 variable). (**g–j**) Bar diagram of the maximum number of IFN complexes (maximum of the sum of blue and gray lines in **a–f**) for monomer and chimeric ligands in ref. 14 (**g–h**) Daudi and (**i–j**) Daudi-EGFR cells. EGF, epidermal growth factor; EGFR, epidermal growth factor receptor; WT, wild-type.

model also allows us to test the dependence of the efficiency of the chimera on receptor abundance, length of the linker between both ligand subunits, and diffusion of membrane receptors. This general model can be easily tailored to other chimeric compounds to be used as a tool to understand the experimental observations as well as to optimize the design of potential chimeric constructs with improved selectivity.

RESULTS

Activity of the chimera is enhanced in cells overexpressing EGFR

Figure 2 compares the dynamics of the different complexes C_i in Daudi (Figure 2a–c) vs. Daudi-EGFR cells (Figure 2d–f). After ligand stimulation at t = 0, the number of complexes increases initially to later drop due to internalization. The amount of IFN ligand–receptor complexes formed decreases when using IFN mutants with reduced affinity. In all cases, the maximum amount of IFN complexes formed is higher in Daudi-EGFR cells (Figure 2d–f) than in Daudi cells, with most of the IFN complexes also bound via the EGF subunit to EGFR (blue line). The dynamics of the EGF and IFN receptors (IFNR) is plotted in **Supplementary Figure S1** online.

Given that transcription of IFN-induced genes has been shown to correlate to IFNR occupancy,[15] the maximum activity of the chimera can be monitored in terms of the maximum number of IFN complexes formed. Figure 2g–j plots the maximum amount of IFN complexes in monomer vs. chimeric configurations in both cell lines. The control cell line shows no difference in activity between monomer and chimeric ligand due to its low endogenous EGFR expression (Figure 2g,h). On the contrary, the chimeric ligand induces higher IFN complex formation in cells overexpressing EGFR, as compared with the monomer (Figure 2i,j). These results correlate with the measurements reported in ref. 14, at which the activity of the pathway is monitored in terms of pSTAT1 levels (a readout of IFN stimulation). Overall, the model shows how the efficiency of chimeric ligands is achieved: the formation of the IFN complex is enhanced by the presence of EGFR, which binds to the EGF subunit of the chimera while maintaining the IFN subunit close to the cell surface. This intermediate configuration increases the local concentration of IFN at the vicinity of the cell surface, facilitating the binding to IFNR. This mechanism increases the effective activity of IFN mutants with very low efficiency as monomers (K133A and R144A). With respect to chimeric configuration, these IFN variants outperform the wild type in terms of selectivity (see Selectivity is enhanced in chimeras with reduced IFN affinity section).

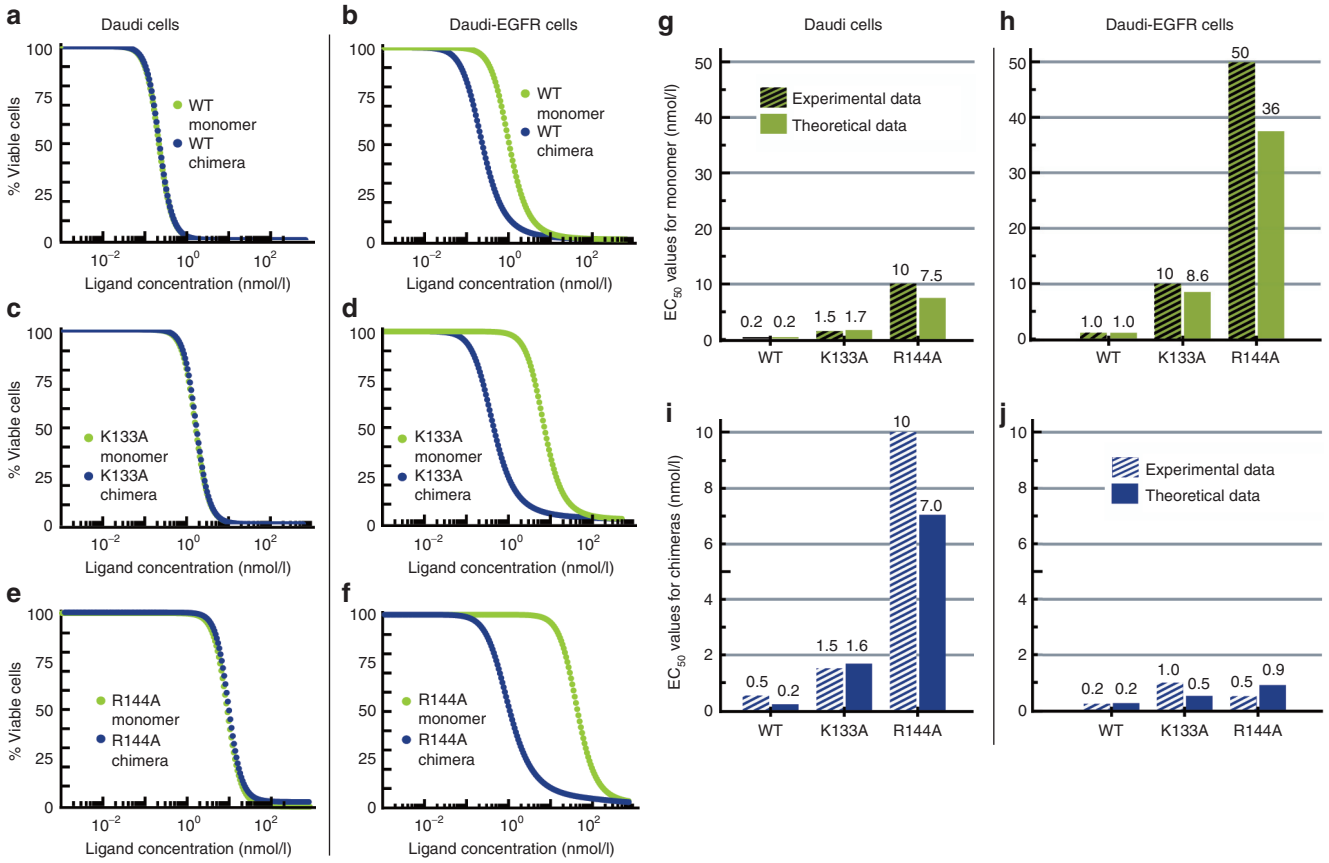

Figure 3 Theoretical dose–response curves predict highest selectivity for lowest affinity interferon mutants. Dose–response curves to compare cytotoxicity of the monomeric (green dotted lines) and chimeric (blue dotted lines) proteins in (**a,c,e**) Daudi and (**b,d,f**) Daudi-EGFR cell lines. (**g–j**) Bar diagram representing experimental and theoretical half maximal effective concentration (EC_{50}) values for (**g–h**) monomer and (**i–j**) chimeric ligands (see Methods section). Numbers above each bar correspond to the EC_{50} (nmol/l) values for each condition. Note the different scale in the *y*-axis. EGFR, epidermal growth factor; WT, wild type.

Selectivity is enhanced in chimeras with reduced IFN affinity

The efficacy of drugs in triggering apoptotic responses is often characterized in terms of percentage of viable cells in a population after treatment, in the form of dose–response curves.[14] To correlate the model predictions with the experimental dose–response curves in ref. 14, we perform a calibration using values for the wild-type IFN monomer in both cell lines tested (see Methods section). This calibration translates the maximum number of IFN complexes formed into percentage of viable cells, and is used to calculate theoretical dose–response curves for the rest of monomer mutants and chimeric constructs, to be compared with their corresponding experimental curves. Other measurements of the chimeric activity, such as the sum of the number of IFN complexes formed until the maximum is reached, have also shown good correlation with experimental data (see **Supplementary Figure S2** online).

Figure 3 shows the dose–response curves calculated for the two cell lines and the three different IFN mutants in monomeric and chimeric configurations. In Daudi cells (**Figure 3a,c,e**) the difference between chimera and monomer is negligible for all mutants. On the other hand, Daudi-EGFR cells (**Figure 3b,d,f**) present stronger response to chimeric ligand vs. monomer for all three IFN mutants. This difference increases when using mutants with reduced IFN affinity, resulting in a wider range of concentrations at which the monomer has a minimal effect whereas the chimera shows a strong effect in terms of percentage of viable cells.

Figure 3g–j plots the half maximal effective concentration (EC_{50}) values of the ligand predicted by the model and the experimental data for each chimera in Daudi and Daudi-EGFR cells in ref. 14. The EC_{50} of the monomer (**Figure 3g,h**) increases as the affinity of the IFN mutants decreases, i.e., progressively higher ligand concentrations are required to trigger apoptosis in 50% of the cells. Of note, each IFN monomer mutant exhibits a higher EC_{50} in Daudi-EGFR cells as compared with the parental Daudi cell line, evidencing higher resistance of Daudi-EGFR cells to treatment with the IFN monomer. We hypothesize that this higher resistance is caused by the proliferative activity derived from EGFR overexpression.

EC_{50} values for the different chimeras are equivalent to their corresponding monomers when applied to Daudi cells, as expected (**Figure 3g,i**). On the contrary, EC_{50} values are lower for all chimeric mutants in Daudi-EGFR cells (compare **Figure 3i** with **Figure 3j**), meaning that low concentrations of the chimera can trigger stronger effect on these cells than on Daudi cells. This difference determines the selective power of chimeric constructs when applied to a population of cells, and

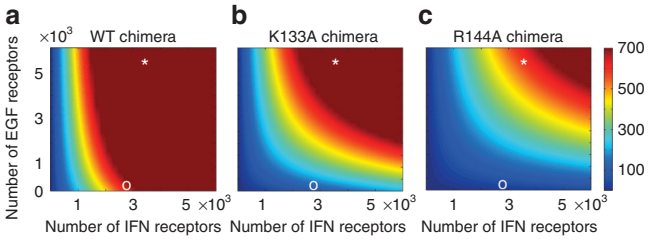

Figure 4 Chimeric ligand activity depending on the number of EGF and interferon (IFN) receptor expression. Activity of the chimera measured as the maximum number of total IFN complexes, C_2 + C_3, in a color map as a function of initial amount of EGF and IFN receptors on the cell membrane. We varied the parameters R_1 (0) and R_2 (0) in **Table 1** from 1 to 6,000 number of molecules. Ligand concentration L = 1 nmol/l. Color threshold has been selected to mark in red the number of IFN complexes that kills all the cells (0% cell viability). White symbols represent experimental values of EGF and IFN number receptors for Daudi (o) and Daudi-EGFR (*) cells, respectively. EGF, epidermal growth factor; EGFR, epidermal growth factor receptor; WT, wild-type.

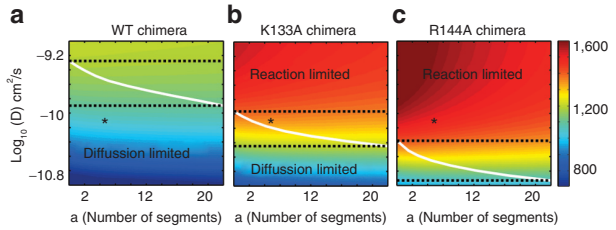

Figure 5 Chimeric ligand selectivity depends on receptor diffusion and linker length. Differential activity between Daudi and Daudi-EGFR cell lines (in a color code) as a function of receptor diffusion coefficient (D) and linker length (number of linker subunits) for the chimeras containing the (**a**) wild type, (**b**) K133A, and (**c**) R144A IFN ligands. The parameters corresponding to the experimental construct[14] are marked with a black asterisk. White line represents maximum selectivity as a function of linker length for each value of the diffusion coefficient. The range in D where a maximum is observed separate the reaction limited regime (selectivity decreases as a function of linker length) from the diffusion limited regime (selectivity slightly increases as a function of linker length). Ligand concentration for each mutant is chosen at the half maximal effective concentration value of activity for the Daudi-EGFR cell line. EGFR, epidermal growth factor receptor.

Table 1 Kinetic parameters used in the chimeric model

Parameter	Value	Ref.
k^1_{off}	0.24 min^{-1}	30
k^1_{on}	0.09 nmol/l^{-1} min^{-1}	30
k^1_e	0.15 min^{-1}	31
h_1	90 Å	32,33
D_1	2–2.4 × 10^{-10} cm^2/s	34
k^2_{off} WT	0.66 min^{-1}	29
k^2_{on} WT	0.22 nmol/l^{-1} min^{-1}	29
k^2_e WT	0.046 min^{-1}	28
k^2_{off} K133A	1.08 min^{-1}	29
k^2_{on} K133A	0.041 nmol/l^{-1} min^{-1}	29
k^2_e K133A	0.046 min^{-1}	28
k^2_{off} R144A	2.58 min^{-1}	29
k^2_{on} R144A	0.021 nmol/l^{-1} min^{-1}	29
k^2_e R144A	0.046 min^{-1}	28
h_2	50 Å	35
D_2	10^{-10} cm^2/s	21
A	900 μm^2	23
a	48.5x10^{-4} µm	14
R_1(0) Daudi cells	22 molecules	14
R_2(0) Daudi cells	2,800 molecules	14
R_1(0) Daudi-EGFR cells	5,640 molecules	14
R_2(0) Daudi-EGFR cells	3,600 molecules	14
$C_1(0) = C_2(0) = C_3(0)$	0 molecules	

Parameter values of EGF and IFN binding, unbinding, and endocytotic rates for a quantitative analysis of our system, corresponding to EGF-EGFR wild-type system and IFN-IFNR wild-type and mutants of IFN, from recent publications. EGF, epidermal growth factor; EGFR, epidermal growth factor receptor; IFNR, interferon receptor.

when the activity element induces a stronger response in cells overexpressing the receptor of the targeting element. When overexpression of this receptor is a marker of disease, these chimeric constructs can trigger cytotoxic activity in unhealthy cells, leaving healthy cells unharmed. Therefore, comparison between **Figure 3i,j** shows that the mutant with the lowest IFN affinity (R144A) presents the highest selectivity, having a strong effect on unhealthy Daudi-EGFR cells whereas leaving healthy cells undamaged for a wide range of ligand concentrations.

Overall, the model quantitatively reproduces the experimental data for different monomers and chimeric constructs,[14] and shows that the most selective chimera is the mutant with reduced affinity toward IFNR, again, consistent with the experiments.

Efficiency of the chimera depends on the balance between EGFR and IFNR expression

In the previous section, the model illustrates how the selectivity of chimeric constructs is achieved between cells expressing low and high levels of the targeting element receptor. However, *in vivo* cells do not express a disease marker in an on/off fashion but in a wide range of expression levels.[16] To understand how the expression level of receptors influences the efficiency of the chimera, we calculate the maximum number of IFN complexes formed for different values of initial EGF and IFNR after stimulation with 1 nmol/l of chimeric ligand. Results are represented in **Figure 4**, in which each point in the graph corresponds to the maximum number of IFN complexes formed at certain values of IFNR and EGFR. Blue color represents harmless levels of IFN complex formed and red represents IFN complex levels high enough to trigger apoptosis in all cells of a population. IFNR and EGFR expression levels for Daudi (white circle) and Daudi-EGFR (white asterisk), in our experimental model system, are marked in all panels.

For a constant ligand concentration, wild-type chimera activity (**Figure 4a**) does not depend on EGFR expression levels, respectively. This means that upon crossing a certain threshold in IFNR levels, all cells will die independently of the expression

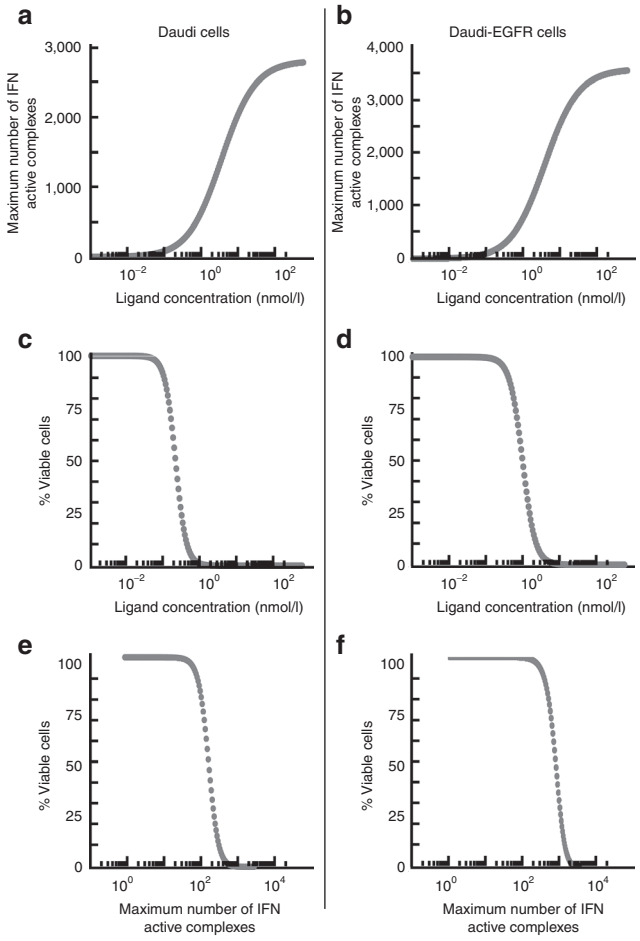

Figure 6 Calibration curves for the IFN wild-type monomer in Daudi-EGFR and Daudi cell lines. (**a,b**) Model prediction of maximum IFNR activation for different ligand concentrations. (**c,d**) Experimental dose–response curves from ref. 14 fitted as sigmoidal curves. (**e,f**) Calibration curves to correlate predicted IFNR activation with experimental cytotoxic activity for a given ligand concentration. Parameters for the sigmoidal fitting of the calibration curves: (**e**) for Daudi cells are maximum value (E_{max}) =100, minimum value (E_0) = 0, Inflection Point (IP) = 160.9, Slope (S) = –3.3 and (**f**) for Daudi-EGFR cells are E_{max} = 100, E_0 = 0, IP = 814, S = –3.4. Sigmoidal fitting perfomed using an in-house MATLAB script. EGFR, epidermal growth factor receptor; IFN, interferon; IFNR, interferon receptor.

levels of our disease marker, EGFR. On the other hand, the R144A mutant chimera (**Figure 4c**) shows low activity in cells with low numbers of EGFR, but also reduced efficiency in cells with intermediate levels of EGFR expression, with the result that potentially harmful cells can be left undamaged. The mutant with intermediate affinity, K133A (**Figure 4b**), exhibits the best trade-off between selectivity and efficiency, with strong activity in cells expressing high and intermediate levels of EGFR (disease cells) and low activity in cells expressing low levels of EGFR (healthy cells).

Taken together, these results show that the expression levels of both targeting and activity receptor elements modulate the efficiency and selectivity of the chimera, and that different versions of the chimera can be designed and optimized in specific situations to achieve the best compromise between selective killing and efficiency.

Selectivity of the chimera depends on linker length and receptor diffusion

As discussed in the Methods section, formation of C_3 complex via Eqs. 4 and 5 depends on two factors: first, both receptor types must become close enough on the cell surface. This process is controlled by diffusion and favored by longer chimera linkers *a* (see Eq. 7). In addition, the effective affinity constant $k^i_{on'}$ (Eq. 9) decreases with linker length because the effective reaction volume increases for longer linkers. The global coupling rate k^i_c in Eq. 6 is dominated by the slowest process: if diffusion of receptors is slow $k^i_c \sim k^i_{diff}$, and the reaction is said to be diffusion limited. On the other hand, for fast diffusive transport, $k^i_c \sim k^i_{on'}$, and the process becomes reaction limited. Between both regimes, there could be an intermediate optimal linker that maximizes the activity.

In ref. 14, the linker is formed by a chain of seven identical subunits of Gly4-Ser residues. The linker length *a* is estimated as the average end-to-end distance of a protein polymer containing N Kuhn segments (the Gly4-Ser subunits), using a worm-like chain model:[17]

$$a^2 = 2l_p l_c \left(1 - l_p/l_c\right)\left(1 - e^{-l_c/l_p}\right) \qquad (1)$$

where N is the number of subunits, $l_c = N \cdot a_K$ and $l_p = a_K/2$ are the contour and persistent lengths, respectively. The Kuhn segment length, a_K, is calculated as $a_K = 5 \cdot C_d$, where $C_d = 3.8$ Å is the length of a residue.

To study the impact of receptor diffusion and linker length on the selectivity of chimeras, we calculated the difference in activity (measured as the maximum number of IFN complexes formed) between Daudi and Daudi-EGFR cells varying systematically the diffusion coefficient and the number of linker subunits. **Figure 5** plots this differential activity in a color code as a function of linker length across a physiologically relevant range of diffusion coefficients for receptors in the membrane ($D \in 10^{-11}$–10^{-9} cm^2/s). Calculations corresponding to the experimental values are marked as asterisks. White lines mark a shallow maximum in differential activity as a function of linker length. For the wild-type chimera (**Figure 5a**), C_3 formation is mainly diffusion limited, because the differential activity slightly increases with the linker length. For the K133A and R144A mutants (**Figure 5b,c**) the selectivity increases as expected, and C_3 formation is mainly reaction limited, meaning that shorter linkers enhance the selective potential of the chimera. This presents a practical advantage because shorter linkers are easier to synthesize and longer chimeras are prone to cleavage *in vivo*.

DISCUSSION

In this article, we present a theoretical model for chimeric ligands that allows us to study and optimize the selectivity of these types of constructs toward specific cell types. Some of these synthetic compounds have been developed as selective drugs,[1,6,7,10,12] allowing high activity at very low drug concentration and therefore, reducing side effects. Our model provides an *in silico* tool to design and test the efficiency of new synthetic compounds, as well as to optimize the existing ones by testing variants with improved selective potential.

When tailored to the specific case of IFN-EGF chimera using parameter values from ref. 14, our model quantitatively

reproduces the experimental results of the different chimeric constructs in terms of pathway activation (**Figure 2g–j**) and cytotoxic potential (**Figure 3g–j**).

We restricted our model to interactions occurring at the membrane level, calibrating downstream events using the experimental dose–response curve for the WT-IFN monomer (see Methods section). A detailed mathematical implementation of all downstream molecular interactions that ultimately trigger cytotoxic response will reduce the generality and simplicity of our model, so we consider this approach far from the scope of this contribution. In addition, internalization of C_3 is computed as the sum of the internalization constants of both C_1 and C_2 complexes, assuming they are independent. However, the proximity of both complexes when in C_3 configuration may induce dependence on the internalization of proximal active receptors linked to the same chimeric molecule.

Membrane diffusion of receptors and complexes is assumed uniform, so the well-known heterogeneity of the plasma membrane can impact diffusion of the components on the membrane. Moreover, the dimeric nature of both EGF and IFN complexes[18,19] is not considered for the sake of generality. Instead, a simpler 1:1 ligand–receptor interaction scheme is considered. Given the accuracy of the 1:1 model reproducing the experimental results (**Figure 3g–j**), we hypothesize that receptor homodimerization is not playing a significant role in the dynamics of the system. In addition, the model does not include synthesis and degradation of free receptors, assuming a dynamic equilibrium that keeps a constant concentration of free receptors in unstimulated conditions.

The model also assumes that both subunits of the chimeric ligand are bound to receptors of the same cell. However, it is known that chimeras can act in a paracrine manner, cross-linking receptors of nearby cells.[7] Finally, as previous studies suggested, EGF may have prosurvival signals, which are not considered in our model, and would counteract the cytotoxic activity of IFN.[20] A detailed model including the effect of EGF stimulation on cell proliferation at cell population level is in progress.

Despite all simplifications and assumptions, the model accurately reproduces the experimental data[14] for all compounds and both cell lines tested in a quantitative fashion. The present model provides a reliable and systematic tool to design chimeric ligands, allowing us to determine optimal configurations before synthesis and *in vivo* tests. All experimental data used here correspond to the IFN-EGF specific scenario, but the generality of the model ensures a straightforward customization to model other chimeric designs, using different combinations of activity and targeting elements to design selective compounds against specific cell types.

METHODS

The chimeric ligand–receptor system can be considered as an extension of the monovalent ligand–receptor interaction model,[21] assuming a sequential process with a single ligand able to interact with two different receptors following the scheme:

$$R_1 + L \underset{k^1_{off}}{\overset{k^1_{on}}{\rightleftharpoons}} C_1 \xrightarrow{k^1_e} \varnothing \tag{2}$$

$$R_2 + L \underset{k^2_{off}}{\overset{k^2_{on}}{\rightleftharpoons}} C_2 \xrightarrow{k^2_e} \varnothing \tag{3}$$

$$C_2 + R_1 \underset{k^1_u}{\overset{k^1_c}{\rightleftharpoons}} C_3 \xrightarrow{k^3_e} \varnothing \tag{4}$$

$$C_1 + R_2 \underset{k^2_u}{\overset{k^2_c}{\rightleftharpoons}} C_3 \xrightarrow{k^3_e} \varnothing \tag{5}$$

Eqs. 2 and 3 correspond to the individual binding of each subunit of the chimeric ligand L to its complementary receptor R_i to produce intermediate complexes C_i, where $i = 1, 2$ corresponds to each of the two targeted species (**Figure 1b,c**). These intermediate complexes are formed by one ligand subunit linked to its corresponding receptor whereas the other subunit is free and available to interact with its receptor via Eqs. 4 and 5 to generate the complex C_3 (**Figure 1d**). This second binding event is modulated by two factors: the two-dimensional diffusion of the receptors at the cell membrane and the increase in local concentration close to the cell membrane due to the first binding event.[22] The coupling rate constant (k^i_c) is calculated as:[21]

$$k^i_c = \left(\frac{1}{k^i_{\text{diff}}} + \frac{1}{k^i_{\text{on}'}} \right)^{-1} \tag{6}$$

The diffusive rate constant, k^i_{diff}, is calculated using the model for binding of cell surface molecules to receptors from ref. 21, where the intermediate complexes C_1 and C_2 are considered as numbers of membrane molecules:

$$k^i_{\text{diff}} = \frac{2\pi \cdot D}{A \cdot \log\left(b_i / a\right)}. \tag{7}$$

Here $D = D_1 + D_2$ is the sum of diffusion coefficients on the cell membrane for both receptor species, and A is the typical cell surface area for mammalian cells.[23] The parameter b_i represents the average half-distance between receptors R_i on the cell surface, and is estimated as:

$$b_i = \sqrt{A/(\pi R_i)} \tag{8}$$

The parameter a corresponds to the linker length between ligand subunits (Eq. 1). Normalization of k^i_{diff} by cell surface area A, Eq. 7, is necessary to express the diffusive rate constant in # molecules^{-1} min^{-1}, the same units as $k^i_{\text{on}'}$ below. We remark that all molecular species, R_i, C_i, are given in molecule numbers.

On the other hand, $k^i_{\text{on}'}$ is the effective affinity constant recalculated for a two-dimensional binding process[21] as follows:

$$k^i_{\text{on}'} = \frac{k^i_{\text{on}}}{N_{av} \cdot V_i} \tag{9}$$

where k^i_{on} is the corresponding three-dimensional rate affinity constant in Eqs. 2 and 3, N_{av} is Avogadro's number, and V_i is the effective reaction volume for the second binding event assumed as a spherical gasket above the cell surface where the free subunit gets distributed after the first binding event (see **Figure 1b,c**). This volume is calculated as $V_i = A \cdot (h_i + a)$, where h_i is the height of the extracellular domain of the receptor. Finally, the uncoupling rate k^i_u in Eqs. 4 and 5 can be written as:

$$k^i_u = \left(1 - \gamma_i\right) k^i_{\text{off}} \tag{10}$$

Where $\gamma_i \equiv k^i_{on'} / \left(k^i_{diff} + k^i_{on'}\right)$ the "capture probability" factor for receptor R_i, quantifying the probability that closely associated R_i and C_j (i, j = 1, 2) bind to become a C_3 complex.[21] k_e represents the internalization constant of each of the different complexes after ligand binding, assuming $k^3_e = k^1_e + k^2_e$, because internalization of the two complexes in C_3 is considered to be independent. The set of reactions 2–5 is translated into the following differential equations:

$$\frac{dR_1}{dt} = k^1_{off}C_1 + k^1_u C_3 - k^1_{on}R_1L - k^1_c R_1 C_2 \quad (11)$$

$$\frac{dR_2}{dt} = k^2_{off}C_2 + k^2_u C_3 - k^2_{on}R_2L - k^2_c R_2 C_1 \quad (12)$$

$$\frac{dC_1}{dt} = k^1_{on}R_1L + k^2_u C_3 - k^1_{off}C_1 - k^2_c C_1 R_2 - k^1_e C_1 \quad (13)$$

$$\frac{dC_2}{dt} = k^2_{on}R_2L + k^1_u C_3 - k^2_{off}C_2 - k^1_c C_2 R_1 - k^2_e C_2 \quad (14)$$

$$\frac{dC_3}{dt} = k^1_c R_1 C_2 + k^2_c R_2 C_1 - \left(k^1_u + k^2_u + k^3_e\right)C_3 \quad (15)$$

Note that, in contrast to other models of signal transduction by receptors,[24] we consider extracellular ligand concentration as a constant in our equations. This choice is justified in **Supplementary Text S1** online. To solve Eqs. 11–15 numerically, we developed an in-house MATLAB (MathWorks, Natick, MA) script (data not shown) using parameters for the chimeric system described.[14] The system is composed by EGF as targeting element linked to different mutants of the IFNα-2a as the activity element. The activity of the chimera corresponds to the cytotoxic effect of the IFNα-2a subunit. This chimeric design is assumed to guide the antiproliferative and apoptotic effect[25,26] of interferon toward cells overexpressing EGFR (upregulated in a number of tumoral cell lines).[27] Mutants of IFN exhibiting different affinity toward the IFNR were tested in Daudi cells engineered to overexpress EGFR cells (~300× the levels of the Daudi control cell line). For our study, we selected the wild-type form of IFNα-2a and the mutant variants, K133A and R144A,[28,29] with progressively less avidity toward IFNR. Parameter values are taken from experimental studies[28–35] and are listed in **Table 1**. Within our modeling scheme, variable R_1 represents EGFR, R_2, IFNR, C_1 and C_2 represent EGF and IFN complexes alone (i.e., complexes formed by the receptor and one end of the chimera, with the other chimera subunit free to bind to its corresponding receptor). C_3 corresponds to the chimera linked to EGFR and IFN at the same time. The initial number of EGFR and IFNR is written as R_1 (0) and R_2 (0), and the initial amount of complexes C_1, C_2, and C_3 is equal to 0 (see **Table 1**).

To compare the theoretical predictions with experimental measurements, we established a correlation between cytotoxic effect of IFN and number of IFN complexes predicted. To do so, we compute the maximum value of IFN ligand–receptor complexes (i.e., $C_2 + C_3$ in the model) for the range of ligand concentrations experimentally used, resulting in the sigmoidal curves in **Figure 6a,b**. The prediction of maximum IFN complexes for each ligand concentration is correlated with its cytotoxic effect using the experimental dose–response curves for the wild-type IFN monomer ligand in ref. 14 for Daudi and Daudi-EGFR cells (both are sigmoidal curves reinterpreted in **Figure 6c,d**). The resulting calibration curves for both cell types are shown in **Figure 6e,f**, correlating the number of IFN complexes predicted with its activity in terms of percentage of viable cells. The calibration curve is then used to calculate the predicted cytotoxicity for other mutants of IFN monomer and all chimeric variants.

Supplementary Figure S2 online plots the dose–response curves and EC_{50} values calculating the IFN activity as the sum of the number of IFN complexes formed before the maximum (to be compared with **Figure 3**, calculated using the maximum value of IFN complexes). Both methods produce equivalent results in complete agreement with the experimental data.

The quantitative fit of the EC_{50} values for the different IFN monomers with the experimental data provides a good validation of the model, because changes in the affinity of the IFN ligand fully correlate with the experimental phenotype.

Acknowledgments. This work has been supported by the Ministry of Science and Technology of Spain via a Ramon Y Cajal Fellowship (Ref. RYC-2010-07450) and a Project from Plan National framework (Ref. BFU2011-30303), and a Marie Curie International Reintegration Grant from the EU (Ref. 248346-NMSSBLS). V.D.M. acknowledges financial support to the Universidad Autónoma de Madrid for a FPI-UAM fellowship. We thank the Instituto Nicolás Cabrera of the Universidad Autónoma de Madrid (Spain) and P. Cironi for helpful insights at the start of the project.

Author Contributions. V.D-.M., R.G., and D.G.M. wrote the manuscript, designed the model, performed the research, and analyzed the data.

Conflict of interest. The authors declared no conflict of interest.

Study Highlights

WHAT IS THE CURRENT KNOWLEDGE ON THE TOPIC?

✓ Chimeric ligands achieved their selective potential by taking advantage of the differential expression of disease markers targeted by one subunit of the chimera, whereas the other subunit triggers repairing or cytotoxic responses.

WHAT QUESTION DID THIS STUDY ADDRESS?

✓ In this study, we present a mathematical model that allows *in silico* design and optimization of chimeric constructs in terms of their selectivity and efficiency.

WHAT THIS STUDY ADDS TO OUR KNOWLEDGE

✓ To our knowledge, our study provides the first mathematical framework that focuses on chimeric drugs, allowing us to understand the results of chimeras already tested experimentally, as well as to investigate new designs with improved selective potential.

HOW THIS MIGHT CHANGE CLINICAL PHARMACOLOGY AND THERAPEUTICS

✓ Our model constitutes a step forward toward a more systematic and reliable design of selective chimeric compounds before their *in vivo* implementation.

1. Kawakami, K., Aggarwal, B.B. & Puri, R.K. Cytotoxins and Immunotoxins for Cancer Therapy: Clinical Applications 1st edn., (CRC Press, Taylor & Francis, Boca Raton, FL, 2004).
2. Turturro, F. Denileukin diftitox: a biotherapeutic paradigm shift in the treatment of lymphoid-derived disorders. *Expert Rev. Anticancer Ther.* **7**, 11–17 (2007).
3. Kreitman, R.J. et al. Phase I trial of recombinant immunotoxin anti-Tac(Fv)-PE38 (LMB-2) in patients with hematologic malignancies. *J. Clin. Oncol.* **18**, 1622–1636 (2000).
4. Kreitman, R.J. et al. Phase I trial of recombinant immunotoxin RFB4(dsFv)-PE38 (BL22) in patients with B-cell malignancies. *J. Clin. Oncol.* **23**, 6719–6729 (2005).
5. Kioi, M., Husain, S.R., Croteau, D., Kunwar, S. & Puri, R.K. Convection-enhanced delivery of interleukin-13 receptor-directed cytotoxin for malignant glioma therapy. *Technol. Cancer Res. Treat.* **5**, 239–250 (2006).
6. Ruoslahti, E., Bhatia, S.N. & Sailor, M.J. Targeting of drugs and nanoparticles to tumors. *J. Cell Biol.* **188**, 759–768 (2010).
7. Bremer, E. et al. Simultaneous inhibition of epidermal growth factor receptor (EGFR) signaling and enhanced activation of tumor necrosis factor-related apoptosis-inducing ligand (TRAIL) receptor-mediated apoptosis induction by an scFv:sTRAIL fusion protein with specificity for human EGFR. *J. Biol. Chem.* **280**, 10025–10033 (2005).
8. Bremer, E. et al. Target cell-restricted apoptosis induction of acute leukemic T cells by a recombinant tumor necrosis factor-related apoptosis-inducing ligand fusion protein with specificity for human CD7. *Cancer Res.* **65**, 3380–3388 (2005).
9. Stieglmaier, J. et al. Selective induction of apoptosis in leukemic B-lymphoid cells by a CD19-specific TRAIL fusion protein. *Cancer Immunol. Immunother.* **57**, 233–246 (2008).
10. Bremer, E., ten Cate, B., Samplonius, D.F., de Leij, L.F. & Helfrich, W. CD7-restricted activation of Fas-mediated apoptosis: a novel therapeutic approach for acute T-cell leukemia. *Blood* **107**, 2863–2870 (2006).
11. Bremer, E. et al. Superior activity of fusion protein scFvRit:sFasL over cotreatment with rituximab and Fas agonists. *Cancer Res.* **68**, 597–604 (2008).
12. Xuan, C., Steward, K.K., Timmerman, J.M. & Morrison, S.L. Targeted delivery of interferon-alpha via fusion to anti-CD20 results in potent antitumor activity against B-cell lymphoma. *Blood* **115**, 2864–2871 (2010).
13. Zhang, B., Gao, B., Dong, S., Zhang, Y. & Wu, Y. Anti-tumor efficacy and pre-clinical immunogenicity of IFNa2a-NGR. *Regul. Toxicol. Pharmacol.* **60**, 73–78 (2011).
14. Cironi, P., Swinburne, I.A. & Silver, P.A. Enhancement of cell type specificity by quantitative modulation of a chimeric ligand. *J. Biol. Chem.* **283**, 8469–8476 (2008).
15. Hannigan, G. & Williams, B.R. Transcriptional regulation of interferon-responsive genes is closely linked to interferon receptor occupancy. *EMBO J.* **5**, 1607–1613 (1986).
16. Spencer, S.L. & Sorger, P.K. Measuring and modeling apoptosis in single cells. *Cell* **144**, 926–939 (2011).
17. O'Brien, E.P., Morrison, G., Brooks, B.R. & Thirumalai, D. How accurate are polymer models in the analysis of Förster resonance energy transfer experiments on proteins? *J. Chem. Phys.* **130**, 124903 (2009).
18. Yarden, Y. & Schlessinger, J. Self-phosphorylation of epidermal growth factor receptor: evidence for a model of intermolecular allosteric activation. *Biochemistry* **26**, 1434–1442 (1987).
19. Uze, G., Lutfalla, G. & Mogensen, K.E. In Guidebook to Cytokines and Their Receptors (ed. Nicola, N.A.), 115–118 (Oxford UniversityPress, Oxford; New York; Tokyo, 1994).
20. Caraglia, M. et al. Interferon-alpha induces apoptosis in human KB cells through a stress-dependent mitogen activated protein kinase pathway that is antagonized by epidermal growth factor. *Cell Death Differ.* **6**, 773–780 (1999).
21. Lauffenburger, D.A. & Linderman, J. Receptors: Models for Binding, Trafficking, and Signaling 130–180 (Oxford University Press, Huntington Beach, CA, 1996).
22. Adam, G. & Delbruck, M. Structural Chemistry in Molecular Biology 198–215 (Freeman, San Francisco, CA, 1968).
23. Zhao, L., Kroenke, C.D., Song, J., Piwnica-Worms, D., Ackerman, J.J. & Neil, J.J. Intracellular water-specific MR of microbead-adherent cells: the HeLa cell intracellular water exchange lifetime. *NMR Biomed.* **21**, 159–164 (2008).
24. Shankaran, H., Resat, H. & Wiley, H.S. Cell surface receptors for signal transduction and ligand transport: a design principles study. *PLoS Comput. Biol.* **3**, e101 (2007).
25. Darnell, J.E. Jr, Kerr, I.M. & Stark, G.R. Jak-STAT pathways and transcriptional activation in response to IFNs and other extracellular signaling proteins. *Science* **264**, 1415–1421 (1994).
26. Pestka, S., Langer, J.A., Zoon, K.C. & Samuel, C.E. Interferons and their actions. *Annu. Rev. Biochem.* **56**, 727–777 (1987).
27. Arteaga, C.L. The epidermal growth factor receptor: from mutant oncogene in nonhuman cancers to therapeutic target in human neoplasia. *J. Clin. Oncol.* **19**, 32S–40S (2001).
28. Dunne, S.L., Bajzer, Z. & Vuk-Pavlovic, S. Kinetics of receptor-mediated uptake and processing of interferon-alpha 2a and tumor necrosis factor-alpha by human tumor cells. *Growth Factors* **2**, 167–177 (1990).
29. Piehler, J., Roisman, L.C. & Schreiber, G. New structural and functional aspects of the type I interferon-receptor interaction revealed by comprehensive mutational analysis of the binding interface. *J. Biol. Chem.* **275**, 40425–40433 (2000).
30. Hendriks, B.S., Orr, G., Wells, A., Wiley, H.S. & Lauffenburger, D.A. Parsing ERK activation reveals quantitatively equivalent contributions from epidermal growth factor receptor and HER2 in human mammary epithelial cells. *J. Biol. Chem.* **280**, 6157–6169 (2005).
31. Resat, H., Ewald, J.A., Dixon, D.A. & Wiley, H.S. An integrated model of epidermal growth factor receptor trafficking and signal transduction. *Biophys. J.* **85**, 730–743 (2003).
32. Ogiso, H. et al. Crystal structure of the complex of human epidermal growth factor and receptor extracellular domains. *Cell* **110**, 775–787 (2002).
33. Garrett, T.P. et al. Crystal structure of a truncated epidermal growth factor receptor extracellular domain bound to transforming growth factor alpha. *Cell* **110**, 763–773 (2002).
34. Xiao, Z., Zhang, W., Yang, Y., Xu, L. & Fang, X. Single-molecule diffusion study of activated EGFR implicates its endocytic pathway. *Biochem. Biophys. Res. Commun.* **369**, 730–734 (2008).
35. Roisman, L.C., Piehler, J., Trosset, J.Y., Scheraga, H.A. & Schreiber, G. Structure of the interferon-receptor complex determined by distance constraints from double-mutant cycles and flexible docking. *Proc. Natl. Acad. Sci. U.S.A.* **98**, 13231–13236 (2001).

Supplementary Information accompanies this paper on the *Pharmacometrics & Systems Pharmacology* website (http://www.nature.com/psp)

3.3 Synergistic Interaction between Selective Drugs in Cell Populations Models

Background, Introduction and Author Contribution

This publication analyzes the effect of combinatorial treatments with chimeric ligands from a theoretical perspective to explore the design of better treatments with reduced side effect and enhanced efficiency. To do that, the author of this thesis developed a population model where two sets of cells expressing different levels of a target molecule are treated with different concentrations of two chimeric drugs simultaneously. inheritance The model used by the author is an extension of the ligand-receptor model presented in the previous section, but it was rewritten to take into account the simultaneous interaction of two chimeric ligands. As in the case of the previous contribution, the model was calibrated with experimental dose-response curves in [77] and informed with experimental parameter values. Finally, it was numerically solved for different ligand combinations — in monomeric and chimeric configuration— and concentrations in proliferating populations of cells. Unlike the previous publication, this model permits to add cell-to-cell receptors variability to the system and also phenotypic inheritance of the amount of receptors (such us in diseases caused by genetic mutations). The model predicts that drug combination of selective drugs can selectively affect a given cell population at reduced concentrations compared to single drug treatment, that is, chimeric ligands are synergistic in terms of their selective potential.

PLOS | ONE

RESEARCH ARTICLE

Synergistic Interaction between Selective Drugs in Cell Populations Models

Victoria Doldán-Martelli, David G. Míguez*

Departamento de Física de la Materia Condensada, Condensed Matter Physics Center (IFIMAC) and Instituto Nicolás Cabrera, Facultad de Ciencias, Universidad Autónoma de Madrid, Madrid, Spain

* david.gomez.miguez@uam.es

OPEN ACCESS

Citation: Doldán-Martelli V, Míguez DG (2015) Synergistic Interaction between Selective Drugs in Cell Populations Models. PLoS ONE 10(2): e0117558. doi:10.1371/journal.pone.0117558

Academic Editor: Jordi Garcia-Ojalvo, Universitat Pompeu Fabra, SPAIN

Received: August 8, 2014

Accepted: December 29, 2014

Published: February 11, 2015

Data Availability Statement: All relevant data are within the paper and its Supporting Information files.

Funding: The authors thank the Instituto Nicolás Cabrera of the Universidad Autónoma de Madrid (Spain). This work has been supported by the Ministry of Science and Technology of Spain via a Ramón Y Cajal Fellowship (Ref. RYC-2010-07450) and a Project from Plan Nacional framework (Ref. BFU2011-30303). VDM acknowledges financial support from the Ministerio de Educación y Ciencia of Spain. The funders had no role in study design, data collection and analysis, decision to publish, or preparation of the manuscript.

Abstract

The design of selective drugs and combinatorial drug treatments are two of the main focuses in modern pharmacology. In this study we use a mathematical model of chimeric ligand-receptor interaction to show that the combination of selective drugs is synergistic in nature, providing a way to gain optimal selective potential at reduced doses compared to the same drugs when applied individually. We use a cell population model of proliferating cells expressing two different amounts of a target protein to show that both selectivity and synergism are robust against variability and heritability in the cell population. The reduction in the total drug administered due to the synergistic performance of the selective drugs can potentially result in reduced toxicity and off-target interactions, providing a mechanism to improve the treatment of cell-based diseases caused by aberrant gene overexpression, such as cancer and diabetes.

Introduction

The field of modern pharmacology aims to develop novel approaches to improve disease treatment, reduce side effects, minimize costs and enhance the efficiency of targeted therapy. These major challenges require a rational design of novel drugs and improved treatment strategies. In this direction, two of the main approaches currently being pursued involve the development of selective drugs and the design of optimal drug combination therapies.

Drug selectivity can be defined as the ability of a compound to exhibit enhanced effect towards a particular cell population in preference to others. To achieve that, a drug must be designed to target specific cellular components that are differentially expressed in two cell types. In the context of diseases that involve cells overexpressing certain genes, such as oncogenes in cancer [1], this targeting potential can be used to selectively affect only cells with increased levels of the overexpressed protein. Once selectivity is achieved, the drug can be designed to either restore normal cellular function when possible, or to trigger apoptosis of the unhealthy cells without harming the healthy cellular environment. In general, selective drugs are composed of a targeting element (TE) that recognizes and binds to the target protein, and an activity element (AE) that is directed towards the selectively targeted cells. Many of these synthetic chimeric

Competing Interests: The authors have declared that no competing interests exist.

compounds have shown good *in vivo* performance, and several of them have been approved by the FDA or currently undergoing clinical trials [2–15].

On the other hand, drug combination therapies have shown enhanced efficiency compared to individual drug therapy in many diseases [16], including cancer [17, 18] and HIV's [19]. The interaction between drugs in multicomponent therapies is a complex and multi-scale problem [20] that requires full characterization of the direct and indirect molecular aspects of the interaction, which are often unknown. Due to this, experimental studies and discoveries of successful drug combinations are often based on empirical intuition and trial-and-error approaches. In general, drug interactions can be classified based on their effect when combined, compared to their effect when applied alone. Drugs that do not interact with each other, or are mutually exclusive by competing for the same target are considered as additive [22]. This basically means that the lower concentration which produces a certain effect corresponds to the most potent drug, and there is no gain due to the combination of the two drugs. On the other hand, antagonism occurs when one of the drugs mitigates or counteracts the action of the other, i.e, the combination is always less effective than the single agents at the same concentration. Finally, synergism occurs when the combination of both drugs is more effective than each agent separately at the same total concentration, i.e., one of the agents enhances the actions of the other [21]. This can occur either via direct interaction, i.e, one drug increases the bioavailability of the other, or indirectly, i.e, the two drugs cooperate on targets on the same or different pathways involved in the same process [23]. Thus, the total concentration of drug administered to achieve a certain effect is reduced, which potentially also reduces side effects, drug resistance and undesired off-target interactions.

In the context of selective drugs, synergism and antagonism can be also defined in terms of the enhanced or reduced selective potential of the two drugs when combined [24], i.e, their ability to target selectively a specific cell population, compared to their selective potential when applied individually. In this way, two drugs are synergistic if their combination is more selective than the two drugs acting alone at the same total concentration. Here, we explore the mechanism of interaction between selective drugs in combination from a theoretical perspective. To do that, we develop a population model where two sets of cells expressing different levels of a target molecule are treated with different concentrations of two drugs simultaneously. In principle, these two drugs can be monomeric non-selective ligands (i.e., they do not differentiate between healthy and unhealthy cells), or chimeric ligands, composed of an AE and linked to a TE, allowing them to selectively target unhealthy cells, leaving the healthy environment undamaged.

Two different approaches are taken into account: first, we analyze the effect of combinations of two different chimeric ligands when applied simultaneously to an heterogeneous population of cells; next, we combine the effect of individual chimeric drugs based on the Loewe additivity model [22]. Both models predict that drug combination of selective drugs is synergistic in terms of their selective potential. Finally, we introduce phenotypic inheritance in the cell population to show that both selectivity and synergism also occur in a context where the amount of target proteins of the daughter cells depends on the mother cell, such as in diseases caused by mutations in specific genes. Our results show that the concentration to obtain a desired selectivity can be minimized by simultaneous treatment of selective drugs.

Models

To analyze the effect of selective drug combinations in a multicellular approach, we develop a mathematical framework where we allow two asynchronous populations of cells with two distinct average number of target molecules to proliferate for a given time. Cells are treated with

different concentrations of monomers and chimeric drugs alone or in combination, to then monitor and compare the dynamics of proliferation of the two cell populations. The dynamics of the effect of chimeric drugs at the cellular level is calculated based on a chemical kinetics model for the ligand-receptor interaction [25]. The model used is an extension of our previous contribution to the study of the dynamics of chimeric ligands, where we develop a mathematical framework to predict the selective potential of chimeric drugs, based on the affinity of both AE and TE subunits of the ligand towards their targets (activity element receptor, AER, and targeting element receptor, TER, respectively), the concentration of the target molecules and the linker length between AE and TE in the chimera [25]. The model is rewritten to take into account the simultaneous interaction of two chimeric ligands, resulting in the following set of interactions:

$$R_i + L_j \underset{k^{off}_{i,j}}{\overset{k^{on}_{i,j}}{\rightleftharpoons}} C_{i,j} \tag{1}$$

$$C_{1,j} + R_2 \underset{k^{u}_{2,j}}{\overset{k^{c}_{2,j}}{\rightleftharpoons}} C_{3,j} \tag{2}$$

$$C_{2,j} + R_1 \underset{k^{u}_{1,j}}{\overset{k^{c}_{1,j}}{\rightleftharpoons}} C_{3,j} \tag{3}$$

$$C_{i,j}, C_{3,j} \xrightarrow{k^{e}_{i,j}, k^{e}_{3,j}} \nexists \tag{4}$$

where R_i corresponds to the i receptor (i = 1,2) and L_j corresponds to each of the two different ligands (j = 1,2) used in the combined treatment. Each ligand L_j is composed of a AE and TE, and it can bind to R_1 or R_2 via reaction 1 to give an intermediate complex $C_{i,j}$ (Fig. 1A–C). These intermediate complexes facilitate reactions 2 and 3 by originating a local concentration of the free subunit of the ligand L_j in the vicinity of the complementary receptor, to generate the complex $C_{3,j}$ (Fig. 1D). The coupling ($k^{c}_{i,j}$) rate constants in reaction 2 and 3 are calculated as follows:

$$k^{c}_{i,j} = \left(\frac{1}{k^{diff}_{i}} + \frac{1}{k^{on'}_{i,j}} \right)^{-1} \tag{5}$$

where the diffusive rate constant k^{diff}_{i} is modulated by the diffusion D_i of the receptors R_i at the membrane as [26, 27]:

$$k^{diff}_{i} = \frac{2\pi \left(\sum D_i \right)}{A \cdot \log \left(b_i / a \right)} \tag{6}$$

being A the average cell surface area, $b_i = \sqrt{A/(\pi R_i)}$ corresponds to half the average distance between R_1 and R_2, and a is the linker length. Effective affinity and dissociation rates for the reactions that take place at the membrane are calculated as [26]:

$$k^{on'}_{i,j} = \frac{k^{on}_{i,j}}{N_{av} \cdot V_i} \tag{7}$$

$$k^{u}_{i,j} = (1 - \gamma_{i,j}) k^{off}_{i,j} \tag{8}$$

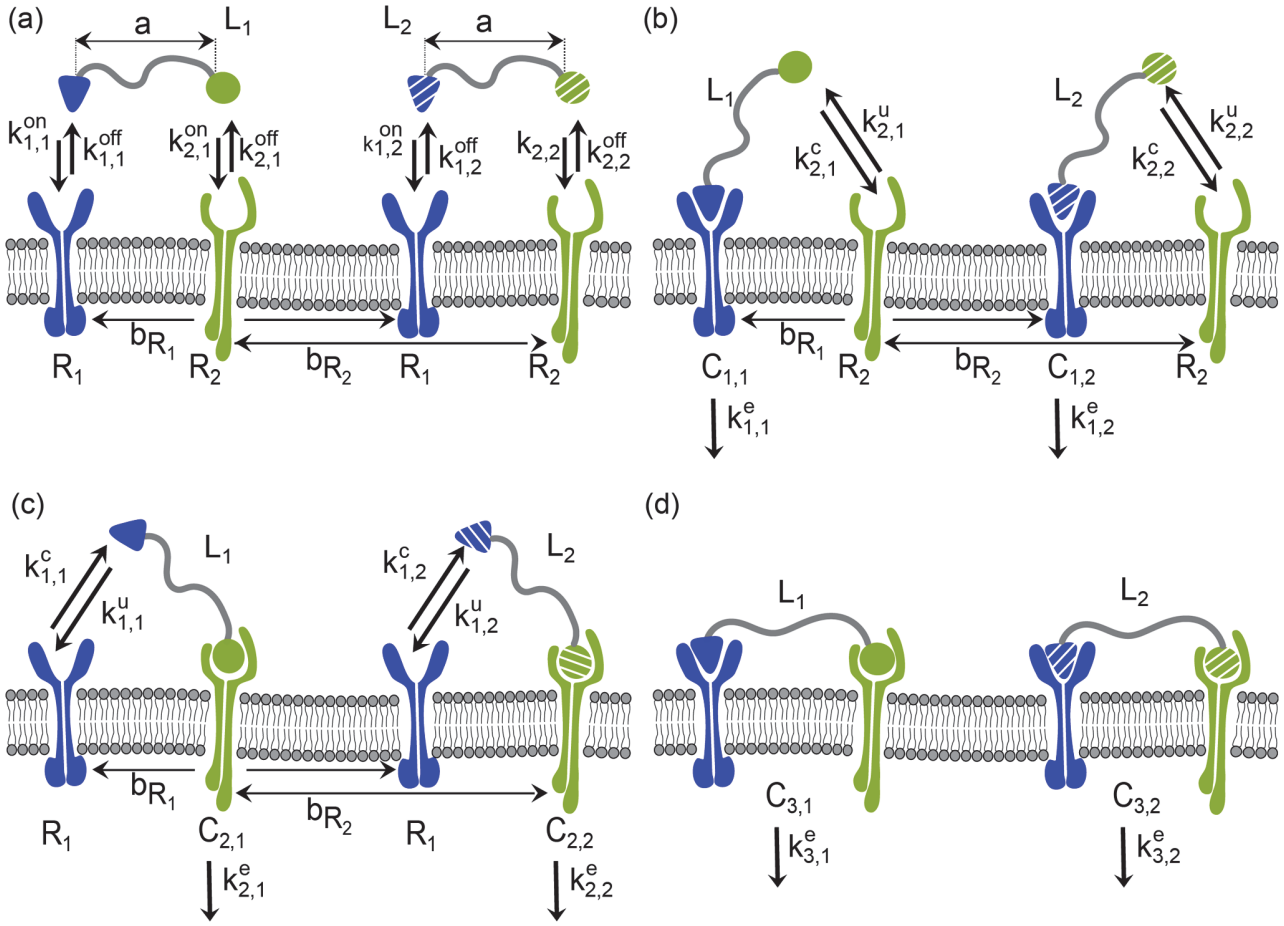

Fig 1. Scheme of the model for the simultaneous interaction of two chimeric ligands with their corresponding receptors. (A) Each one of the ligands L_j consists of two subunits which can interact with their corresponding receptors to form intermediate complexes $C_{i,j}$. (B,C) This first binding event induces an increase in the local concentration of the free subunit of the ligand facilitating the interaction with its corresponding receptor to form complex $C_{3,j}$ (D).

doi:10.1371/journal.pone.0117558.g001

where N_{av} is Avogadro's number and $V_i = A \cdot (h_i + a)$ is the effective reaction volume for the second binding event, assumed as a spherical gasket above the cell surface where the free subunit gets distributed after the first binding event (see [25]), being h_i the height of R_i above the cell surface. $\gamma_{i,j} = k^{on\prime}_{i,j}/(k^{diff}_i + k^{on\prime}_{i,j})$ corresponds to the capture probability factor for receptor R_i and ligand L_j, explained in detail in [26].

For a given constant concentration of both ligands L_j, the equations are solved for each individual cell in the population, based on its amount of R_1 and R_2 receptors, identified as TER and AER, respectively. The maximum value of AER-AE complexes formed in each cell is then correlated with the physiological response produced by the AE using experimental dose-response curves (this correlation is a multi-step process explained in detail in Ref. [25]). Typical dose-response curves are often fitted to a four-parameter sigmoidal [25], such as:

$$R(L) = \frac{A - D}{1 + (L/EC_{50})^B} + D \tag{9}$$

where the physiological response $R(L)$ for a given drug concentration L is characterized by its maximal D and minimal A asymptotes, B is the slope parameter of the curve, and EC_{50} is the

half-maximal effective concentration of the ligand, that is, the inflection point of the curve. S1A Fig. shows a schematic representation of the workflow used to solve the model equations and obtain the dynamics of growth of the heterogeneous cell population.

As a numerical solution, the model is informed with data from a synthetically designed chimeric ligand composed of the Epidermal Growth Factor (EGF) as TE and different mutants of Interferon alfa-2a (IFNα-2a) as AE [15]. Thus, the apoptotic effect triggered by IFNα-2a stimulation is directed towards cells overexpressing the Epidermal Growth Factor Receptor (EGFR). The physiological response of the cells to the treatment corresponds to the apoptotic effect induced by IFNα-2a, measured experimentally as the percentage of surviving cells after 60 hours of treatment.

Since EGFR is an oncogene overexpressed in a number of tumor cells [28], this chimera can be potentially used to selectively target cancer cells without affecting the healthy surrounding tissue. Different mutants of the IFNα-2a molecule are tested as monomers (M_{wt}, M_1, M_2 and M_3), and as AE's in chimeric configuration, identified here as Ch_{wt} for the chimera composed of the wild type version of the IFNα-2a linked to EGF, and Ch_1, Ch_2 for the experimentally available mutants of IFNα-2a with reduced affinity towards the IFNα-2a receptor linked to the targeting element EGF [15]. Other potential chimeras composed of EGF linked to IFNα-2a mutants with decreasing affinity towards the AER combined with EGF, named Ch_3 and Ch_4, are included in the analysis (Table 1 shows the dissociation constants for each IFN monomer).

To mimic the experimental conditions, cells in the population are allowed to proliferate for 60 hours in the presence of the drug treatment, and the physiological response of each cell to the treatment depends on the amount and efficiency of each ligand, the amount of TER and AER receptors expressed, and the exposure time to treatment. Given that the physiological response of the cells is apoptosis, we set the decision between survival or death for each cell in the population as follows: for a given physiological response ($0 < R(L) < 1$), the probability of undergoing apoptosis at every time point is computed as $\theta = (1 - R(L))^{\Delta t/T}$, being T the total length of the experiment and Δt the time step in the simulation. Then, a random number ($0 < \gamma < 1$) from a uniform distribution is assigned for each cell in the population and

Table 1. Parameters used in the population model. Values of IFNα-2a (AE) dissociation rates (k_D), corresponding to IFNα-2a-IFNR wild type and mutants of IFNα-2a, from recent publications [15, 39] and theoretical ligands (M_3 and M_3). Mean values of EGF and IFN receptors expressed by Daudi and Daudi-EGFR cells, extracted from [15].

Parameter	Value	Units	Reference
k_D M_{wt}	3	*nM*	Ref. [39]
k_D M_1—K133A	26	*nM*	Ref. [39]
k_D M_2—R144A	120	*nM*	Ref. [39]
k_D M_3	240	*nM*	theoretical
k_D M_4	480	*nM*	theoretical
k_D *EGF*	2.47	*nM*	theoretical
$[EGFR]_{healthy}$	22	*molecules*	Ref. [15]
$[IFNR]_{healthy}$	2800	*molecules*	Ref. [15]
$[EGFR]_{unhealthy}$	5640	*molecules*	Ref. [15]
$[IFNR]_{unhealthy}$	3600	*molecules*	Ref. [15]
# of cells at t = 0	100	*cells*	theoretical
Average cell cycle	27.5	*hours*	Ref. [29, 40]
Total time	60	*hours*	theoretical

doi:10.1371/journal.pone.0117558.t001

compared to the value of θ at every time step. If $\gamma \geq \theta$, the cell survives. On the contrary, if $\gamma < \theta$, then the cell dies and it is no longer considered in the simulation.

A cell division occurs when the age of a given cell reaches the numerical value for the cell cycle length assigned to that particular cell. This value is obtained from a gamma distribution with mean m = 27.5 hours [29, 30] and standard deviation of 2 hours. The amount of surface receptors are also gamma distributed [31], with a mean value obtained from experimental data [15] (see Table 1) and a coefficient of variation of 0.3, to mimic cell-to-cell variability in both populations. Mean values of the final cell numbers are obtained from 10 independent runs of the model. Numerical solution of the model equations and other calculations are performed using a in-house Matlab script (code available upon request).

Results

Selectivity of chimeric drugs versus monomers in a cell population

The model described above is used to illustrate the effect of monomers versus chimeric ligands in a heterogeneous cell population. Fig. 2 illustrates the dynamics of growth of healthy (blue curve) and unhealthy (red curve) cell populations under nonselective monomers versus selective chimeric ligand treatment. To characterize and compare its selective potential, we define a threshold based on the amount of cells of both populations that remain after 60 hours of treatment (i.e., the duration of the experiments in [15], where the dose-response curves and other experimental data are obtained). Thus, a given treatment is considered as efficient when the number of unhealthy cells does not increase, while the population of healthy cells grows to at least 80% of its potential size. These two threshold values are marked in Fig. 2A–I as dashed red and blue horizontal lines for the unhealthy and healthy cells, respectively. These threshold values will be used to categorize the selective potential of a given treatment.

Low concentrations of M_{wt} are harmless to both cell populations, which can grow exponentially (Fig. 2A). Intermediate concentrations (Fig. 2B) have a much stronger effect in healthy cells than in unhealthy cells, due to higher resistance to IFNα-2a treatment in the unhealthy cell population (reported experimentally in [15], where authors hypothesized that this effect is mainly due to the anti-apoptotic potential of the EGFR overexpression [32] that may counteract the effect of IFNα-2a stimulation). Higher concentrations of the monomer are able to reduce the number of unhealthy cells in the system, but affecting the healthy population even more (Fig. 2C). This type of response is similar for all mutants of the monomer of IFNα-2a, as shown in the S2 Fig.

On the other hand, chimeric ligands show enhanced effect in cells overexpressing EGFR. The dynamics of Ch_{wt} ligand treatment, composed of EGF linked to wild type IFNα-2a, is shown in Fig. 2D–F. Low concentrations do not affect the growth rate of both cell populations. Intermediate and high values of chimeric ligand affect both healthy and unhealthy cells, reducing both cell populations simultaneously.

Optimal treatment can be achieved by the chimeric ligand composed of EGF linked to a mutant of IFNα-2a with reduced affinity towards the IFN receptor, as shown in Fig. 2G–I. Low concentrations of ligand Ch_2 do not affect any of the populations, while intermediate values do allow the healthy cells to proliferate and prevent the unhealthy cell population to expand in size. Again, high concentrations of the ligand start to affect the healthy population that cannot grow above its 80% potential size. Dynamics for other chimeric ligands are plotted in S3 Fig.

Fig. 2J–M plots the amount of TER and AER for each cell of the healthy (blue) and unhealthy (red) population before treatment (Fig. 2J) and after 60 hours of treatment with intermediate concentrations of M_{wt} (Fig. 2K), Ch_{wt} (Fig. 2L) and Ch_2 (Fig. 2M). Interestingly, despite the fact that the apoptotic potential of the monomers and chimeras directly depends on the amount of

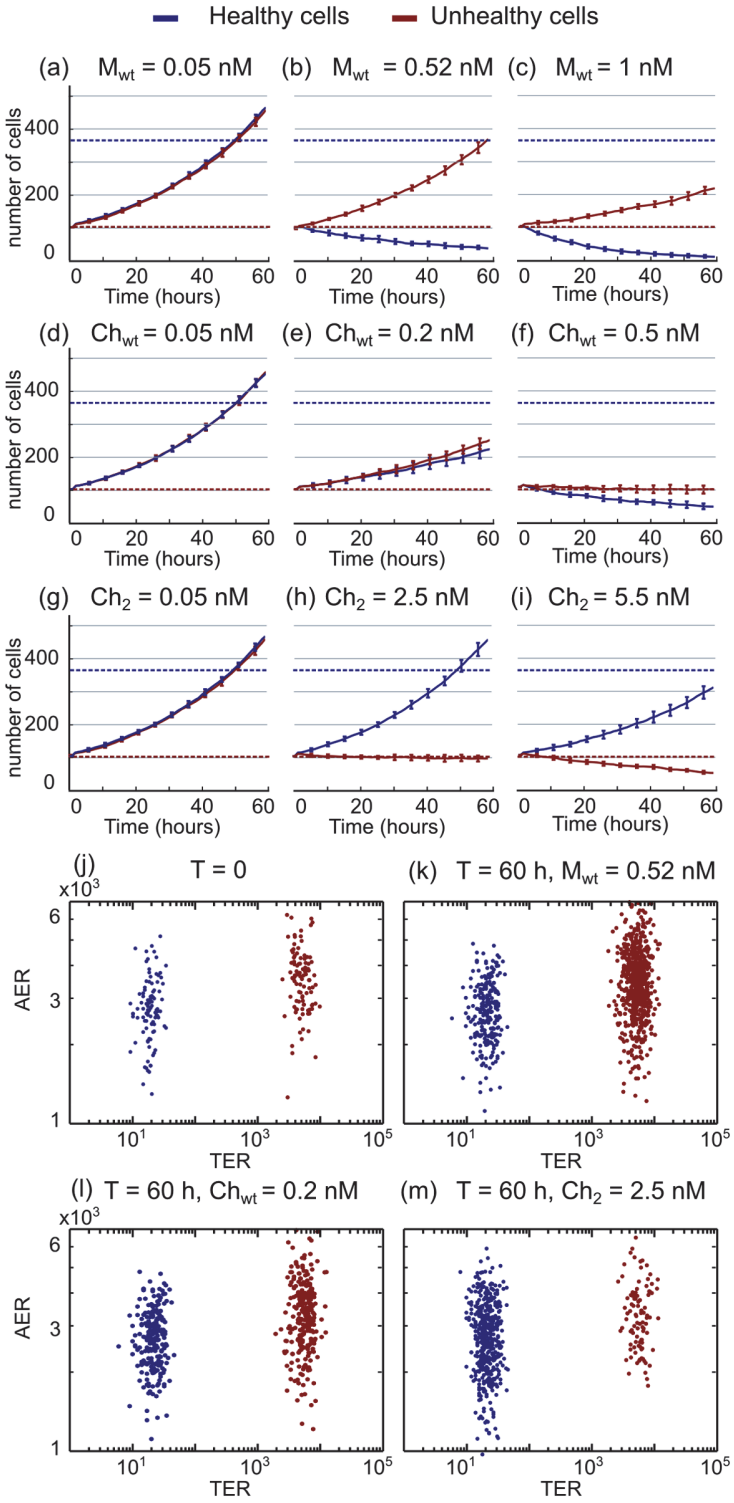

Fig 2. Dynamics of the cell populations after individual drug treatment. (A–C) Numerical solution of the model equations showing the time evolution of healthy (blue line) and unhealthy (red line) cells after treatment with low, intermediate and high concentrations of the M_{wt} monomer. (D–F) Time evolution after treatment with different concentrations of Ch_{wt}. (G–I) Time evolution after treatment with different concentrations of Ch_2, which at intermediate values is able to achieve the threshold of 80% survival of healthy

cells, while the unhealthy cells are maintained. Solid line and error bars correspond to the average and standard deviation of 10 independent runs of the model. (J–M) Distribution of the AER and TER receptors for the two cell populations at (J) initial conditions, and after 60 hours of treatment with (K) M_{wt} = 0.52 nM, (E) Ch_{wt} = 0.2 nM and (M) Ch_2 = 2.5 nM (i.e, same concentrations of Fig. 2B,E,H, respectively) Each dot corresponds to a cell in the population. Notice that M_{wt} treatment affects mainly the unhealthy cells (blue line, B,C), while Ch_2 treatment shows a greater effect on the unhealthy population (red line, H–I).

doi:10.1371/journal.pone.0117558.g002

AER expressed by each individual cell, the model predicts that a number of cells with high values of AER does not undergo apoptosis after 60 hours of treatment. This is due to the fact that the physiological response of a given cell depends on the time that it has been under treatment and, since cells are continuously being born during the simulation, at t = 60 hours some recently born cells may not have been enough time under the influence of the drug to trigger apoptosis.

The above data evidences that selectivity in terms of the threshold of 80% can only be achieved using low affinity mutants of the AE subunit of the chimera, which are only efficient at very high concentrations of ligand (around 2 nM concentration for Ch_2). This concentration representes a 4X increase compared to the concentration for $Ch_{wt} = 0.5nM$, which is the minimum concentration required to prevent the expansion of the unhealthy cell population at the expense of affecting strongly the healthy cells. This increase is also reported experimentally in [15], where the minimum concentration of Ch_2 to prevent the unhealthy cell population to expand leaving the 80% of the healthy surrounding undamaged is 1.5nM, 3 times higher than the value of 0.5nM of Ch_{wt} that prevents the growth of the unhealthy cell population. Unfortunately, this higher doses of drug required to achieve selectivity can result in the emergence of other potential undesired effects, such as toxicity, or increased off-target interactions [33]. Therefore, strategies to reduce the total drug concentration for a given selective effect are relevant. In the next section, we show how combinations of selective chimeric ligands can reduce the concentration of total drug administered maintaining the selective potential.

Synergistic interaction of selective chimeric drugs

Mutant monomers of the same molecule act against the same target, therefore they behave as mutually exclusive and their interaction when combined is additive by definition. In this way, the lowest concentration to obtain a given effect always corresponds to the monomer with stronger binding affinity towards its receptor. Fig. 3A–C corresponds to simultaneous treatment of a fixed concentration of M_{wt} = 0.5nM with the minimal concentration of the mutants of IFNα-2a able to affect at least 20% of the unhealthy cells. According to their additive interaction, none of the potential combinations tested allows us to reduce the total drug concentration of IFNα-2a administered. In addition, none of the multiple combinations tested is able to mitigate the strong effect that the monomers exhibit towards the healthy cell population, as illustrated also in the next section.

Multi-drug treatment using selective drugs is shown by Fig. 3D–I, where we plot the dynamics of the two cell populations at the minimal concentration of total drug required to achieve the selectivity threshold for different combinations of the chimeras. Combinations of the poorly selective Ch_{wt} with chimeras Ch_2, Ch_3 and Ch_4 are able to mitigate the expansion of the unhealthy cell population while meeting the 80% survival threshold of the healthy cells (Fig. 3D–F). The threshold is also achieved when combining the rest of the chimeras with Ch_1, as shown in Fig. 3G–I.

Bars in each panel represent the minimal concentration of total drug to achieve the threshold of selectivity for each combination of ligands, compared to the same ligands as single treatment. We observe a slight reduction in the total concentration used for the combinatorial

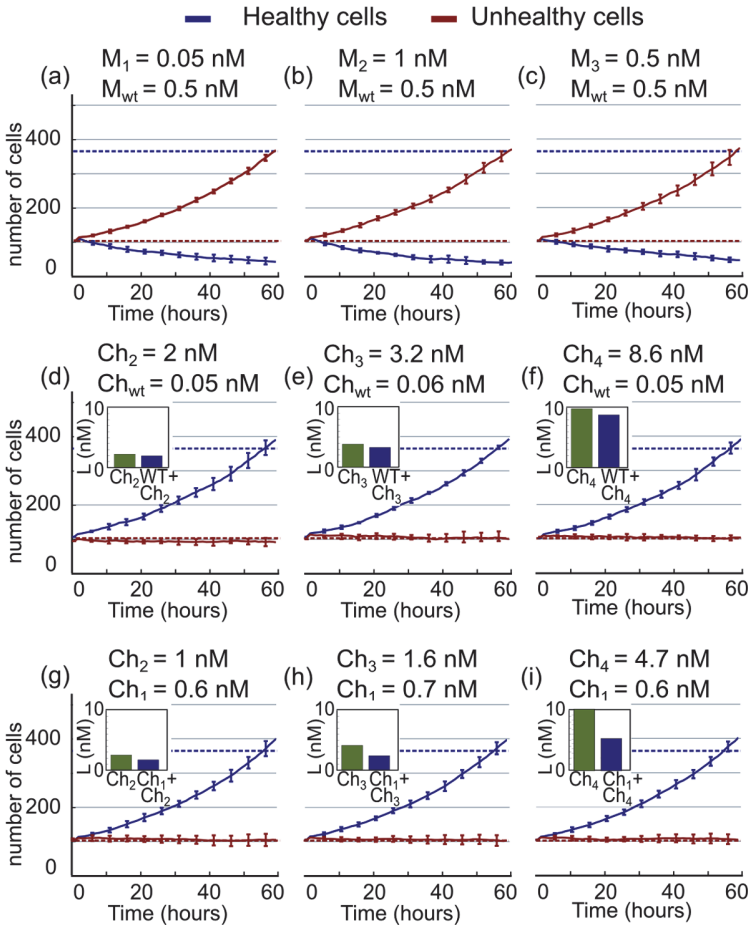

Fig 3. Synergistic performance of selective ligands. (A–C) Numerical solution of the model equations showing the time evolution of healthy (blue line) and unhealthy (red line) cells after treatment with different combinations of monomers, at the minimal concentration required to affect 20% of the unhealthy cell population. (D–F) Time evolution of different combinations of Ch_{wt} with other chimeric ligands at the minimal concentration required to achieve the threshold for selectivity. (G–I) Time evolution of different combinations of Ch_1 with other chimeric ligands at the minimal concentration required to achieve the threshold for selectivity. Bars in each figure correspond to the minimal concentration for the threshold for single treatment and dual treatment with the chimeras used in each panel.

doi:10.1371/journal.pone.0117558.g003

treatment compared to the individual treatment (values for the percentage of each reduction in the total concentration at threshold are listed in Table 2). Overall, the gain in performance of the dual treatment is more evident when combining a poorly selective ligand as Ch_1 with a low affinity but highly selective chimera, such as Ch_3. In this situation, we can achieve the threshold of optimal selectivity with a 50% reduction in the total drug concentration administered, compared to the concentration of Ch_3 as individual treatment.

The effect of combinatorial treatment can be estimated based on the effect of single treatment strategies

Detailed analysis of the drug interaction for each combination of two given ligands, as performed in the previous section, requires extensive computational resources. To overcome this, we use an additional approach to calculate the effect of a combination of drugs based on their

Table 2. Reduction in concentration at threshold for optimal selectivity. Percentage of reduction of total drug concentration of combinatorial treatment versus single drug treatment for different selective drug combinations.

Single drug	Drug combination	Reduction percentage
Ch_1 = -	Ch_{wt} + Ch_1 = -	-%
Ch_2 = 2.2	Ch_{wt} + Ch_2 = 2.0	7%
Ch_3 = 4.2	Ch_{wt} + Ch_3 = 3.3	22%
Ch_4 = 10.1	Ch_{wt} + Ch_4 = 8.6	14%
Ch_2 = 2.4	Ch_1 + Ch_2 = 1.6	33%
Ch_3 = 4	Ch_1 + Ch_3 = 2.3	42.5%
Ch_4 = 10.1	Ch_1 + Ch_4 = 5.3	47.5%

doi:10.1371/journal.pone.0117558.t002

effect when applied individually, using the following equation [22]:

$$I = \frac{L_{c,1}}{L_1} + \frac{L_{c,2}}{L_2} \tag{10}$$

where $L_{c,1}$ and $L_{c,2}$ correspond to the concentrations of the two drugs that produce a given effect when applied together, and L_1 and L_2 are the concentrations that induce the same effect when applied alone. The interaction index I depends on the type of interaction between the two drugs: synergistic ($I < 1$) additive ($I = 1$) or antagonistic ($I > 1$). In our particular case, since both ligands share common binding sites (i.e., they are mutants of the same molecule with reduced affinity), they behave as mutually exclusive and therefore, they follow the principle of Loewe additivity so the interaction index I in Eq. 10 is set to 1 [22] (a detailed analysis of the general equation for drug interaction in conditions of drug additivity, synergy or antagonism can be found as S1 Text).

Next, the Loewe additivity model is applied to drugs that induce a typical dose-response curve [25], as described in Eq. 9. Thus, we solve Eq. 9 for L and substitute into Eq. 10 for both ligands ($L = L_1$ and $L = L_2$), to obtain:

$$1 = \frac{L_{c,1}}{EC_{50,1}}\left(\frac{R(L_{c,1}, L_{c,2}) - D_1}{A_1 - R(L_{c,1}, L_{c,2})}\right)^{(1/B_1)} + \frac{L_{c,2}}{EC_{50,2}}\left(\frac{R(L_{c,1}, L_{c,2}) - D_2}{A_2 - R(L_{c,1}, L_{c,2})}\right)^{(1/B_2)} \tag{11}$$

This equation can be solved numerically to obtain the physiological response $R(L_{c,1}, L_{c,2})$ for each potential combination of $L_{c,1}$ and $L_{c,2}$. The typical shape of the curve is shown in S4A Fig.

Therefore, Eq. 11 allows us to calculate directly the effect of the two drugs when applied simultaneously, significantly reducing the computational cost of the process. S5 Fig. plots the dynamics of several combinations of monomers and chimeras using this method (to be compared with Fig. 3, computed using the simultaneous drug stimulation of the system to show that both methods produce equivalent results). This simplified method allows us to compute the effect of any combination between two given drugs to develop isobolograms representing the final number of cells, after 60 hours of combined treatment for each combination of monomers (Fig. 4A–B) and chimeras (Fig. 4D–E).

Finally, to compare the selective effect of multiple combination of ligands, we define the performance $P(L_{c,1}, L_{c,2})$ of a given treatment as:

$$P(L_{c,1}, L_{c,2}) = N_f^*(L_{c,1}, L_{c,2})_{healthy} - N_f^*(L_{c,1}, L_{c,2})_{unhealthy} \tag{12}$$

where $N_f^*(L_{c,1}, L_{c,2})_{healthy}$ and $N_f^*(L_{c,1}, L_{c,2})_{unhealthy}$ correspond to the final number N_f of healthy and unhealthy cells respectively, after 60 hours of combined treatment (i.e., the final point of

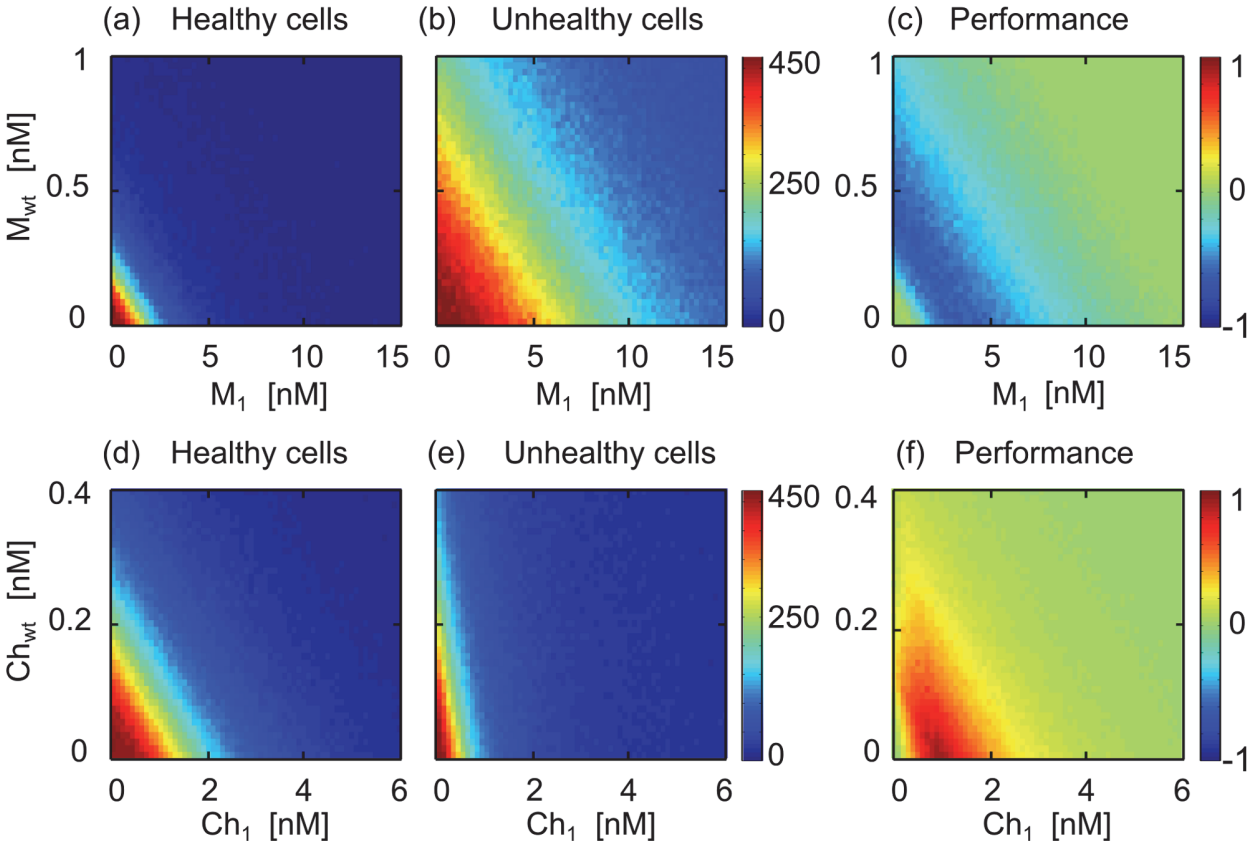

Fig 4. Isobolograms and performance colormaps for monomer and chimera combinations. (A–B) Isobolograms of the effect of the combination of monomers M_{wt} and M_1 for (A) healthy and (B) unhealthy cells (final number of cells after 60 hours of treatment). (C) Performance of the combinatorial monomer treatment, where all values are below 0, evidencing that the combination affects more strongly the healthy population. (D–E) Isobolograms of the effect of chimeras Ch_{wt} + Ch_1 for (D) healthy and (E) unhealthy cells. (F) Performance of the combinatorial chimeric treatment, where all values are above 0, evidencing that the combination affects more strongly the unhealthy population.

doi:10.1371/journal.pone.0117558.g004

the curves in Fig. 3) normalized to obtain values for the performance $P(L_{c,1}, L_{c,2})$ between −1 (minimal selectivity of treatment, i.e., 0% survival of the healthy cells) and 1 (optimal selectivity, i.e., ≥80% survival of healthy and no growth in the unhealthy cell population). A workflow scheme of this approach is shown in S1B Fig.

Fig. 4A–B illustrates the isobolograms for any concentration of monomers M_{wt} and M_1 for healthy (Fig. 4A) and unhealthy cells (Fig. 4B) for a range of concentration values. The performance map (Fig. 4C) evidences that monomer combinations are not selective (i.e, $P \leq 0$ at any concentration). Isobolograms for Ch_{wt} and Ch_1 combinations are shown for healthy (Fig. 4D) and unhealthy (Fig. 4E) cell populations. The performance map (Fig. 4F) illustrates that the combination shows regions of positive performance ($P > 0$), i.e., regions where the combinatorial treatment acts selectively towards the unhealthy cell population.

Performance colormaps for other combinations of chimeric drugs are shown in Fig. 5, where regions in which the threshold of selectivity is achieved are marked in dark red. Simultaneous treatment of Ch_{wt} with Ch_2, Ch_3 and Ch_4 show that, for each combination, optimal selectivity can be achieved at slightly lower concentrations when using the two drugs simultaneously, compared to the same drugs acting alone (i.e., $[Ch_{wt}] = 0$ in each panel). This is more evident when combining Ch_1 with the other chimeras (Fig. 5D–F), where the optimal

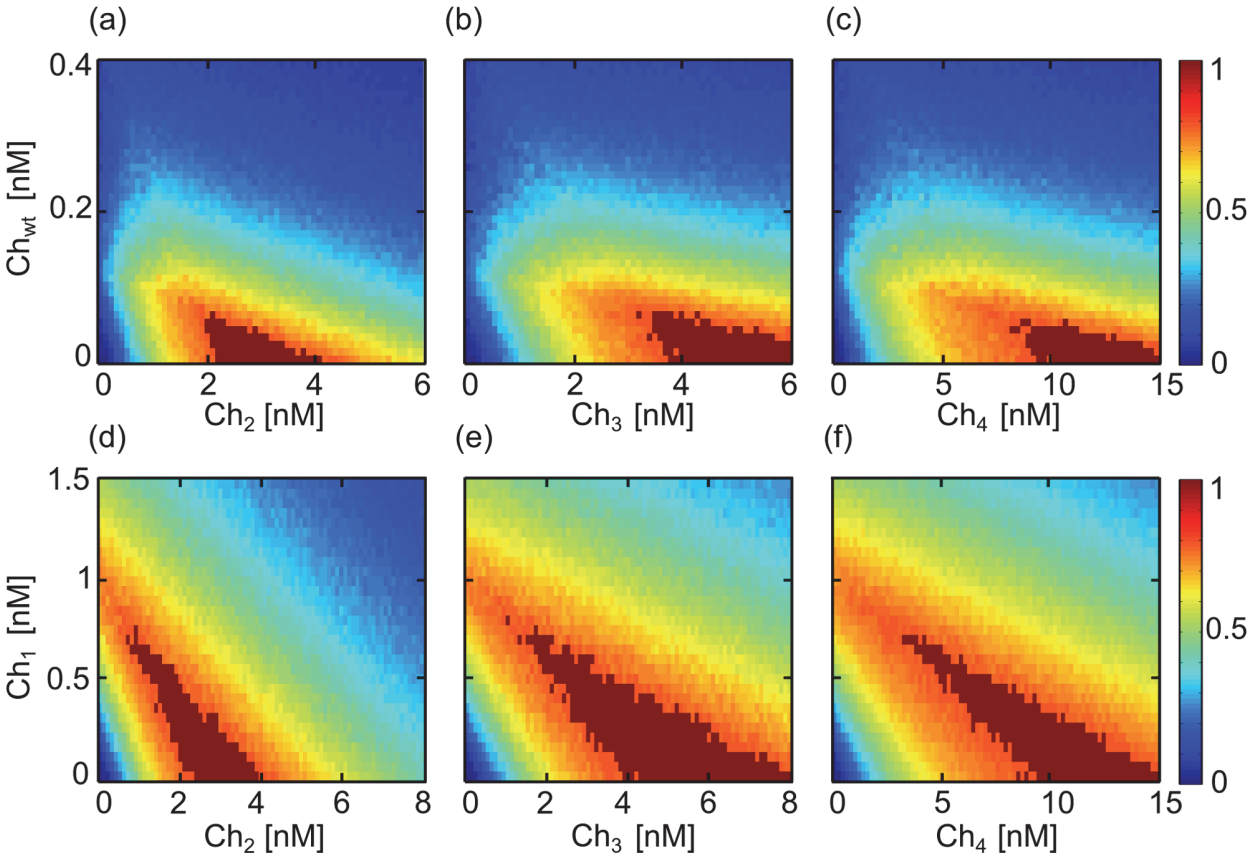

Fig 5. Performance colormaps for different chimera combinations. (A–C) Combination of Ch_{wt} with other chimeras. (D–F) Combination of Ch_1 with other chimeras. Areas where the threshold of selectivity is achieved are marked in dark red. Since there is no negative values for the performance P, color bars are now presented between 0 and 1.

doi:10.1371/journal.pone.0117558.g005

selectivity threshold is achieved at significantly lower concentrations using two selective drugs instead of one (numerical values for the minimal concentration for the threshold of selectivity as well as the reduction in total final concentration due to the combinatorial treatment are shown in Table 2).

Synergistic interaction for selective chimeric drugs in cell populations with heritability

Previous simulations assumed that both healthy and unhealthy cells are, as a first approximation, phenotypically different, with the expression levels of TER and AER obtained from gamma distributions. Therefore, the amount of receptors expressed by a daughter cell depends on its cell type, but it is independent on the amount of receptors expressed by the mother cell. In other potential scenarios, the difference in phenotype between healthy and unhealthy cells can be caused by genetic mutations, and therefore, the amount of receptors expressed by the mother cell is inherited by the daughter cells. In these situations, a given treatment can become inefficient, and it can potentially act as selective pressure, acting more strongly over weak cells and ultimately inducing resistance to treatment in the population. This scenario has been explored extensively *in vivo* and *in silico*, and is one of the main causes of the short-lived response

of targeted therapy in cancer [18]. Recently, it has been shown theoretically and experimentally that dual treatment strategies can dramatically reduce the possibility of development of resistant cells, resulting in long-term disease control compared to single drug treatment, or even sequential drug treatment [18].

To test the performance of dual selective treatment in the context of genetic inheritance of the amount of receptors, we set the average amount of TER and AER expressed by a given daughter cell as directly given by the amount of receptors expressed by the mother (with a coefficient of variation of 0.3). Simulations are performed as in the previous section, and performance colormaps can be computed for all possible concentrations of different ligand combinations (Fig. 6). Comparison of Fig. 6A–F with the corresponding Fig. 5A–F evidences that selectivity is more difficult to achieve in conditions of heritability (i.e., regions of optimal selectivity (marked in dark red) are reduced and occur at higher concentrations). Numerical values for the minimal concentration for the threshold of selectivity, as well as the reduction in total final concentration due to the combinatorial treatment in conditions of heritability, are shown in Table 3. Fig. 6 G–H, plots the values of AER and TER of the cells in the population before (Fig. 6G) and after (Fig. 6H) 60 hours of treatment for the minimal concentration of Ch_2 that meets the threshold in conditions of heritability. Comparison of both distributions with conditions of no heritability (Fig. 2J,M) evidences that heritability increases the variability in the expression levels of AER and TER in the population, resulting in a decrease in the performance of the drug combinations and a reduction in the region of optimal selectivity (Fig. 6A–F).

Conclusions and Discussion

Chimeric ligands with selective potential constitute one of the forefronts in modern pharmacology. The development of strategies to affect only malfunctioning cells inside a healthy tissue based on a sequential mechanisms of targeting is still in its early stages. Rational approaches based on modulating the strength of the interaction between ligand and target has shown that selectivity can be improved in a rational predictive manner [15, 25, 34]. Unfortunately, this results in a marked increase of the total concentration of drug that needs to be administered, which potentially increases the risk of toxicity and other undesired effects. Therefore, the problem of achieving selectivity at reduced drug concentrations is a main concern when developing selective drugs.

Our previous modeling approaches [25, 34] allow us to predict the optimal value of the affinity and dissociation rates of both AE and TE for improved selectivity at the lowest drug concentration. Unfortunately, the affinity and dissociation rates in a given ligand-receptor interaction cannot be modulated gradually, since single mutations in the ligand change abruptly the binding and unbinding rates with the complementary receptor. In this sense, combination of two ligands can, in principle, result beneficial to improve the selective potential of the treatment since, for instance, highly potent ligands could affect cells expressing high TER concentrations, while more selective chimeras (i.e., with reduced potency in the AE subunit) could discriminate better between healthy and unhealthy levels of the target protein.

To our knowledge, our results constitute the first studies focused on the combination of selective drugs, by generalizing our previous results of single treatments with selective drugs [25] to study selective drug combinations in cell population models. Our studies show that the combination of selective drugs is synergistic in terms of their selective potential, i.e., the combination of selective drugs can reduce the total drug administered to achieve a given selective effect, compared to the same drugs acting alone. We also show that using a explicit model of two selective drugs is equivalent to a simplified model where the two drugs are assumed to interact additively. This alternative method allows us to develop performance maps where selectivity is

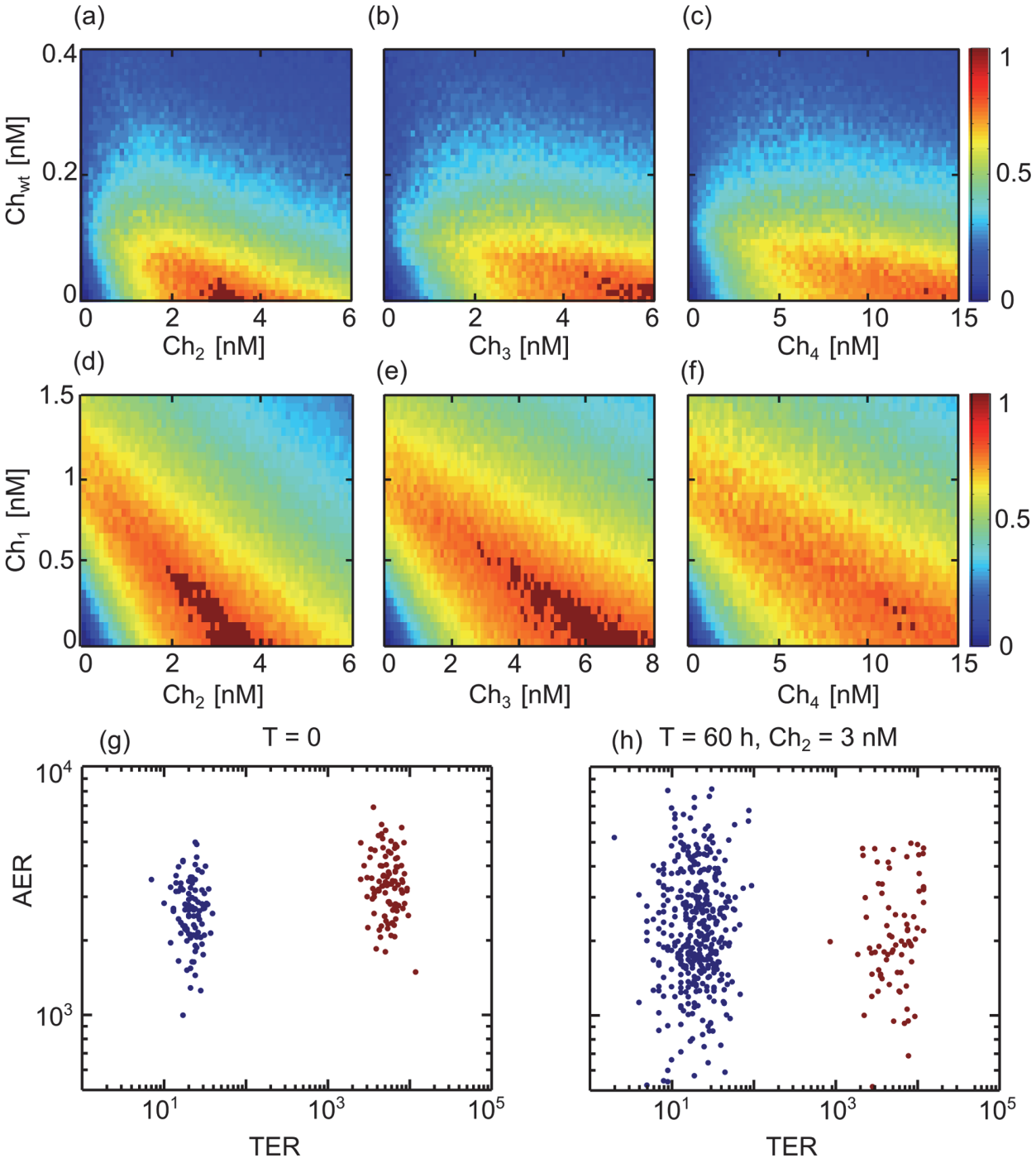

Fig 6. Performance colormaps for different chimera combinations in conditions of heritability. (A–C) Combination of Ch_{wt} with other chimeras. (D–F) Combination of Ch_1 with other chimeras. Areas where the threshold of selectivity is achieved are marked in dark red. Since there is no negative values for the performance P, color bars are now presented between 0 and 1. (G–H) Distribution of the AER and TER receptors for the two cell populations before (G) and after (H) 60 hours of treatment with $Ch_2 = 3$ nM.

doi:10.1371/journal.pone.0117558.g006

Table 3. Reduction in concentration at threshold for optimal selectivity in conditions of heritability. Percentage of reduction of total drug concentration of combinatorial treatment versus single drug treatment for different selective drug combinations.

Single drug	Drug combination	Reduction percentage
Ch_2 = 2.9	Ch_{wt} + Ch_2 = -	-%
Ch_3 = 5.3	Ch_{wt} + Ch_3 = 4.5	15%
Ch_4 = -	Ch_{wt} + Ch_4 = -	-%
Ch_2 = 2.9	Ch_1 + Ch_2 = 2.35	19%
Ch_3 = 6	Ch_1 + Ch_3 = 3.45	42.5%
Ch_4 = -	Ch_1 + Ch_4 = -	-%

doi:10.1371/journal.pone.0117558.t003

computed for any given concentration of the combined drugs. We used a cell population based model to study how these types of treatments respond in a context of cell-variability and their robustness in condition where the amount of target proteins is inherited from mother to daughter cells. Interestingly, despite assuming additive interaction of the different chimeras when combined (i.e., they compete for the same molecular targets), when looking at the selective potential of the treatment, chimeras behave as synergistic.

Several main assumptions are taken into account while developing the model. First, we assume that production and degradation of each receptor is balanced in conditions of no ligand stimulation. We also simplified all potential downstream regulation in receptor expression after activation, focusing only on the regulation that takes place due to direct ligand stimulation. We also assume that the activity triggered by the ligand-receptor interaction is proportional to the amount of maximum active complexes formed. Other potential values such as the total value of active complexes at a given time also produce equivalent results, as discussed in [25] at the single cell level. Regarding the simulations of the population dynamics, we assumed that all cells proliferate at the same mean rate, independently of the amount of EGFR receptors. It is well-known that EGFR stimulation is correlated with the activation of proliferative signals [32], but experimental data monitoring differences in cell cycle length for Daudi versus Daudi-EGFR cells used to inform our model are not available [15]. In addition, the effect of heritability in the expression of receptors was assumed to simply depend on the amount of receptors expressed by the mother cells. Other potential scenarios to capture the effect of mutations in the regulation of the expression of receptors will be more realistic, but they will result in more free parameters and assumptions. In addition, we assume that the effect of heritability will be more relevant in longer experiments, i.e., when more generations of cells are allowed to develop. Unfortunately, experimental data are only available at the time point of t = 60h, corresponding to an average of 2.2 generations, insufficient to observe the selective pressure effect induced by the drug treatment. To mimic cell-to-cell variability in the population, we assumed gamma distributions for the amount of receptors expressed and the cell cycle length, based on several publications. Other types of distributions were also tested (gaussian, lognormal), with almost no difference in the results compared to the gamma distribution [35–38]. To quantitatively compare the different combinatorial treatments, a threshold is defined in terms of the potential selectivity of the treatment towards the different cell types expressing different concentrations of the target proteins (80% survival of the healthy cells while the number of unhealthy cells is maintained). Other potential threshold values defined also evidence the reported synergism when combining two selective ligands, but at different drug concentrations.

In conclusion, we have shown that combination of selective drugs can selectively affect a given cell population at reduced concentrations compared to single drug treatment. These

types of theoretical studies focused on the rational design of selective drugs and treatments can complement experimental efforts, allowing researches to develop a more reliable and efficient approach to quantitative pharmacology.

Supporting Information

S1 Text. Response surface plots for drug interaction in conditions of drug additivity, synergy or antagonism.
(TEX)

S1 Fig. Workflow to obtain the effect of a drug combination on a cell population. (A) Direct simulation of two simultaneous treatments (see section Models: Eqs. 1–4 are solved directly for two simultaneous ligands (j = 1,2) at a constant concentration. The value of AER-AE complexes formed is then translated into a physiological effect using calibration with experimental dose response curves obtained from [15]. Two populations of cells are defined with values for AER and TER from gamma distributions for healthy and unhealthy cells. Eqs. 1–4 are solved numerically for each cell in the two populations, obtaining the dynamics of growth for healthy and unhealthy cell populations for a given constant concentration of L_1 and L_2. (B) Calculation of the effect of combinatorial treatment assuming additive interaction between ligands: the maximum number of AER-AE complexes is calculated for each combination of AER and TER receptors concentrations by solving Eqs. 1–4 for a single ligand treatment (j = 1). The output of the model is translated to a calibration curve [25], obtaining the theoretical dose-response curves for each ligand. Physiological response curves are fitted to a four-parameter sigmoidal (Eq.9), and the physiological response for any concentration of two ligands is then calculated using the Loewe approximation for additive ligand interaction (Eq. 11). This response is then used to perform simulations for healthy and unhealthy cell populations, following the same procedure as in (A). Finally, the number of healthy and unhealthy cells after 60 hours of treatment is plotted in the corresponding isobologram for each ligand combination. The final performance colormap for each value of the combination of ligands is obtained by subtracting the normalized isobolograms for unhealthy minus healthy cells. Values above threshold of performance are highlighted in dark red.
(TIFF)

S2 Fig. Dynamics of the cell populations after individual monomer treatment. Numerical solution of the model equations showing the time evolution of healthy (blue line) and unhealthy (red line) cells after treatment with low, intermediate and high concentrations of (A–C) M_1 monomer, (D–F) M_2 monomer, and (G–I) M_3 monomer.
(TIFF)

S3 Fig. Dynamics of the cell populations after individual chimeric treatment. Numerical solution of the model equations showing the time evolution of healthy (blue line) and unhealthy (red line) cells after treatment with low, intermediate and high concentrations of (A–C) Ch_1 chimera, (D–F) Ch_3 chimera, and (G–I) Ch_4 chimera.
(TIFF)

S4 Fig. Response surfaces for $L_1 + L_2$ combinations. Response surface plots using Eq.13 (see S1 Text) for two ligands showing (A) additivity, $\alpha = 0$, (B) synergy, $\alpha = 5$ and (C) antagonism, $\alpha = -0.5$. The black curve is the isobol curve (i.e., curve of equal effect) for 50% (EC_{50}) of physiological response and it has different curvature depending on the interaction type.
(TIFF)

S5 Fig. Numerical solution of the model equations showing synergistic performance of selective ligands using the Loewe approximation (to be compared with Fig. 3 in the main text, obtained using chemical dynamics simulation of two ligands simultaneously). (A–C) Time evolution of healthy (blue line) and unhealthy (red line) cells after treatment with different combinations of monomers, at the minimal concentration required to affect 20% of the unhealthy cell population. (D–F) Time evolution of different combinations of Ch_{wt} with other chimeric ligands at the minimal concentration required to achieve the threshold for selectivity. (G–I) Time evolution of different combinations of Ch_1 with other chimeric ligands at the minimal concentration required to achieve the threshold for selectivity.
(TIFF)

Acknowledgments

We thank the Instituto Nicolás Cabrera of the Universidad Autónoma de Madrid (Spain) and Raul Guantes for very helpful input.

Author Contributions

Conceived and designed the experiments: VDM DGM. Performed the experiments: VDM DGM. Analyzed the data: VDM DGM. Contributed reagents/materials/analysis tools: VDM DGM. Wrote the paper: VDM DGM.

References

1. Croce CM (2008) Oncogenes and cancer. New England Journal of Medicine 358: 502–511. PMID: 18234754
2. Verma S, Miles D, Gianni L, Krop IE, Welslau M, et al. (2012) Trastuzumab Emtansine for HER2-Positive Advanced Breast Cancer. New England Journal of Medicine. 367(19), 1783–1791. doi: 10.1056/NEJMoa1209124 PMID: 23020162
3. Taylor ND, Way JC, Silver PA, Cironi P. (2010) Anti-glycophorin single-chain Fv fusion to low-affinity mutant erythropoietin improves red blood cell-lineage specificity. Protein Engineering, Design and Selection. 23(4):251–60. doi: 10.1093/protein/gzp085 PMID: 20083493
4. Turturro F (2007) Denileukin diftitox: a biotherapeutic paradigm shift in the treatment of lymphoid-derived disorders. Expert Review of Anticancer Therapy 7: 11–17. doi: 10.1586/14737140.7.1.11 PMID: 17187516
5. Kreitman RJ, Wilson WH, White JD, Stetler-Stevenson M, Jaffe ES, et al. (2000) Phase i trial of recombinant immunotoxin anti-tac (fv)-pe38 (lmb-2) in patients with hematologic malignancies. Journal of Clinical Oncology 18: 1622–1636. PMID: 10764422
6. Kreitman RJ, Squires DR, Stetler-Stevenson M, Noel P, FitzGerald DJ, et al. (2005) Phase i trial of recombinant immunotoxin rfb4 (dsfv)-pe38 (bl22) in patients with b-cell malignancies. Journal of clinical oncology 23: 6719–6729. doi: 10.1200/JCO.2005.11.437 PMID: 16061911
7. Kioi M, Husain SR, Croteau D, Kunwar S, Puri RK (2006) Convection-enhanced delivery of interleukin-13 receptor-directed cytotoxin for malignant glioma therapy. Technology in cancer research & treatment 5: 239–250. doi: 10.1177/153303460600500307
8. Bremer E, Samplonius DF, van Genne L, Dijkstra MH, Kroesen BJ, et al. (2005) Simultaneous inhibition of epidermal growth factor receptor (egfr) signaling and enhanced activation of tumor necrosis factor-related apoptosis-inducing ligand (trail) receptor-mediated apoptosis induction by an scfv: strail fusion protein with specificity for human egfr. Journal of Biological Chemistry 280: 10025–10033. PMID: 15644326
9. Bremer E, Samplonius DF, Peipp M, van Genne L, Kroesen BJJ, et al. (2005) Target cell–restricted apoptosis induction of acute leukemic t cells by a recombinant tumor necrosis factor–related apoptosis-inducing ligand fusion protein with specificity for human cd7. Cancer research 65: 3380–3388. PMID: 15833872
10. Stieglmaier J, Bremer E, Kellner C, Liebig TM, ten Cate B, et al. (2008) Selective induction of apoptosis in leukemic b-lymphoid cells by a cd19-specific trail fusion protein. Cancer Immunology, Immunotherapy 57: 233–246. doi: 10.1007/s00262-007-0370-8 PMID: 17665197

11. Bremer E, ten Cate B, Samplonius DF, de Leij LF, Helfrich W (2006) Cd7-restricted activation of fas-mediated apoptosis: a novel therapeutic approach for acute t-cell leukemia. Blood 107: 2863–2870. doi: 10.1182/blood-2005-07-2929 PMID: 16332967
12. Bremer E, ten Cate B, Samplonius DF, Mueller N, Wajant H, et al. (2008) Superior activity of fusion protein scfvrit: sfasl over cotreatment with rituximab and fas agonists. Cancer research 68: 597–604. doi: 10.1158/0008-5472.CAN-07-5171 PMID: 18199557
13. Xuan C, Steward KK, Timmerman JM, Morrison SL (2010) Targeted delivery of interferon-alpha via fusion to anti-cd20 results in potent antitumor activity against b-cell lymphoma. Blood 115: 2864–2871. doi: 10.1182/blood-2009-10-250555 PMID: 20139095
14. Zhang B, Gao B, Dong S, Zhang Y, Wu Y (2011) Anti-tumor efficacy and pre-clinical immuno-genicity of ifnα2a-ngr. Regulatory Toxicology and Pharmacology 60: 73–78. doi: 10.1016/j.yrtph.2011.02.007 PMID: 21338646
15. Cironi P, Swinburne IA, Silver PA (2008) Enhancement of cell type specificity by quantitative modulation of a chimeric ligand. Journal of biological chemistry 283: 8469–8476. doi: 10.1074/jbc.M708502200 PMID: 18230610
16. Fitzgerald JB, Schoeberl B, Nielsen UB, Sorger PK (2006) Systems biology and combination therapy in the quest for clinical efficacy. Nature chemical biology 2: 458–466. doi: 10.1038/nchembio817 PMID: 16921358
17. Yuan S, Wang F, Chen G, Zhang H, Feng L, et al. (2013) Effective elimination of cancer stem cells by a novel drug combination strategy. Stem Cells 31: 23–34. doi: 10.1002/stem.1273 PMID: 23132831
18. Bozic I, Reiter JG, Allen B, Antal T, Chatterjee K, et al. (2013) Evolutionary dynamics of cancer in response to targeted combination therapy. Elife 2. doi: 10.7554/eLife.00747 PMID: 23805382
19. Tan X, Hu L, Luquette LJ III, Gao G, Liu Y, et al. (2012) Systematic identification of synergistic drug pairs targeting hiv. Nature biotechnology 30: 1125–1130. doi: 10.1038/nbt.2391 PMID: 23064238
20. Jia J, Zhu F, Ma X, Cao ZW, Li YX, et al. (2009) Mechanisms of drug combinations: interaction and network perspectives. Nature reviews Drug discovery 8: 111–128. doi: 10.1038/nrd2683 PMID: 19180105
21. Borisy AA, Elliott PJ, Hurst NW, Lee MS, Lehár J, et al. (2003) Systematic discovery of multi-component therapeutics. Proceedings of the National Academy of Sciences 100: 7977–7982. doi: 10.1073/pnas.1337088100
22. Berenbaum MC (1977) Synergy, additivism and antagonism in immunosuppression. a critical review. Clinical and experimental immunology 28: 1.
23. Zimmermann GR, Lehar J, Keith CT. (2007) Multi-target therapeutics: when the whole is greater than the sum of the parts. Drug Discovery Today 12: 34–42 doi: 10.1016/j.drudis.2006.11.008 PMID: 17198971
24. Lehaŕ J, Krueger AS, Avery W, Heilbut AM, Johansen LM, et al. (2009) Synergistic drug combinations tend to improve therapeutically relevant selectivity. Nature Biotechnology 27, 659–666 doi: 10.1038/nbt.1549 PMID: 19581876
25. Doldán-Martelli V, Guantes R, Miguez DG (2013) A mathematical model for the rational design of chimeric ligands in selective drug therapies. CPT: Pharmacometrics & Systems Pharmacology 2: e26.
26. Lauffenburger DA, Linderman JJ (1993) Receptors: models for binding, trafficking, and signaling, volume 365. Oxford University Press New York:.
27. Míguez DG (2010) The role of asymmetric binding in ligand–receptor systems with 1: 2 interaction ratio. Biophysical chemistry 148: 74–81. doi: 10.1016/j.bpc.2010.02.012 PMID: 20332059
28. Arteaga CL (2001) The epidermal growth factor receptor: from mutant oncogene in nonhuman cancers to therapeutic target in human neoplasia. Journal of Clinical Oncology 19: 32s–40s. PMID: 11560969
29. Gewert DR, Shah S, Clemens MJ (1981) Inhibition of cell division by interferons. European Journal of Biochemistry 116: 487–492. doi: 10.1111/j.1432-1033.1981.tb05362.x PMID: 6167441
30. Klein E, Klein G, Nadkarni JS, Nadkarni JJ, Wigzell H, et al. (1968) Surface igm-kappa specificity on a burkitt lymphoma cell in vivo and in derived culture lines. Cancer Research 28: 1300–1310. PMID: 4174339
31. Cai L, Friedman N, Xie XS (2006) Stochastic protein expression in individual cells at the single molecule level. Nature 440: 358–362. doi: 10.1038/nature04599 PMID: 16541077
32. Oda K, Matsuoka Y, Funahashi A, Kitano H (2005) A comprehensive pathway map of epidermal growth factor receptor signaling. Molecular systems biology 1. doi: 10.1038/msb4100014 PMID: 16729045
33. MacDonald ML, Lamerdin J, Owens S, Keon BH, Bilter GK, et al. (2006) Identifying off-target effects and hidden phenotypes of drugs in human cells. Nature Chemical Biology 2: 329–337. doi: 10.1038/nchembio790 PMID: 16680159

34. Ruiz-Herrero T, Estrada J, Guantes R, Miguez DG (2013) A tunable coarse-grained model for ligand-receptor interaction. PLoS computational biology 9: e1003274. doi: 10.1371/journal.pcbi.1003274 PMID: 24244115

35. Weddell JC, Imoukhuede PI (2014) Quantitative characterization of cellular membrane-receptor heterogeneity through statistical and computational modeling. PloS one 9: e97271. doi: 10.1371/journal.pone.0097271 PMID: 24827582

36. Bengtsson M, Stahlberg A, Rorsman P, Kubista M (2005) Gene expression profiling in single cells from the pancreatic islets of langerhans reveals lognormal distribution of mrna levels. Genome research 15: 1388–1392. doi: 10.1101/gr.3820805 PMID: 16204192

37. Dowling MR, Milutinović D, Hodgkin PD (2005) Modelling cell lifespan and proliferation: is like-lihood to die or to divide independent of age? Journal of The Royal Society Interface 2: 517–526. doi: 10.1098/rsif.2005.0069

38. Friedman N, Cai L, Xie XS (2006) Linking stochastic dynamics to population distribution: An analytical framework of gene expression. Phys Rev Lett 97: 168302. doi: 10.1103/PhysRevLett.97.168302 PMID: 17155441

39. Piehler J, Roisman LC, Schreiber G (2000) New structural and functional aspects of the type i interferon-receptor interaction revealed by comprehensive mutational analysis of the binding interface. Journal of Biological Chemistry 275: 40425–40433. doi: 10.1074/jbc.M006854200 PMID: 10984492

40. Schwarz MA, Tardelli L, Macosko HD, Sullivan LM, Narula SK, et al. (1995) Interleukin 4 retards dissemination of a human b-cell lymphoma in severe combined immunodeficient mice. Cancer research 55: 3692–3696. PMID: 7641177

Supporting Information

Text S1: Response surface plots for drug interaction in conditions of drug additivity, synergy or antagonism.

To explain graphically drug synergy, additivity, or antagonism we chose a response surface model developed by Greco et al. [1], based on the equation for Loewe additivity (Eq. 10) and the extension for logistic dose-response curves (Eq. 11), adding a third term multiplied by the interaction parameter α:

$$1 = \frac{L_{c,1}}{EC_{50,1}}\left(\frac{R(L_{c,1},L_{c,2})-D_1}{A_1-R(L_{c,1},L_{c,2})}\right)^{(1/B_1)} + \frac{L_{c,2}}{EC_{50,2}}\left(\frac{R(L_{c,1},L_{c,2})-D_2}{A_2-R(L_{c,1},L_{c,2})}\right)^{(1/B_2)} + \\ + \frac{\alpha\cdot L_{c,1}L_{c,2}}{EC_{50,1}EC_{50,2}}\left(\frac{(R(L_{c,1},L_{c,2})-D_1)\cdot(R(L_{c,1},L_{c,2})-D_2)}{(A_1-R(L_{c,1},L_{c,2}))\cdot(A_2-R(L_{c,1},L_{c,2}))}\right)^{(1/2B_1+1/2B_2)} \quad (13)$$

where α is the interaction parameters, $R(L_{c,1},L_{c,2})$ is the physiological response for each potential combination of $L_{c,1}$ and $L_{c,2}$ and all remaining parameters have been explain in the main text (see Eq. 11). The first two terms on the right-hand expression of this equation are equivalent to the right-hand terms of Eq. 11. It follows that Eq. 13 defines the interaction index I for a combination of two drugs with dose-response curves following Eq. 9.

$$I = \frac{L_{c,1}}{EC_{50,1}}\left(\frac{R(L_{c,1},L_{c,2})-D_1}{A_1-R(L_{c,1},L_{c,2})}\right)^{(1/B_1)} + \frac{L_{c,2}}{EC_{50,2}}\left(\frac{R(L_{c,1},L_{c,2})-D_2}{A_2-R(L_{c,1},L_{c,2})}\right)^{(1/B_2)} = \\ = 1 - \frac{\alpha\cdot L_{c,1}L_{c,2}}{EC_{50,1}EC_{50,2}}\left(\frac{(R(L_{c,1},L_{c,2})-D_1)\cdot(R(L_{c,1},L_{c,2})-D_2)}{(A_1-R(L_{c,1},L_{c,2}))\cdot(A_2-R(L_{c,1},L_{c,2}))}\right)^{(1/2B_1+1/2B_2)} \quad (14)$$

Therefore, when $\alpha > 0$, the interaction index I is less than 1, Loewe synergism is indicated; when $\alpha < 0$, interaction index is greater than one, Loewe antagonism is indicated; and when $\alpha = 0$, Loewe additivity is indicated (defaults to Eq. 10). The larger positive α is, the smaller the interaction index and the stronger the synergy.
Plots of the physiological response, $R(L_{c,1},L_{c,2})$, of different combinations of two drugs that show additivity, synergy or antagonism are shown in Fig. S4A-C, respectively.

References

1. Greco WR, Bravo G, Parsons JC. (1995) The search for synergy: a critical review from a response surface perspective. Pharmacological Reviews. 1995 Jun;47(2):331-85

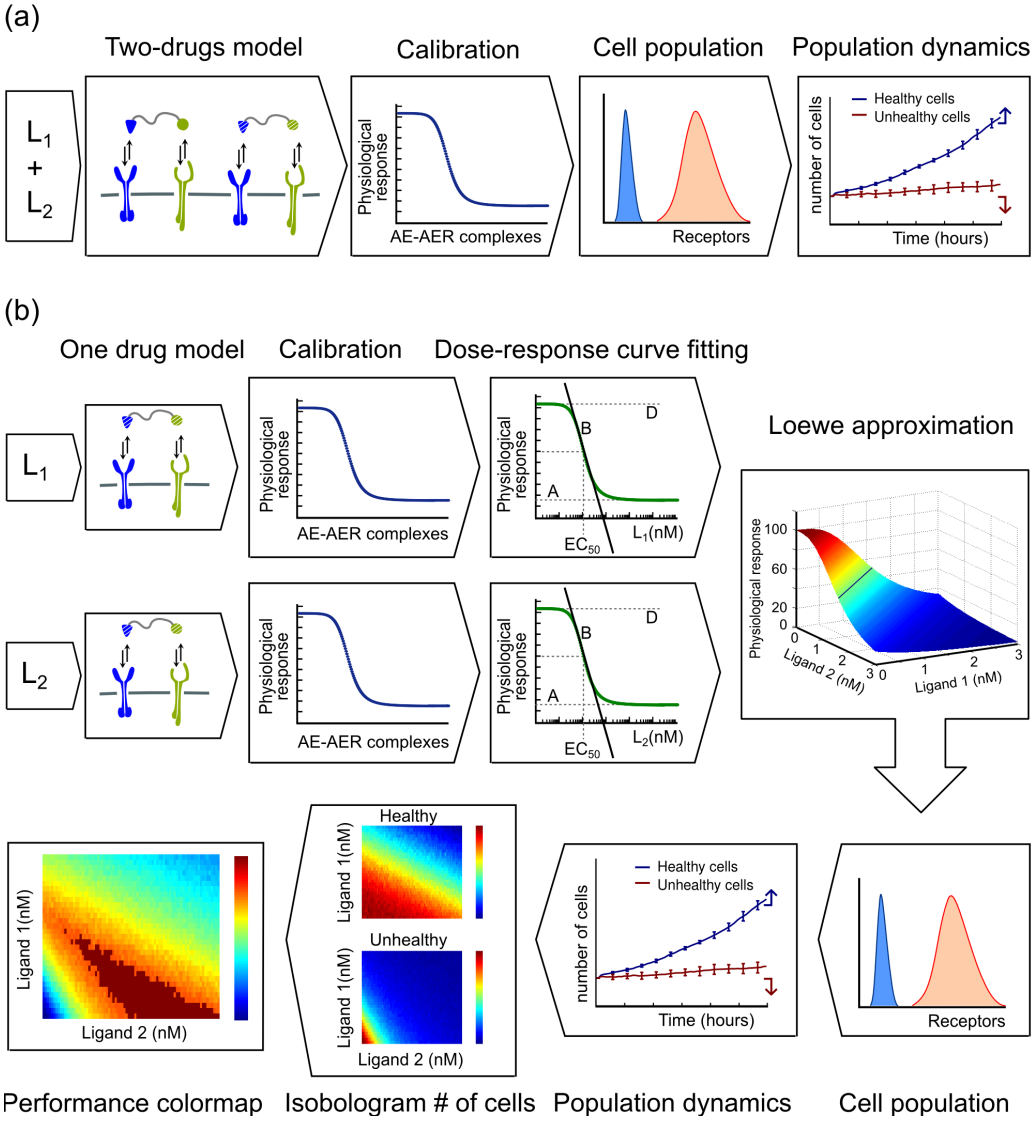

Figure S1. Workflow to obtain the effect of a drug combination on a cell population. (A) Direct simulation of two simultaneous treatments (see section *Models*: Eqs. 1-4 are solved directly for two simultaneous ligands ($j = 1, 2$) at a constant concentration. The value of AER-AE complexes formed is then translated into a physiological effect using calibration with experimental dose response curves obtained from [15]. Two populations of cells are defined with values for AER and TER from gamma distributions for healthy and unhealthy cells. Eqs. 1-4 are solved numerically for each cell in the two populations, obtaining the dynamics of growth for healthy and unhealthy cell populations for a given constant concentration of L_1 and L_2. (B) Calculation of the effect of combinatorial treatment assuming additive interaction between ligands: the maximum number of AER-AE complexes is calculated for each combination of AER and TER receptors concentrations by solving Eqs. 1-4 for a single ligand treatment ($j = 1$) . The output of the model is translated to a calibration curve [25], obtaining the theoretical dose-response curves for each ligand. Physiological response curves are fitted to a four-parameter sigmoidal (Eq.9), and the physiological response for any concentration of two ligands is then calculated using the Loewe approximation for additive ligand interaction (Eq. 11). This response is then used to perform simulations for healthy and unhealthy cell populations, following the same procedure as in (A). Finally, the number of healthy and unhealthy cells after 60 hours of treatment is plotted in the corresponding isobologram for each ligand combination. The final performance colormap for each value of the combination of ligands is obtained by subtracting the normalized isobolograms for unhealthy minus healthy cells. Values above threshold of performance are highlighted in dark red.

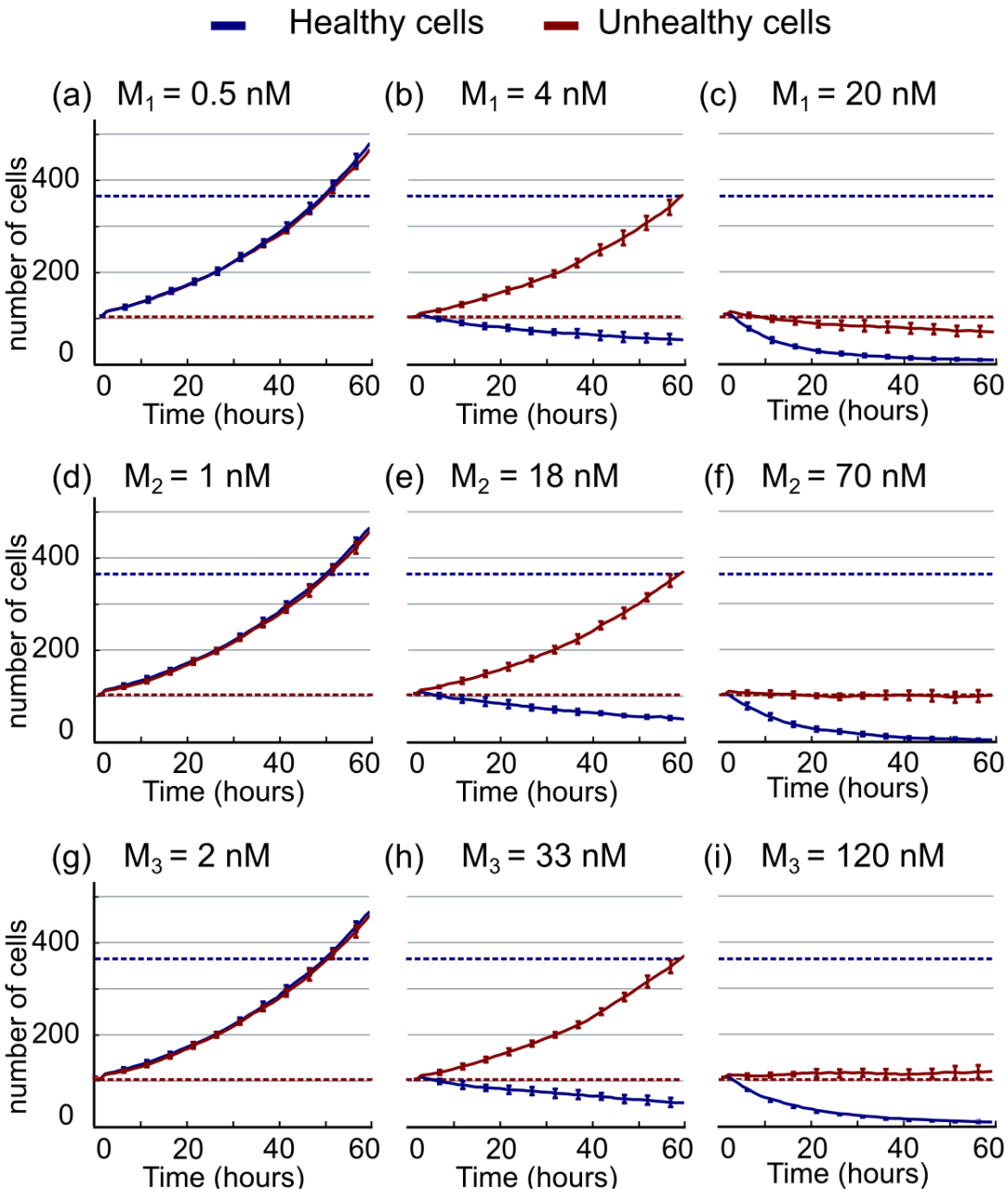

Figure S2. Dynamics of the cell populations after individual monomer treatment. Numerical solution of the model equations showing the time evolution of healthy (blue line) and unhealthy (red line) cells after treatment with low, intermediate and high concentrations of (A-C) M_1 monomer, (D-F) M_2 monomer, and (G-I) M_3 monomer.

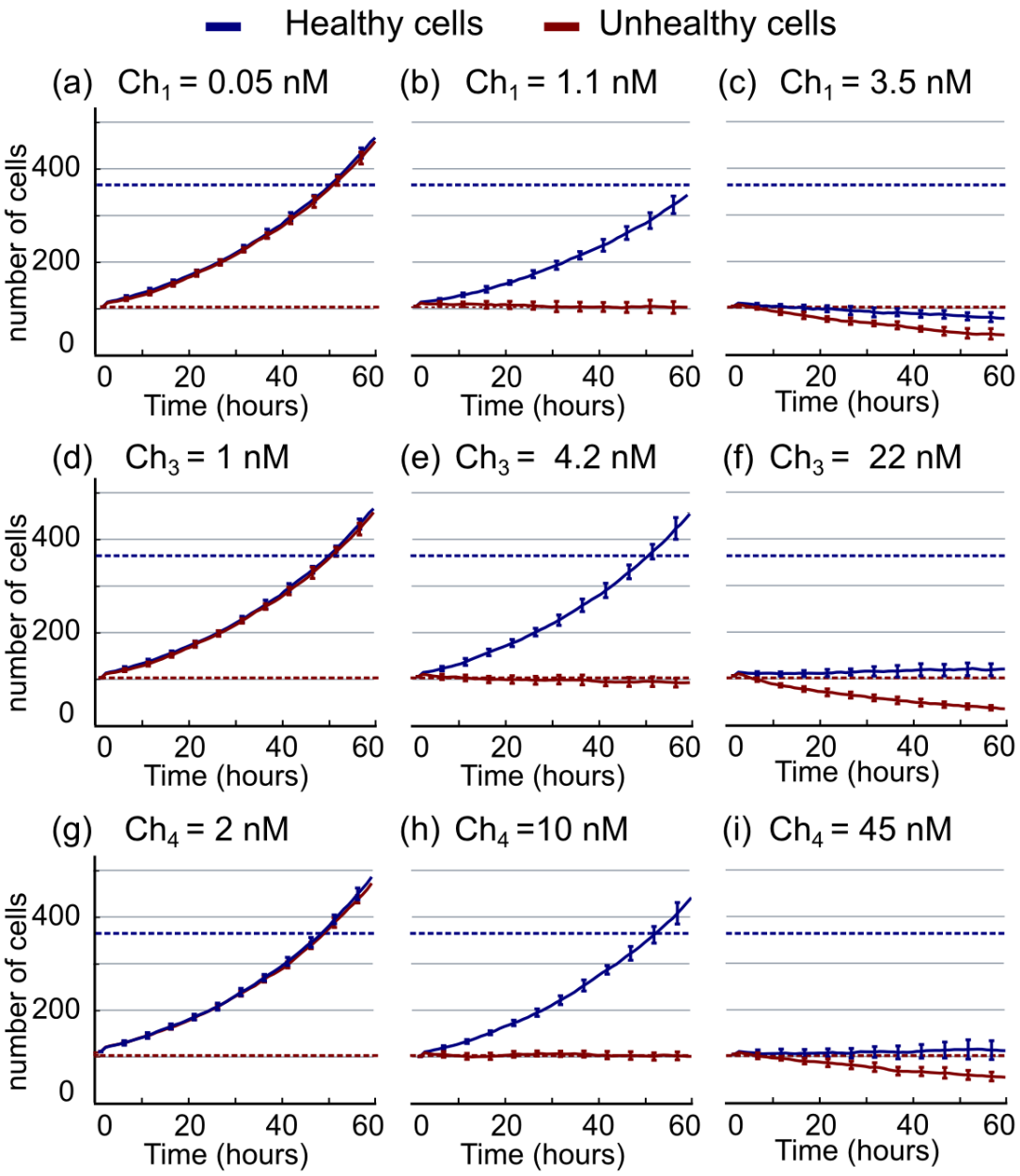

Figure S3. Dynamics of the cell populations after individual chimeric treatment. Numerical solution of the model equations showing the time evolution of healthy (blue line) and unhealthy (red line) cells after treatment with low, intermediate and high concentrations of (A-C) Ch_1 chimera, (D-F) Ch_3 chimera, and (G-I) Ch_4 chimera.

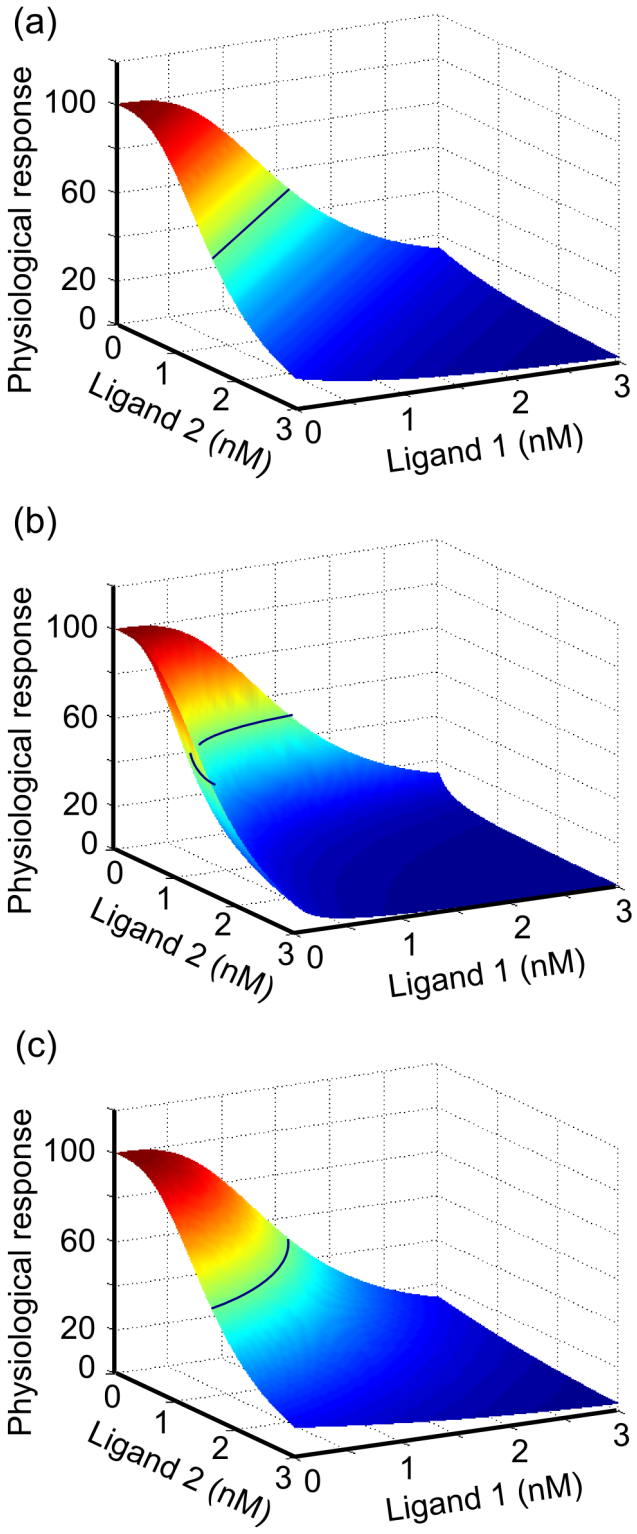

Figure S4. Response surfaces for $L_1 + L_2$ combinations. Response surface plots using Eq.13 (see *Text S1*) for two ligands showing (A) additivity, α=0, (B) synergy, α=5 and (C) antagonism, α=-0.5 . The black curve is the isobol curve (i.e., curve of equal effect) for 50% (EC_{50}) of physiological response and it has different curvature depending on the interaction type.

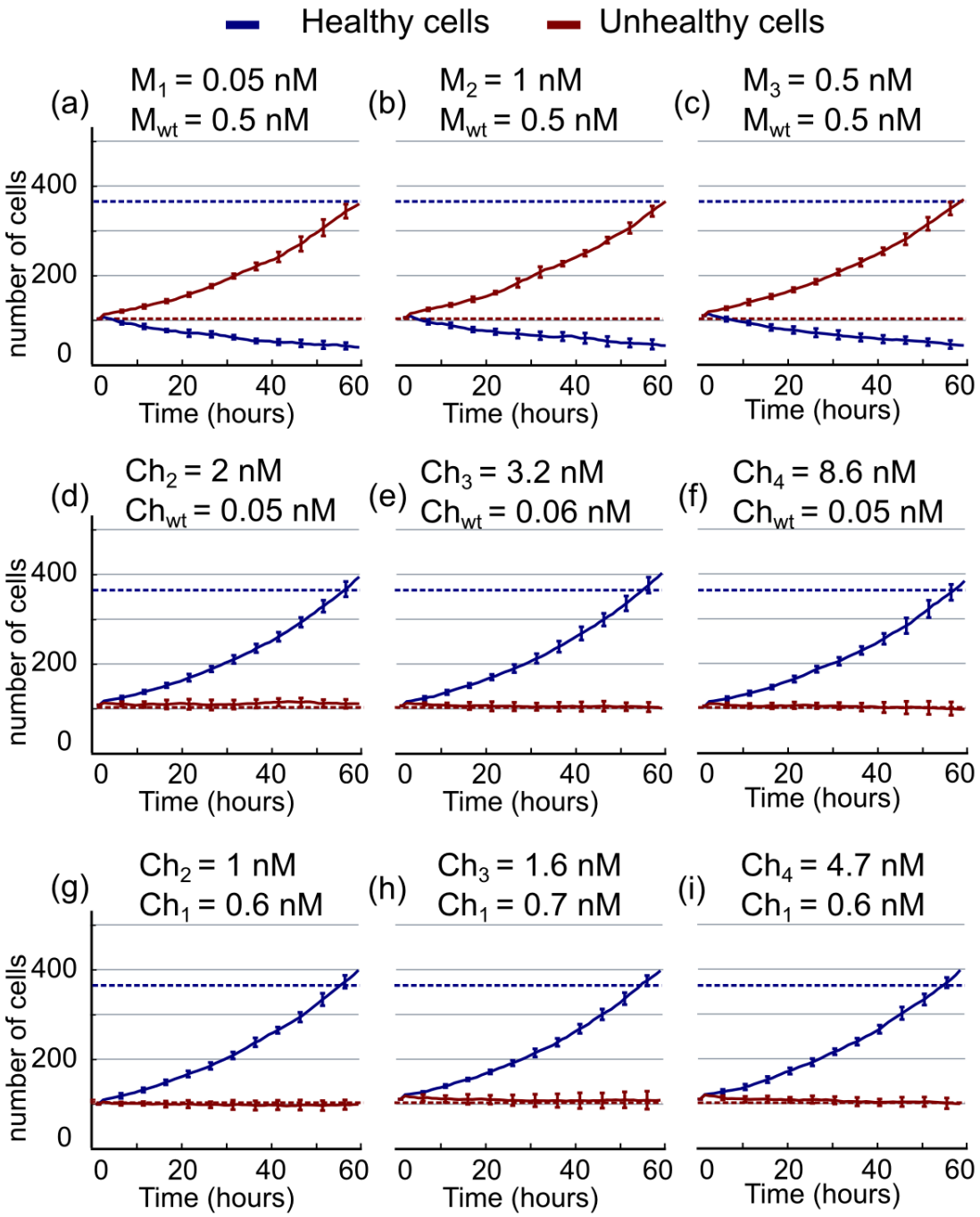

Figure S5. Numerical solution of the model equations showing synergistic performance of selective ligands using the Loewe approximation (to be compared with Fig. 3 in the main text, obtained using chemical dynamics simulation of two ligands simultaneously). (A-C) Time evolution of healthy (blue line) and unhealthy (red line) cells after treatment with different combinations of monomers, at the minimal concentration required to affect 20% of the unhealthy cell population. (D-F) Time evolution of different combinations of Ch_{wt} with other chimeric ligands at the minimal concentration required to achieve the threshold for selectivity. (G-I) Time evolution of different combinations of Ch_1 with other chimeric ligands at the minimal concentration required to achieve the threshold for selectivity.

3.4 The influence of network topologies in periodic drug treatments

Background, Introduction and Author Contribution

The last contribution of this thesis belongs to the line of work of 'Nonlinear regulation in pathways and its impact on disease treatment' which includes different publications ([45, 79] and addresses different questions at many biological levels, such as: How can signaling networks integrate and process information from different signals? How can they operate robustly in the presence of noise and undesirable fluctuations? What is the relation between structure and function of simple signaling networks? Which are the underlying mechanisms inducing variability in the cellular response to drug treatments?

Herein, the author presents the last contribution (in preparation) of this thesis, which uses tools from Nonlinear Dynamics to explore how the architecture of a signaling network influences a given drug treatment.In this direction, the author created a computational high-throughput screening platform to explore all posible three-node network topologies and monitored their response to inhibition, using different initial conditions for the system (i.e., the phosphorylation levels of each of the involved nodes). The author of this thesis performed the analysis of the resulting dose-response curves and characterized their behavior in terms of the type of dependence on the initial value of the treatment. Using this approach, the author found interesting novel ways of response, suggesting that the topology of the signaling network can induce complex dose-response curves and nonlinear effects.

The influence of network topologies in drug treatments

Victoria Doldán-Martelli, David G. Míguez*

May 22, 2017

Centro de Biología Molecular Severo Ochoa, Depto. de Física de la Materia Condensada, Instituto Nicolás Cabrera and IFIMAC, Universidad Autónoma de Madrid, Campus de Cantoblanco, 28046 Madrid, Spain

* Corresponding Author: David G. Míguez: david.miguez@uam.es

Keywords: In silico screening, Mathematical Models, Systems Biology

Abstract

An accurate prediction of the outcome of a given drug treatment requires quantitative values for all parameters and concentrations involved, as well as a detailed characterization of the network of interactions where the target molecule is embedded. Here, we present a high-throughput *in silico* screening of all potential networks of three interacting nodes to study the effect of the initial conditions of the network in the efficiency of a given drug treatment. Our study shows that most network topologies can induce multiple dose-response curves, where different initial conditions can enhance, reduce or even suppress the effect of treatment. The type of dual response observed depends on how the potential bistable regimes interplay with the inhibition of one of the nodes inside a nonlinear pathway architecture. We propose that this dependence of the strength of the drug on the initial state of activation of the pathway may be affecting the outcome and the reproducibility of drug studies and clinical trials.

Introduction

Some of the main potential contributions of Systems Biology to the field of Pharmacology are to help design better drugs [10, 26]), to find better targets [21] or to optimize treatment strategies [11]. To do that, a number of studies focus on the architecture of the biomolecular interaction networks that regulate signal transduction and how they introduce ultrasensitivity, desensitization, adaptation and even oscillatory dynamics [31, 15]. To identify the source of these effects, large scale signaling networks are often dissected into minimal sets of recurring interaction patterns called network motifs [23], which can be understood using computational and analytical tools. Many of these motifs are nonlinear, combining positive and negative feedback and feed-forward loops that introduce a rich variety of dynamic responses to a given stimuli.

In the context of protein-protein interaction networks, these loops of regulation are mainly based on interacting kinases and phosphatases. The strength of these interactions can be modulated by small molecules that can cross the plasma membrane [5] and block the activity of a given kinase in a highly specific manner [4]. Inhibition of a dysfunctional component of a given pathway via small-molecule inhibition has been successfully used to treat several diseases, such as cancer or auto-immune disorders. Nowadays, 31 of these inhibitors are approved by the FDA, while many more are currently undergoing clinical trials [36].

Characterization of inhibitors and its efficiency and specificity towards all human kinases constitutes a highly active area of research [13, 24, 18]. Importantly, since these inhibitors target interactions that are embedded in highly nonlinear biomolecular networks, the response to treatment is often influenced by the architecture of the network. For instance, treatment with the mTOR-inhibitor rapamycin induces reactivation of the Akt pathway due to negative feedback regulation via IRS1, upstream of Akt [34]. In addition, this nonlinear interplay induces a new steady state in the pathway with high Akt phosphorylation on T308 but not S473. [25].

In addition, the nonlinear interactions in the MEK/ERK pathway have been shown to induce different modes of response to inhibition [33], and even bimodal MAP kinase (ERK) phosphorylation responses after inhibition in T-lymphocytes [3]. The same interplay between positive and negative feedbacks induces ERK activity pulses, with a frequency and amplitude that can be modulated by EGFR (epidermal growth factor receptor) and MEK (Mitogen-activated protein kinase kinase) inhibition, respectively [1].

One of the basic characteristics that nonlinear interactions can induce in a system is multi-stability, commonly associated with the presence of a positive or a double negative feedback loop in the network. Bistability has been observed *in vitro* [32, 22], *in vivo* [12, 19], as well as in synthetic circuits [8, 6]. In the context of biological networks and drug treatment, multi-stability also induces dependence on initial conditions, i.e., the same concentration of a given drug may result in different responses, depending on the initial state of the system.

In general, an accurate prediction of the efficiency of a given drug treatment requires quantitative values for all kinetic constants involved, as well as the concentration of each protein. As argued above, the architecture of the network is also relevant, since the dynamics of deactivation and activation depends strongly on the topology of the interactions [2, 21]. Here, we investigate whether the initial conditions of activation or deactivation in the proteins in a system also influence drug treatment efficiency. To do that, we set a computational high-throughput screening to explore all possible 3-node network topologies and monitor the response to inhibition. Starting from two different initial conditions, we generate two dose-response curves for each set of parameter values. The comparison of these two curves allows us to characterize each network topology in terms of its impact in the outcome of drug inhibition. Using this approach, we found novel types of response, suggesting that the topology of the network of interactions can induce complex dose-response curves, increasing, decreasing or even disrupting the strength of inhibition. Our results reveal that the initial state of the system determines the efficiency of a given drug in most of the possible networks topologies, suggesting that this may compromise the reproducibility of *in vitro* and *in vivo* studies that involve inhibitory treatments.

Materials And Methods

To study all potential network topologies that induce multiple dose-response curves and their dependence on initial conditions, we set up a high-throughput approach that explores all possible connections between

an input, a target and an output node, including positive and negative feedback auto-regulation (see Figure 1). This computational screening is inspired by previous studies that focus on network topologies inducing adaptation [20], bistability and ultra-sensitivity [27]. Our approach introduces the effect of a drug inhibitor in one of the nodes of the network, and focuses mainly on the characterization of the effect of the network in shaping the response to the inhibition.

The core network is composed of three main components: an input node that receives a constant external stimulus, a target node that is inhibited by the drug, and the output node, which is used as a readout of the system activity. Details of the dynamics of the interaction between the nodes and automatization of the screening are described in the Supplementary Material. In brief, the set of interactions can be generalized in the following equation:

$$\frac{\partial X_j}{\partial t} = \sum_{i=1}^{9} (\delta_{(I_{i,j})(1)} \frac{(1 - X_j) \cdot X_i \cdot k_{i,j}}{K_{i,j} + 1 - X_j} - \delta_{(I_{ij})(-1)} \frac{X_i \cdot X_j \cdot k_{i,j}}{K_{ij} + X_j}) \tag{1}$$

where X_j is the state vector that contains the concentration of the active version of the 9 interacting species (X_1 for input, X_2 for the target and X_3 for output), a background activator (X_4,X_5,X_6), and a deactivator (X_7,X_8,X_9) enzyme for each of them. Parameters $k_{i,j}$ and $K_{i,j}$ correspond to the catalytic and Michaelis-Menten constants for the activation or deactivation of X_j by X_i. I_{ij} are the components of the interaction matrix, which defines interactions between the nodes. Here, a given component I_{ij} of the matrix is zero if X_i does not affect X_j, 1 if the X_i activates X_j and -1 if X_i deactivates X_j. $\delta_{(I_{ij})(1)}$ and $\delta_{(I_{ij})(-1)}$ are Kronecker delta functions that are 1 when the value I_{ij} is 1 or -1, respectively. This way, the left part of the sum is nonzero when the component X_i activates X_j, while the right side is nonzero when X_i deactivates X_j.

Values of the interaction matrix $I_{i,j}$ are set to represent all possible interactions between input, target and output (see Supplementary Material). To ensure that each node receives at least one activating and one deactivating interaction, the required background enzymes (X_4...X_9) are automatically set for each of the 5103 possible network topologies.

The effect of inhibitor is incorporated as a Hill function, assuming fast dynamics of binding and unbinding to its target (quasi-steady state approximation) (see Supplementary material). Considering this, X_2 is substituted by the expression $X_2/(1 + (K_a \times inh))$ when $i = 2$ in Eq. 1 (i.e., whenever X_2 acts as an activating or deactivating enzyme). This way, the effect of the inhibitor can be directly incorporated into the equations independently of the architecture of the network, strongly facilitating the screening process. This approach excludes from our screening all topologies where X_2 autoregulates itself (see Supplementary Material).

To characterize the dependence on initial conditions, we proceed as follows (see Fig. 1): For each particular network topology, all components $k_{i,j}$ and $K_{i,j}$ of the catalytic and Michaelis-Menten constant matrices are randomly set between a desired range of values (see Supplementary Material). Then, the system is numerically solved for two different constant concentrations of inhibitor (low and $high$) until a steady state is reached. The two resulting sets of concentrations for input, target and output for low and high inhibitor are used as initial conditions $IC_{low} = [X_1^f, X_2^f, X_3^f]_{low}$ and $IC_{high} = [X_1^f, X_2^f, X_3^f]_{high}$ for numerical simulations where different concentrations of inhibitor are applied. For each simulation, a new steady state is reached, labeled as $SS_{low} = [X_1^f, X_2^f, X_3^f]_{low}$ and $SS_{high} = [X_1^f, X_2^f, X_3^f]_{high}$ where the subindexes low and $high$ refer to the initial condition used in the simulation. This is repeated for different constant concentrations of inhibitor to ultimately draw dose-response curves of the output of the network X_3^f against the inhibitor concentration. Finally, the two generated dose-response curves DS_{low} and DS_{high} are analyzed, compared and classified.

This process is repeated for each network topology 10000 times for different sets of parameters to sample the phase space and determine regions where the treatment depends on initial conditions. Based on this, all network topologies are classified depending on the relationship between the two dose-response curves. This way, if both curves DS_{low} and DS_{high} are identical, the response of the inhibitor does not depend on the initial conditions, while if the two curves are different, this means that the effect of the inhibitor is dependent on the initial state of activation of the system.

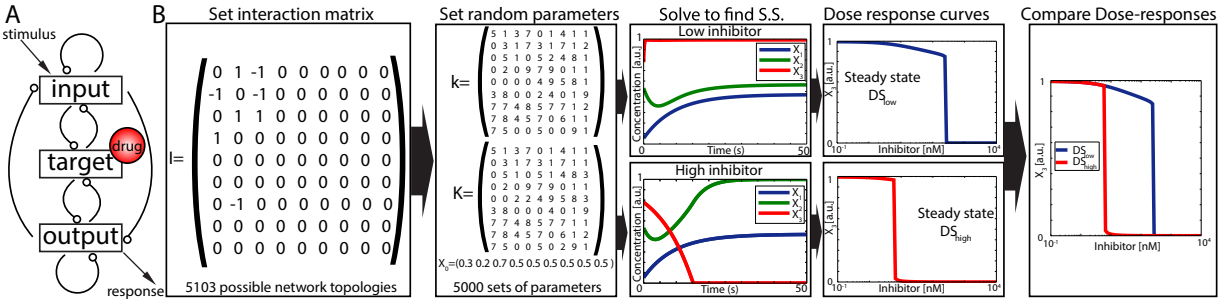

Figure 1: **Scheme of the workflow for the high-throughput analysis**. (A) Scheme of network with all possible interactions between input, target, and output. (B) For each possible interaction matrix, we sample the parameter space by randomly generate 10000 sets of parameter values for the catalytic (k), Michaelis-Menten (K) matrices, and for initial values of active input, target and output (X_1^0, X_2^0, X_3^0). For each of these parameter sets, we numerically solve the system for two different inhibitor concentrations (low and $high$). The two steady states are used as initial conditions for numerical simulations with several concentrations of inhibitor. The steady state value of the output node (X_3) is plotted against the inhibitor concentration to generate dose-response curves DS_{low} and DS_{high}. Finally, both dose-response curves are compared.

Results

The strength of inhibition depends on the initial conditions for most of the networks.

At first inspection, our screening reports differences between the two dose-response curves for around 80% of all network topologies. This suggests that, for a region in the parameter space, the efficiency of the inhibition depends on the initial conditions for most of the possible three-node network topologies. The percentage of networks where the two dose-response curves do not coincide increases with the connectivity of the network, as shown in Fig. 2 (blue bars and left vertical axis), up to 97% for networks with 8 links between input, target and output (251 of all possible 256 networks of 8 links in our study). The percentage of simulations that show multiple dose-response curves also increases with the number of links in the network (green bars and right vertical axis in Fig. 2) up to 5.5% for the more connected topologies. The existence of these dual dose-response curves is based on the presence of direct or indirect positive autoregulation in one or more nodes of the network. These nonlinear loops induce regions of bistability in the phase space, inducing a dependence of the strength of inhibition on the initial conditions of the system.

When comparing the effect of the initial steady state on the two dose-response curves, we can identify different scenarios of how the initial conditions affect the efficiency of the drug treatment. The most common scenario corresponds to a shift in the dose-response curve, i.e., when the initial condition changes, the efficiency of the inhibitor changes. This behavior is characterized by a shift in the $EC50$ of the dose-response curve (i.e., the concentration of inhibitor that induces a half-maximal effect in the output). An example of this type of response is illustrated in Fig. 3a-d. The typical dual response in this mode is shown in Fig. 3b, where the two dose-responsecurves for the two initial conditions IC_{low} and IC_{high} are plotted in blue (DS_{low}) and red (DS_{high}), respectively. For this network configuration and these conditions, the $EC50$ of the inhibitor changes around 1.5 orders of magnitude. This type of dependence on the initial conditions is simply a result of a bistable regime, as shown in the phase plane in Fig. 3c. Inside the bistable regime, the nullclines for the inhibitor concentration marked in Fig. 3b show two stable fixed points coexisting for the same conditions (blue and red circles), with each initial condition (IC_{low} and IC_{high}) evolving towards a different final steady state SS_{low} and SS_{high}. Fig. 3d shows the bifurcation diagram with two stable branches that coexist for a particular range of values of inhibitor. Supp. Movie 1 is an animation of how the two initial conditions transit to their corresponding steady states for increasing concentrations of the inhibitor.

Another common scenario corresponds to one of the dose-response curves showing a standard response to treatment, while the other is not responding for the same range of concentrations of inhibitor. An example of this dual two dose-response curves is shown in Fig. 3f for the network illustrated in Fig. 3e.

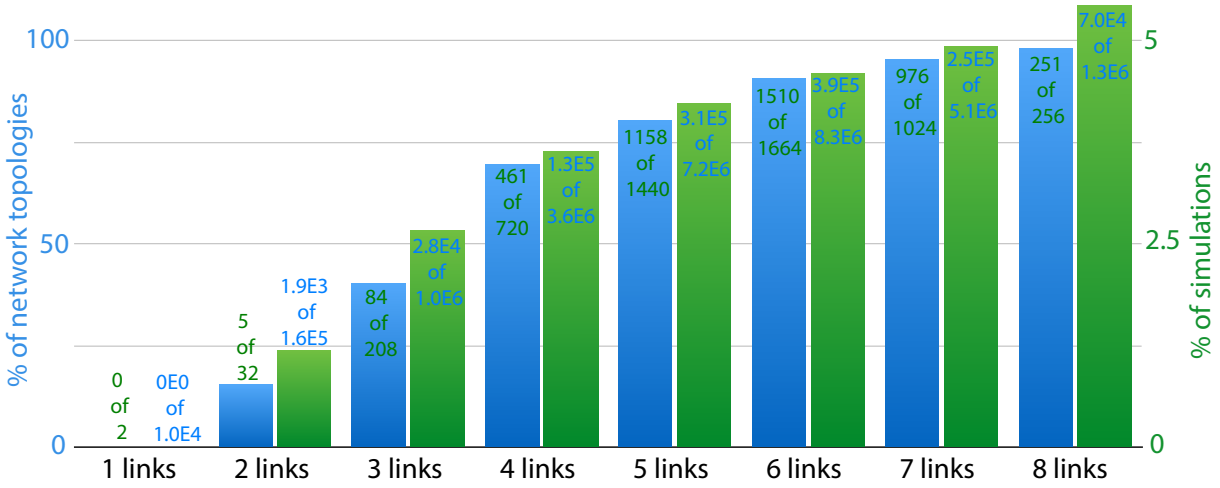

Figure 2: **The percentage of cases with multiple dose-response curves to inhibition increases with the network connectivity**. Blue bars correspond to the percentage of network topologies (left vertical axis) and green bars correspond to the percentage of simulations (right vertical axis). Values in each bar illustrate the number of positive cases over the total number of cases.

In this scenario, the inhibitor acts as an activator of X_3 when we start from IC_{low}, but if the system starts from IC_{high}, it remains insensitive to changes in the concentration of inhibitor. This occurs when one of the two stable branches in the bifurcation diagram (Fig. 3h) is stable for all the range of inhibitor concentration tested, so X_3 cannot switch from the upper to the lower stable branch when the concentration of inhibitor is reduced.

Alternatively, different initial conditions can also switch the effect of a given drug. For instance, the same treatment can result in inhibition or activation of the output signal, simply depending on the initial conditions. An example of this behavior is shown in Fig.3i-l. The two dose-response curves in Fig. 3j for the network in Fig. 3i show one of the curves (DS_{low}) increasing when we increase the concentration of inhibitor, while the other (DS_{high}) decreases in X_3 when the inhibitor increases. The phase diagram (Fig. 3k) for intermediate values of the inhibitor shows also two stable fixed points while the bifurcation diagram (Fig. 3l) shows the shape of the two stable branches, with the upper one decreasing and the lower one increasing due mainly to a transition from a bistable to a monostable regime with higher X_3. This discontinuous jump in the dose-response curve is less pronounced for networks with higher connectivity, but we selected this example since its simplicity allows us to illustrate its nullclines in a two-dimensional phase plane, instead of a three-dimensional plot.

Different initial conditions can induce increased or decreased treatment efficiency

Among all motifs that induce multiple dose-response curves, we can further characterize the topologies in terms of the comparison between the two curves with respect to the two initial conditions. The most common scenario corresponds to the situation illustrated in Fig. 3b, where the less sensitive curve (higher $EC50$) corresponds to the initial condition of low inhibitor IC_{low}, and the more sensitive curve occurs when the system starts from high inhibitor IC_{low}. This increased sensitivity at intermediate concentrations of inhibitor occurs whether the treatment results in deactivation (as in Fig. 3b) or activation (as in Supp. Fig. 3b) of the target. This situation occurs because, in the bistable regime, each initial condition IC_{low} and IC_{high} evolves to its closest steady state in the parameters space. An animation of how the steady states change for the two initial conditions when the concentration of inhibitor is increased is presented as Supp. Movie 1.

Several network topologies also exhibit a different scenario, characterized by an inversion in the sensitivity of the treatment between the two dose-response curves. This scenario is presented in Fig. 4b), and shows the red (DS_{high}) and blue curves (DS_{low}) swapped compared to Fig. 3b. In this particular scenario, the IC_{high} has a reduced final X_3 compared to IC_{low} (red and blue circles in Fig. 3c), but, for intermediate

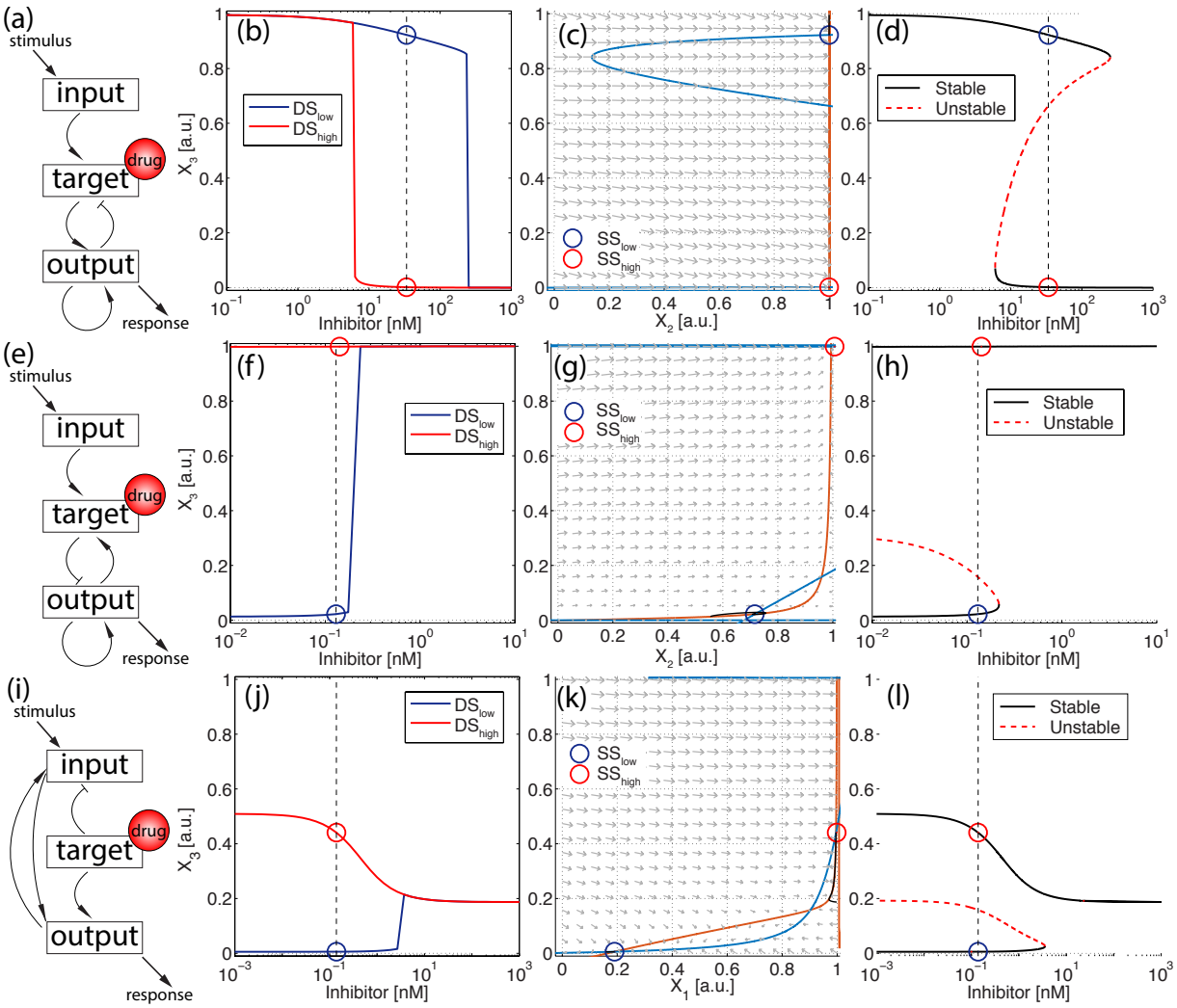

Figure 3: **The effect of initial conditions can shape the dose-response curve in different ways.** (a-d) Shift in the EC50, (e-h) insensitization of one of the dose-response curves, (i-l) Switch in the effect of the drug. Panels (a,e,i) represent the network topologies for each mode. Arrows represent positive interactions (activation) and no-arrow represents negative interaction (de-activation). Panels (b,f,j) represent the dose-response curves DS_{low} (blue) and DS_{high} (red) for initial conditions IC_{low} and IC_{high}, respectively. The rest of parameter values are the same between the two curves. Blue and red circles SS_{low} and SS_{high} represent the steady state solutions for a given concentration of inhibitor. Panels (c,g,k) show the phase plane with vector field and nullclines (nullclines for X_3 in blue and nullclines for X_2 (c,g) and X_1 (k) in orange), representing the two steady states SS_{low} (blue) and SS_{high} (red) respectively. Panels (d,h,l) show the bifurcation diagram of X_3. Black curves are the stable branches and the dash red curve is the unstable branch.

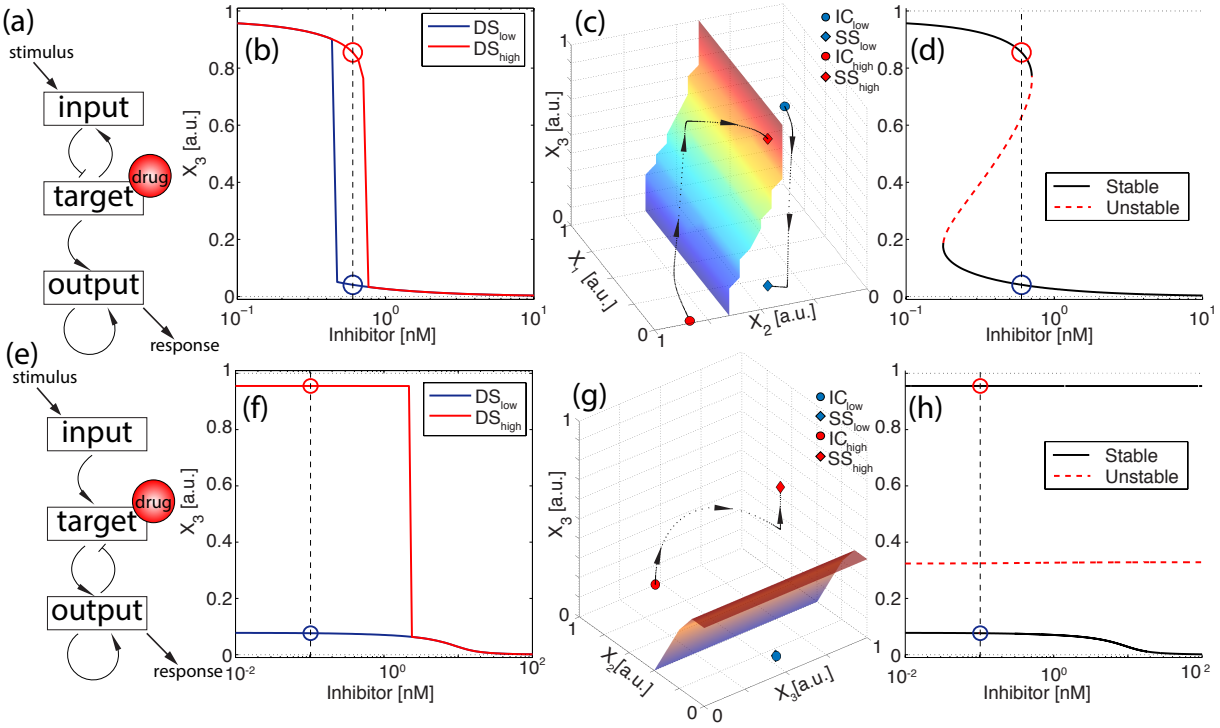

Figure 4: **The network architecture can induce inverse bistability**. (a-d) Shift in the EC50. (e-h) Insensitization of one of the dose-response curves. Panels (a,e) represent examples of network topologies that show two different cases of inverse bistability. Panels (b,f) represent the dose-response curves DS_{low} (blue) and DS_{high} red for initial conditions IC_{low} and IC_{high}, respectively. The rest of parameter values are the same for the two curves. Blue and red circles SS_{low} and SS_{high} represent the steady state solutions for a given concentration of inhibitor. Panels (c,g) represent the three-dimensional phase plane, with the trajectories of each simulation starting from each of the two initial conditions, and the separatrix between the two basins of attraction. Panels (d,h) show the bifurcation diagram of X_3. Black curves are the stable branches and the red dash curve is the unstable branch.

values, higher X_3 transits to a steady state with low X_3, while the lower X_3 evolves to a steady state with high X_3 (blue and red rhombus in Fig. 3c). This is clearly shown by the trajectories (black dotted lines) corresponding to two simulations with the same exact parameter values, but starting from the two different initial conditions (IC_{low} and IC_{high}).

In terms of the effect of drug treatment, starting from a fully inhibited situation (IC_{high}) reduces the efficiency of the drug, compared to the non-inhibited initial condition (IC_{low}). In other words, the $EC50$ of DS_{high} is now higher than DS_{low}, as shown in Fig. 3b. This contrasts with the scenario of Fig. 3b, where the $EC50$ of the drug is lower for DS_{high} compared to DS_{low}. To understand this behavior, we plot the three-dimensional separatrix between the two basins of attraction of the bistable regime in Fig. 4c. Since the separatrix divides the phase space vertically, the initial states $EC50$ of DS_{high} are forced to perform a long transition in X_3 concentration towards the steady state in its basin of attraction. This is translated into a shift in the dose-response curves in the bistable regime, and therefore, an increase in the $EC50$ when the system is initially inhibited.

Since now each initial condition IC_{low} and IC_{high} does not transit to its closest steady state, but instead it evolves to the steady state that is further away in X_3 concentration, we will refer to this scenario as inverse bistability. Supp. Movie 2 is an animation of how the two initial conditions transit to their corresponding steady state for increasing concentrations of the inhibitor. This inversion of the bistable solutions, can also occur in conditions where the inhibitor is acting as an activator of the output node, as illustrated in Supp. Fig. 4b.

Analog to the situation of Fig. 3e-h where the dose-response curve (DS_{high}) becomes insensitive to the drug, other topologies present the opposite scenario, i.e., the DS_{high} responds to the drug but the DS_{low} is insensitive. This scenario is illustrated in Fig. 4f for the network topology of Fig. 4e. Here, DS_{low} responds by reducing X_3 activation in less than 10%, while if we start from the highly inhibited initial condition IC_{high}, the dose-response curve (DS_{high}) shows a much stronger inhibition of the output. Fig. 4g plots the three-dimensional phase space for a particular inhibitor concentration in the bistable regime. Again, the separatrix divides the space in such a way that the initial IC_{high} transits to the steady state SS_{high} with higher X_3.

The network architecture can induce inverse hysteresis loops

As discussed above, the appearance of inverse bistability is based mainly on the interplay in phase space between the initial conditions and the basins of attraction of the two final steady states. Nonetheless, our screening revealed another family of topologies that show an equivalent scenario (i.e., initial states transit to the farthest final steady state), but based on a different underlying mechanism. An illustrative example of this behavior is shown in Fig. 5. The first example corresponds to a network topology of four links that shows inverse bistability as defined in the previous section, i.e, two dose-response curves where the DS_{high} has a higher $EC50$ than DS_{low}. Luckily, since X_2 does not receive input from X_1 and X_3, the phase space is plotted in two dimensions to show the nullclines and the vector field (Fig. 5c). For a concentration of inhibitor inside the bistable domain, we observe the two stable states, and the separatrix dividing vertically the phase plane. Interestingly, the bifurcation diagram in Fig. 5d shows a more complex configuration than in Fig. 4d, with the two stable branches now extending from low to high X_3. This configuration induces another interesting property to these types of networks: Inverse bistability does not only occur when we start with fixed initial conditions, but also if the concentration of the inhibitor is gradually increased or decreased from each initial condition. In other words, if the concentration of inhibitor is adiabatically varied, the system follows a hysteresis loop that is reversed compared to the normal hysteresis observed in magnetism, optical and other physical systems. To illustrate that, we developed an animation where the concentration of inhibitor is gradually increased and decreased, and the evolution of steady states form an inverse hysteresis loop (Supp. Movie 4).

To understand the interactions that induce this inverse hysteresis response, we compared (Fig. 5e) 100 different sets of parameters in a box plot where this topology produces normal (orange) and inverse bistability (blue). This plot allows us to see that most values show overlapping distributions for both types of bistability, while two of them are clearly separated (K_{23} and k_{13} for this particular network). Next, dose-response curves are generated by changing these two parameters between their average values that produce normal or inverse bistability (the rest of parameters are fixed and correspond to the average of the mean for both orange and blue distributions). This analysis reveals that K_{23} mainly affects the response of X_3 in the range of low inhibition, k_{13} mainly affects the steady state in the range of high inhibition, while the intermediate bistable region remains almost unchanged. When we vary both simultaneously (Fig. 5f), we clearly observe that these changes in low and high range of inhibitor interplay to change the nature of the drug from inhibitor to activator of the node X_3.

This sequence also illustrates how, changing a set of parameters to reverse the effect of the inhibitor, while maintaining a bistable region at intermediate inhibitor concentrations, the systems go from normal to inverse bistability. To do that in this particular topology, the strength of the interaction between X_1 and X_3 is reduced, while the interaction between X_2 and X_3 goes from a linear to a unconstrained regime. A different topology with a similar mode of response, and similar transition from normal to inverse bistability is shown in Supp. Fig. 6.

Another example of a network topology able to produce inverse bistability and inverse hysteresis is shown in Fig. 6, with a different configuration of the dose-response curves (Fig. 6b), nullclines (Fig. 6c) and bifurcation diagram (Fig. 6d). The box plot in Fig. 6e again shows two distributions of parameters that do not overlap for both normal (orange) and inverse (blue) bistability (K_{13} and K_{23}). In this particular scenario, the normal bistability is irreversible (as in Fig. 3f), i.e., X_3 is insensitive to changes in the inhibitor for one of the initial steady states. Again, the Michaelis-Menten activation of X_3 by X_1 changes from saturated to linear, affecting mainly the dose-response curves at high inhibitor concentrations. On the other hand, the activation of X_3 by X_2 becomes saturated, mainly affecting the regime at low inhibitor concentrations. Combination of these two effects, while maintaining a bistable regime at intermediate inhibitor concentrations, is able to

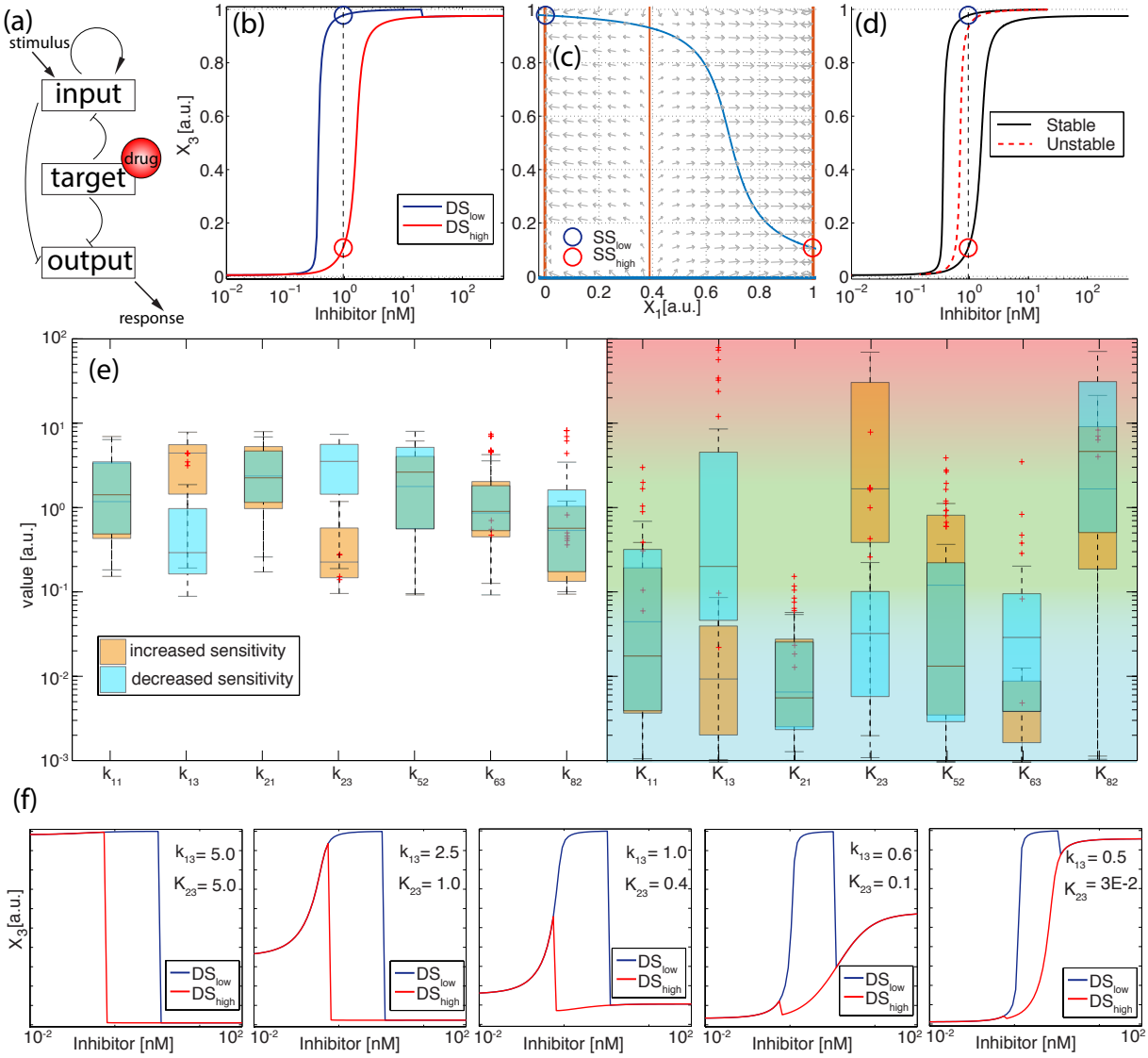

Figure 5: **The network architecture can induce inverse hysteresis**. (a) Example of a network architecture that induces inverse hysteresis. (b) Dose-response curves DS_{low} (blue) and DS_{high} red for initial conditions IC_{low} and IC_{high}, respectively. The rest of parameter values are the same between the two curves. Blue and red circles SS_{low} and SS_{high} represent the steady state solutions for a given concentration of inhibitor. (c) Phase plane with vector field and nullclines (nullclines for X_1 in orange, nullcline for X_3 in blue), representing the two steady states SS_{low} (blue) and SS_{high} (red) respectively. (d) Bifurcation diagram of X_3. Black curves are the stable branches and the red dash curve is the unstable branch. (e) Box plot for all parameter sets that show normal and inverse hysteresis. Blue, green and red background represents the saturated, unconstrained and linear regimes of the Michaelis-Menten kinetics, respectively. (f) Changes in the dose-response curves when two parameters are varied from normal to inverse hysteresis conditions.

transform an irreversible bistability to an inverse bistability. Fig. 6f shows the evolution of the dose-response curves when K_{13} and K_{23} are simultaneously changed from their average value at normal and inverse bistability (the rest of parameters are kept constant and correspond to the average of the means of the two distributions).

An overall characterization of the topologies reveals the minimal motifs that exhibit inverse bistability.

To characterize the basic ingredients underlying the inverse bistability illustrated in Fig. 5 and 6, we proceed to analyze all potential topologies that exhibit this behavior and find relationships and similarities between them. When grouped by number of links, we observe that the percentage of networks that exhibit inverse bistability increases with the connectivity of the network (yellow columns in Fig. 7a). To determine the minimal ingredients for inverse bistability, we represent in Fig. 7b an atlas that correlates topologies by their architecture, identifying topologies that contain another topology of lower connectivity. This representation allows us to isolate 19 minimal motifs of 4 links that are contained in almost all the higher connected topologies that show inverse bistability. These 19 minimal motifs are represented in Fig. 7b as matrix plots (the three first rows and columns of the interaction matrix) are represented as follows: white is "1" (activation), black is "-1" (deactivation) and grey is "0" (no interaction). The 4-link topologies that can also induce an inverse hysteresis loop are highlighted in red. In the row below, these 19 topologies are grouped in sets that only differ by two interactions (a given topologies can belong to different sets).

For all the topologies of four links, we always observe a combination of positive and negative interactions (i.e, no networks where all interactions are positive or negative). In addition, all topologies contain at least a positive feedback that can be direct or indirect (i.e, the self-activation of a node involves another node of the network). The negative interaction can take the form of an indirect feedback loop (as in Fig. 6a), an incoherent feed-forward loop, or not being part of a loop at all (as in Fig. 5a). We have found topologies where the interactions modulated by the inhibitor can either influence the positive, the negative feedback and feedforwad loops, and even several of them simultaneously. We suggest that inverse bistability results from the interplay between the positive feedbacks (that generates the bistability) and the negative interactions that shape the basins of attraction. Additionally, the inhibitor has to directly or indirectly affect the positive feedback and induce a change between the two stable states at a given concentration.

Discussion

In this paper, we present the first global analysis to study how the network topology influences a given drug treatment. To do that, we focus on small network motifs of three interacting nodes where one of the nodes is the target of a small molecule inhibitor. To characterize the effect of the network topology, we compare the dose-response curves of the same drug treatment starting from two different initial conditions in the activity of the network. Our analysis reveals that the initial conditions affect the efficiency of the treatment in most network topologies of three nodes. This dependence is translated into modifications in the dose-response curves and changes in the $EC50$ as well as in the overall effect of the inhibitor.

Our analysis shows that this can occur in the majority of topologies of three nodes. Moreover, we found network configurations that show a novel behavior characterized by the inversion of the steady states respect to the initial conditions. In some conditions, this “inverse bistability” of the target node can also result in “inverse hysteresis loops”, where the reduction of the efficiency of the treatment also occurs when the concentration of inhibitor is varied gradually. Finally, our study shows that most of the topologies that show this inverse bistability and hysteresis contain core motifs of four links composed by a positive feedback and a negative regulation.

The design of the workflow mimics the experimental methodology to determine dose-response curves, where serial dilutions of the drug are administered to equivalent samples in equivalent initial conditions. This workflow is different from the typical studies of bistability in physical and chemical systems [32, 22], where an input parameter is gradually increased or decreased (i.e., the initial condition for each point in the curve is the previous point in the analysis). The fact that all the points in a dose-response curve have the same initial condition influences how the bistable nature of a given network affects the treatment. Nonetheless, some

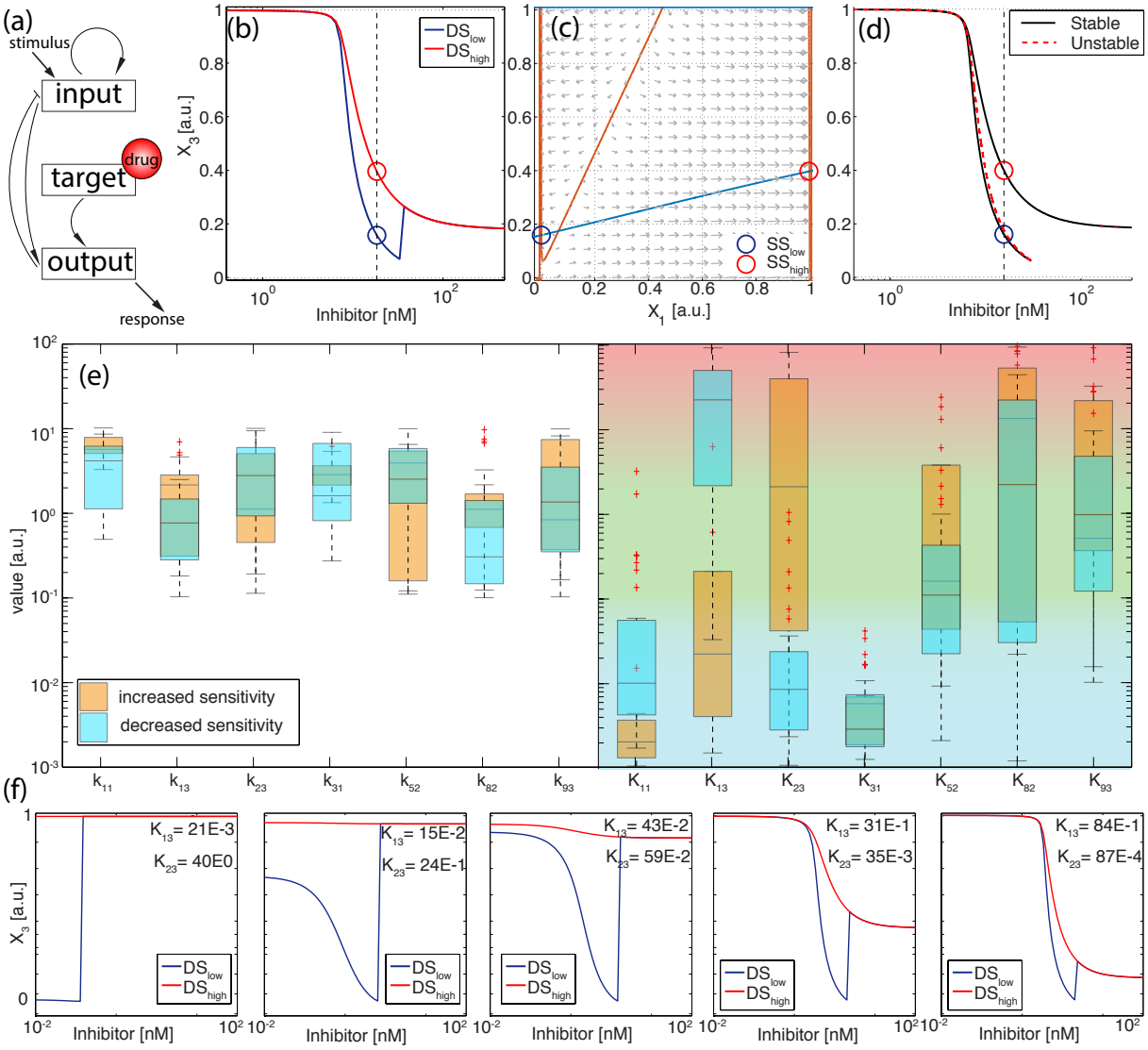

Figure 6: **The network architecture can induce inverse hysteresis**. (a) Example of a network architecture that induces inverse hysteresis. (b) Dose-response curves DS_{low} (blue) and DS_{high} red for initial conditions IC_{low} and IC_{high}, respectively. The rest of parameter values are the same between the two curves. Blue and red circles SS_{low} and SS_{high} represent the steady state solutions for a given concentration of inhibitor. (c) Phase plane with vector field and nullclines (nullclines for X_1 in orange, nullcline for X_3 in blue), representing the two steady states SS_{low} (blue) and SS_{high} (red), respectively. (d) Bifurcation diagram of X_3. Black curves are the stable branches and the red dash curve is the unstable branch. (e) Box plot for all parameter sets that show normal irreversible bistability and inverse bistability. Blue, green and red background represents the saturated, unconstrained and linear regimes of the Michaelis-Menten kinetics, respectively. (f) Changes in the dose-response curves when two parameters are changed from normal irreversible bistability to inverse bistability conditions.

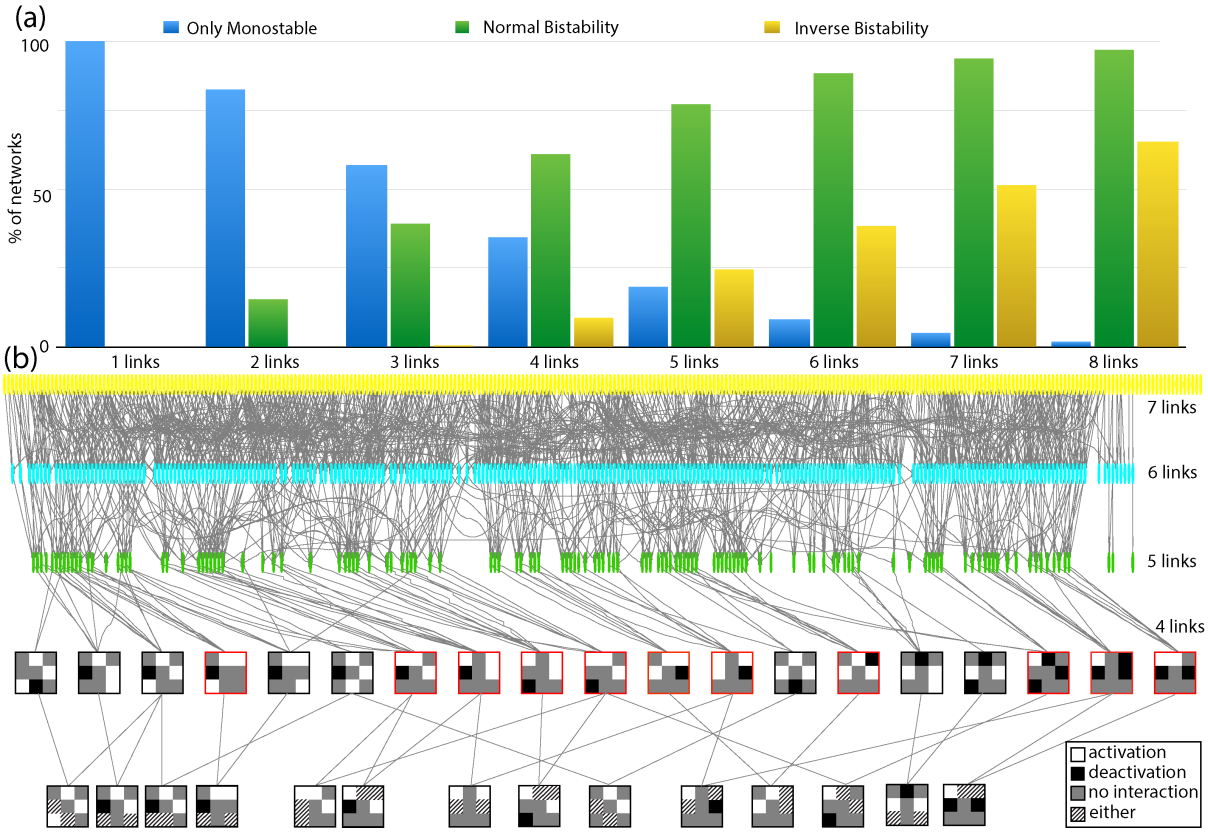

Figure 7: **Characterization of reverse bistability and reversed hysteresis**. (a) The percentage of topologies that show inverse bistability increases with the network connectivity. Blue bars correspond to the percentage of topologies with the same dose-response curve for both initial conditions; green and yellow bars correspond to the percentage of topologies that show increase or decrease of the EC50, respectively. (b) Atlas for all network topologies that induce inverse bistability. Circles represent each of the topologies where our screening has shown inverse bistable response to drug treatment. Networks of different connectivity are represented in different colors. Gray lines link topologies that contain another topology of lower connectivity. Networks of lower connectivity are represented as matrixplots for the interactions, where white represents activation, black is deactivation and grey means no interaction. These minimal networks are then grouped in families where just one or two interactions change. Matrix plots highlighted in red correspond to topologies that can also produce inverse hysteresis loops.

topologies also show inverse bistability when the inhibitor is gradually increased or decreased, generating inverse hysteresis loops.

When comparing dose-response curves in normal bistability, DS_{high} has increased sensitivity (reduced $EC50$) compared to DS_{low}, while in conditions of inverse bistability, DS_{high} has decreased sensitivity (increased $EC50$) compared to DS_{low}. This reduction in sensitivity is very different from the well-studied homologous or heterologous desensitization after repeated or prolonged receptor stimulation [14, 29]. Receptor desensitization is achieved mainly by negative feedback loop that reduces the number or the efficiency of receptors on the cell surface after a initial stimulation [16, 17]. This is translated into a initial strong transient activation of the targets downstream, while a second application of the stimulus does not show the same transient activation. While receptor desensitization focuses on transients responses, inverse bistability refers to the final steady state of the network.

Our study is limited to topologies of three main nodes that play different roles in the network, in an attempt to identify the minimal motifs that induce these dual dose-response curves. In principle, our results also apply to more larger networks with increasing number of nodes that interact linearly, since linear protein-protein interactions can be reduced to smaller networks with equivalent dynamics without reducing the spectrum of reported behaviors [2, 21, 35]. In larger networks with more nonlinear interactions, we expect a similar or even higher dependence on initial conditions, since our analysis shows that the percentage of the networks with multiple dose-response curve increases with the connectivity of the network.

The characterization of the effect of a drug starts with an accurate and reproducible *in vitro* or *in vivo* dose-response curve to establish the optimal dose or the optimal schedule or treatment. The fact that, for most topologies, different initial conditions give different dose-response curves may compromise the reproducibility of drug treatment between biological samples or even patients. In conclusion, when designing drugs and treatments that target proteins embedded in highly inter-connected networks such as signal regulatory pathways, the efficiency of a given compound cannot be predicted if the initial state of activation of the network is not known.

Acknowledgements

This work has been supported by the Ministry of Science and Technology of Spain via a Ramon y Cajal Fellowship (Ref. RYC-2010-07450), a grant from Plan Nacional framework (Ref. BFU2011-30303 and & BFU2014-53299-P) and a FPU fellowship. We thank Raul Guantes, Juan Diaz Colunga, Rosa Martinez Corral, Saul Ares, Katherine Gonzales and Jordi Garcia Ojalvo for invaluable help and technical assistance.

Author Contributions

DGM and VDM: Designed research, performed research, wrote the manuscript.

Supplementary Material

High-throughput *in silico* screening of three-node networks. All programs and scripts have been developed in-house using Matlab© (The Mathworks©, Natick, MA). Code available as Supplementary Material.

This computational high-throughput screening strategy is inspired on previous studies focused on network topologies that induce adaptation [20], bistability and ultrasensitivity [27]. The network is composed of three interacting nodes: an input node, which receives a constant stimulus, a target node that is affected by the presence of the inhibitor, and the output node, which serves as a readout of the network activity. We use a Michaelis-Menten type of interaction kinetics [7] between these three nodes that can result in activation or de-activation of each other. We also allow direct positive and negative feedback in input and output nodes, and indirect feedback and feed-forward loops between all nodes. For simplicity, X_1 is defined as the concentration of the active form for the input node, X_2 for the target and X_3 for the output. We use normalized values for the total concentration thus, $1 - X_1$ is the concentration of the inactive form of the

input node, $1-X_2$ for the target and $1-X_3$ for the output. The conversion between both states is reversible. The set of interactions is therefore simplified as one single equation:

$$\frac{\partial X_j}{\partial t} = \sum_{i=1}^{9} (\delta_{(I_{i,j})(1)} \frac{(1-X_j)\cdot X_i \cdot k_{i,j}}{K_{i,j}+1-X_j} - \delta_{(I_{ij})(-1)} \frac{X_i \cdot X_j \cdot k_{i,j}}{K_{ij}+X_j}) \tag{2}$$

As explained in the main text, X_j is the state vector (X_1 is the concentration of active input, X_2 is the target and X_3 is the output, X_4, X_5, X_6 are the background activators, and X_7, X_8, X_9 are the background de-activators for input, target and output, respectively).

These background enzymes (X_4,...,X_9) are incorporated to provide a constant stimulus to balance the activating or deactivating effect of the other nodes of the network when they do not receive an activating or deactivation interaction. This way, when a given node X_i does not receive a deactivating interaction from either itself or the other nodes, a background enzyme X_j is automatically added to compensate this, otherwise the node will be always in its active form ($X_i = 1$). The same occurs when a node does not receive an activating interaction (a deactivating background reaction is automatically set). For simplicity, the concentration of all background enzyme is fixed at 0.5 (a.u.).

Parameters $k_{i,j}$ and $K_{i,j}$ are the components of the k and K matrices, corresponding to the kinetic rate and Michaelis-Menten constants for the interaction of X_i on X_j. For each given topology, we generate 10000 different k and K matrices where each component of the matrix is obtained from a uniform distribution in logarithmic scale between values 0.1 and 10 for $k_{i.j}$, and between 10^{-3} and 10^2 for the Michaelis-Menten constant ($K_{i,j}$). Taking into account that the concentration of all substrates is normalized to 1, the range for the Michaelis-Menten constant allows us to sample the regime of saturated $K_{ij} << 1$, unconstrained $0.1 < K_{ij} < 1$ and linear $K_{ij} >> 1$ regimes for the Michaelis-Menten dynamics. The kinetics for three values illustrating these regimes are plotted in Supp. Figure 1a. These regimes are illustrated in the box plots in Figures 5, 6 and Supp. Figure 7 as blue, green and red background colors, respectively.

The interaction matrix I_{ij} defines the links between the nodes, and takes the following explicit form:

$$I = \begin{pmatrix} I_{1,1} & I_{1,2} & I_{1,3} & 0 & 0 & 0 & 0 & 0 & 0 \\ I_{2,1} & 0 & I_{2,3} & 0 & 0 & 0 & 0 & 0 & 0 \\ I_{3,1} & I_{3,2} & I_{3,3} & 0 & 0 & 0 & 0 & 0 & 0 \\ I_{4,1} & 0 & 0 & 0 & 0 & 0 & 0 & 0 & 0 \\ 0 & I_{5,2} & 0 & 0 & 0 & 0 & 0 & 0 & 0 \\ 0 & 0 & I_{6,3} & 0 & 0 & 0 & 0 & 0 & 0 \\ I_{7,1} & 0 & 0 & 0 & 0 & 0 & 0 & 0 & 0 \\ 0 & I_{8,2} & 0 & 0 & 0 & 0 & 0 & 0 & 0 \\ 0 & 0 & I_{9,3} & 0 & 0 & 0 & 0 & 0 & 0 \end{pmatrix}$$

This matrix is used to generate all networks between input, target and output relevant to our study. This way, a given component I_{ij} of the matrix is zero if X_i does not affect X_j, 1 if the X_i activates X_j and -1 if X_i deactivates X_j.

$\delta_{(I_{ij})(1)}$ and $\delta_{(I_{ij})(-1)}$ are Kronecker delta functions that are 1 when the value I_{ij} is 1 or -1, respectively. This way, the left part of the subtraction is nonzero when the component X_i activates X_j, while the right part is nonzero when X_i deactivates X_j.

Finally, a constant stimulus in the input node is set as a constant ligand stimulation upstream of the pathway. The dynamics of this stimulus is set as:

$$X_1(t) = X_1(0) - (1/e^{k\cdot t}) \tag{3}$$

The value at $t \to \infty$ is set at $X_1^0 = 0.5$, i.e, the stimulus is set to maintain a constant activation of the input node at intermediate levels. Therefore, the following term is added in its differential form to the node X_1 in all simulations:

$$dX_1/dt = (0.5 - X_1)\cdot k \tag{4}$$

For our simulations, the value of k is fixed at 0.1 [s^{-1}].

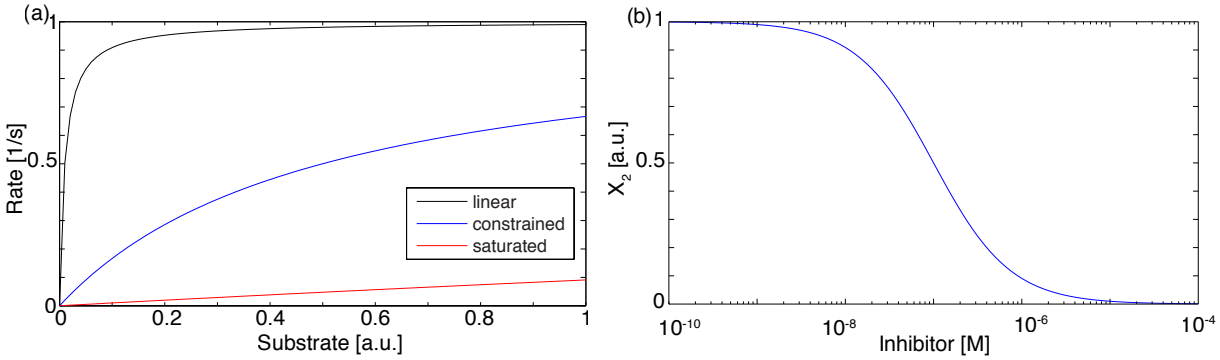

Supplementary Figure 1. (a) Profile of the dynamics of the amount of target in active form depending on the concentration of inhibitor. $k_+ = 10^7$ $[s^{-1}M^{-1}]$, $k_- = 1$ $[s^{-1}]$, (a) Profile of the rate of Michaelis-Menten kinetics for conditions of linear ($K_{ij} >> 1$ [M]), unconstrained ($0.1 > K_{ij} > 1$ [M]) and saturated ($K_{ij} << 0.1$ [M]) regimes.

Modeling Small Molecule Inhibition. Fundamentally, a chemical inhibitor acts by reversibly binding to its target to reduce or block its enzymatic activity [33], following the scheme:

$$[X_2] + [inh] \underset{k_-}{\overset{k_+}{\rightleftarrows}} [X_2 - inh] \tag{5}$$

that takes into account the reversible binding of inhibitor inh and its target X_2, to form a complex $X_2{-}inh$. Ideally, inhibitors should have high rates of binding (k_+) and slow rates of unbinding (k_-) to maximize residence time with the target enzyme [28]. If these values are around 10^6 $s^{-1}M^{-1}$ for k_+ and 10^{-2} s^{-1} for k_-, as reported form some small molecules inhibitors in the literature [30], equilibrium is reached within a few seconds. This equilibrium concentrations is:

$$[X_2 - inh]_{eq} = \frac{k_+}{k_-}[X_2]_{eq} \cdot [inh]_{eq} = K_A \cdot [X_2]_{eq} \cdot [inh]_{eq} \tag{6}$$

where $K_A = k_+/k_-$ is the association constant of the interaction. Typically, the amount of molecules present for the inhibitor is several orders of magnitude higher than the target (inhibitor is in the range of 10^{-9}... 10^{-6} M), so $[X_2 - inh]_{eq} << [inh]_{eq}$ [10]. In these conditions, we can safely assume that the concentration of inhibitor remains constant, so $[inh]_{eq} \approx [inh]_T$ (total concentration of inhibitor). Also, taking into account that $[X_2(0)] = [X_2 - inh]_{eq} + [X_2]_{eq}$, ($X_2(0)$ is the initial concentration of the active target node) we can rewrite Eq. 6 as:

$$[X_2(0)] - [X_2]_{eq} = K_A \cdot [X_2]_{eq} \cdot [inh]_T \tag{7}$$

that rearranging terms becomes,

$$[X_2]_{eq} = \frac{[X_2(0)]}{1 + K_A \cdot [inh]_T} \tag{8}$$

Which expresses the equilibrium concentration of the target X_2 in terms of the initial amount of target $X_2(0)$ and the concentration of inhibitor. The typical shape of this curve is shown in Supp. Fig. 1b.

We assume the general case of reversible non-competitive inhibition, i.e, the inhibitor is a small compound that binds to the active site of the target reducing its activity, without affecting the binding to its substrate. This way, the inhibitor does not affect the K_M of the interaction between enzyme and substrate. Under these conditions, in the presence of inhibitor, X_2 in Eq.1 can be substituted by its effective concentration, calculated via Eq. 8. This approximation allows us to automatically perform the screening of all possible topologies using the same set of equations independently of the interactions where X_2 is involved.

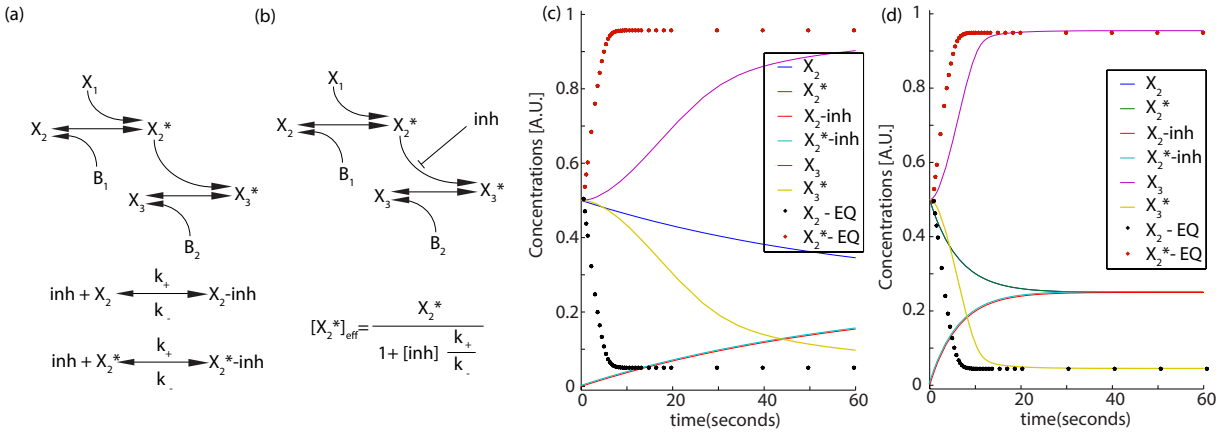

Supplementary Figure 2: Comparison of mass-action dynamics and quasi-steady state approximation for inhibitor concentration. (a-b) Scheme of interaction for the (a) mass action simulation and (b) quasi-steady state approximation. (c-d) Simulations for (c) slow and (d) fast dynamics of inhibitor binding. Solid curves correspond to mass action simulations, dotted curves correspond to the steady state assumption. Kinetic constants for slow binding: $k_+ = 8 \cdot 10^4\ s^{-1}M^{-1}$, $k_- = 8 \cdot 10^{-2}\ s^{-1}$. Kinetic constants for values of binding and unbinding similar to experimental data [30]: $k_+ = 8 \cdot 10^5\ s^{-1}M^{-1}$, $k_- = 8 \cdot 10^{-3}\ s^{-1}$.

To test the validity of this equilibrium approximation, we performed numerical simulations where we compared the dynamics of the activation of the output X_3 using mass action (Supp. Figure 2a) and the equilibrium approximation (Supp. Figure 2b). The output is plotted in Supp. Figure 2c-d, for different kinetics of binding k_+ and unbinding k_- but maintaining the same value of $K_A = k_+/k_-$.

When values of k_+ around $10^5\ s^{-1}M^{-1}$ are used, the amount of active target X_3 using mass action (yellow line) and equilibrium approach (black dotted line) do not match even after 60 seconds of the simulation. On the other hand, when we use values of k_+ closer to 10^6, comparable to several small molecule inhibitors found in the literature [30], the equilibrium approximation is equivalent to the mass action dynamics after 15 seconds.

Unfortunately, the equilibrium approximation cannot be used in conditions where the target node is activating or deactivating itself. Therefore, in these networks, the effect of the inhibitor cannot be simplified as an effective concentration of active X_2 at equilibrium, and full mass action has to be simulated explicitly as a sequestering interaction. To study these types of topologies, a different set of equations has to be written for each particular network topology, and the simulation and analysis can not be automated using the same script for all topologies. Therefore, we exclude from our analysis the possibility of positive or negative autoregulation in X_2 (i.e, $I_{2,2} = 0$).

Calculation of all possible network topologies. The first three rows and columns of the interaction matrix I_{ij} between the three nodes of the network is:

$$I_{i,j} = \begin{pmatrix} I_{1,1} & I_{1,2} & I_{1,3} \\ I_{2,1} & I_{2,2} & I_{2,3} \\ I_{3,1} & I_{3,2} & I_{3,3} \end{pmatrix}$$

Where each value of $I_{i,j} = [-1, 0, 1]$, i.e if the component X_i activates or deactivates X_j, the value is $I_{i,j} = 1$, or $I_{i,j} = -1$ respectively. $I_{i,j} = 0$ if X_i does not act on X_j. To calculate all possible topologies, we consider all 3 potential types of interaction between the three nodes. This gives us a total number of possible networks of $N = 3^{3\times3} = 19683$.

Based on the previous section, all network topologies that contain positive or negative autoregulation of the target node are not considered in our analysis. These topologies correspond to the interaction matrices with the following form:

$$I_{i,j} = \begin{pmatrix} I_{1,1} & I_{1,2} & I_{1,3} \\ I_{2,1} & 1 & I_{2,3} \\ I_{3,1} & I_{3,2} & I_{3,3} \end{pmatrix} \text{ or } I_{i,j} = \begin{pmatrix} I_{1,1} & I_{1,2} & I_{1,3} \\ I_{2,1} & -1 & I_{2,3} \\ I_{3,1} & I_{3,2} & I_{3,3} \end{pmatrix}$$

Therefore, we only take into account the networks where the interaction $I_{2,2} = 0$, resulting in $N = 3^{(3\times3)-1} = 6561$ networks.

Next, since we are interested in the effect of inhibition, we do not consider the topologies where the target node X_2 does not act on the other two nodes, i.e., all network topologies take the form:

$$I_{i,j} = \begin{pmatrix} I_{1,1} & I_{1,2} & I_{1,3} \\ 0 & 0 & 0 \\ I_{3,1} & I_{3,2} & I_{3,3} \end{pmatrix}$$

That constitute a total of $N = 3^{(3\times3)-3} = 729$ network topologies. Finally, we eliminate from our analysis all topologies where the output does not receive an interaction from the other two nodes, i.e., all interaction matrices that take the form:

$$I_{i,j} = \begin{pmatrix} I_{1,1} & I_{1,2} & 0 \\ I_{2,1} & 0 & 0 \\ I_{3,1} & I_{3,2} & I_{3,3} \end{pmatrix}$$

Which constitute another $N = 3^{(3\times3)-3} = 729$ network topologies. Considering this, the total number of possible network topologies evaluated in our screening is N=5103.

Organization of all network topologies that show inverse bistability and inverse hysteresis.

We organized the 712 topologies that showed inverse bistability in a undirected graph or *complexity atlas*, similarly to the work of Coterell and Sharpe [9]. Herein, the topologies are represented by nodes while the bidirectional edges represent the similarity between topologies: Linked topologies (neighbors) present the same connectivity pattern except for one interaction i.e., we could go from one to another neighbor by adding or removing one interaction. The resulting connectivity matrix was reorganized by number of links and plotted using the *biograph* function included in the Bioinformatics Toolbox of Matlab (The Mathworks, Natick, MA). The 19 minimal motifs are represented as matrix plots, taking into account the three first rows and columns of the interaction matrix for each of the topologies. This way, a positive interaction from component i to component j of the network (i.e.,"1" in the parameter I_{ij} in the interaction matrix) is represented as a white square; a black square corresponds to a negative interaction from component i to component j ("-1" in the parameter I_{ij} of the interaction matrix) while a grey square means that there is no interaction ("0" in the I_{ij} in the interaction matrix).

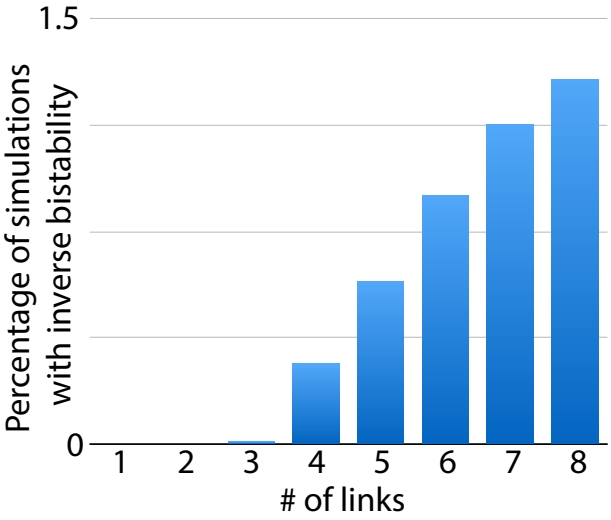

Supplementary Figure 3: The percentage of simulations with inverse bistability increases with the connectivity of the network.

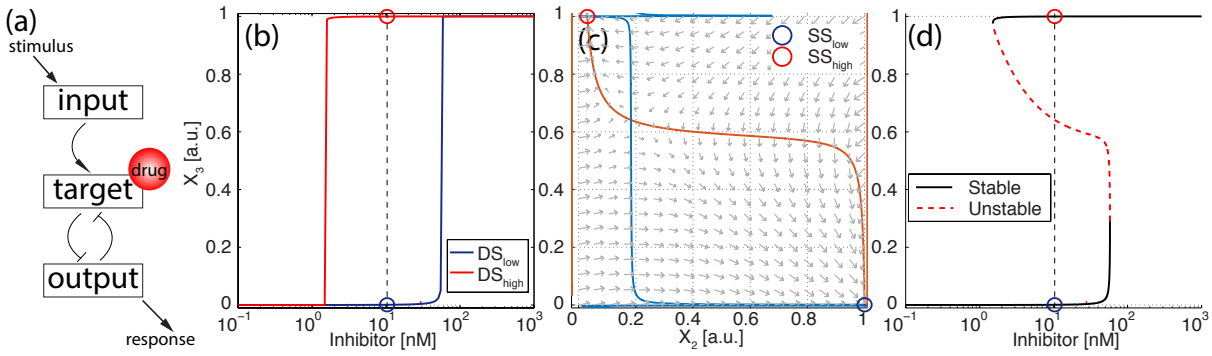

Supplementary Figure 4: Dependence on the initial conditions with the inhibitor acting as activator of the output node. Panel (a) represents the network topology used in this simulation. Arrow-headed lines represent positive interactions (activation) and bar-headed lines correspond to negative interactions (de-activation). Panel (b) represents the dose-response curves DS_{low} (blue) and DS_{high} red for initial conditions IC_{low} and IC_{high}, respectively. The rest of the parameter values are the same between the two curves. Blue and red circles SS_{low} and SS_{high} show the steady state solutions for a given concentration of inhibitor. Panel (c) represents the phase plane with vector field and nullclines, representing the two steady states SS_{low} (blue) and SS_{high} (red) respectively. Panel (d) shows the bifurcation diagram of X_3. Black curves are the stable branches and the dash red curve is the unstable branch.

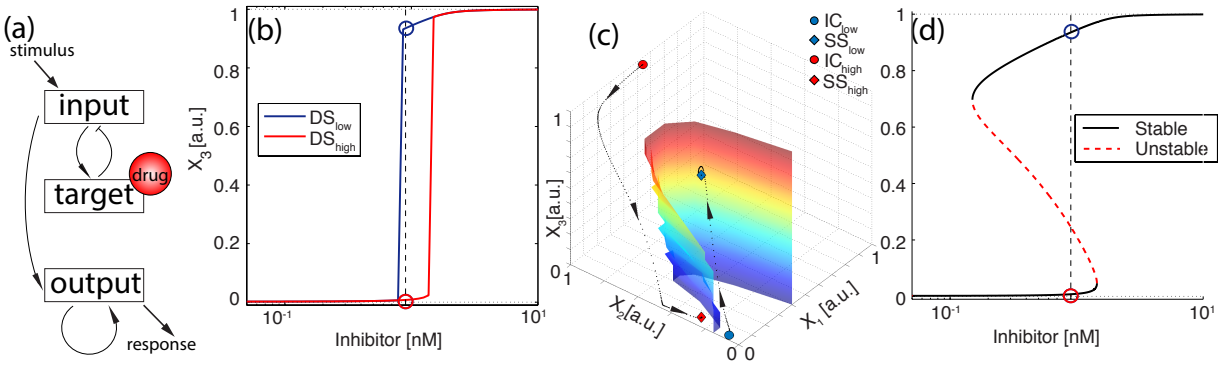

Supplementary Figure 5: Inverse bistability in conditions where the drug acts as an activator of the output node. Panel (a) represents an examples of network topology that show inverse bistability. Panel (b) represents the dose response curves DS_{low} (blue) and DS_{high} red for initial conditions IC_{low} and IC_{high}, respectively. The rest of the parameter values are the same between the two curves. Blue and red circles SS_{low} and SS_{high} represent the steady state solutions for a given concentration of inhibitor. Panel (c) represents the three-dimensional phase plane, with the trajectories of each simulation starting from the two initial conditions, and the separatrix between the two basins of attraction. Panel (d) shows the bifurcation diagram of X_3. Black curves are the stable branches and the red dash curve is the unstable branch.

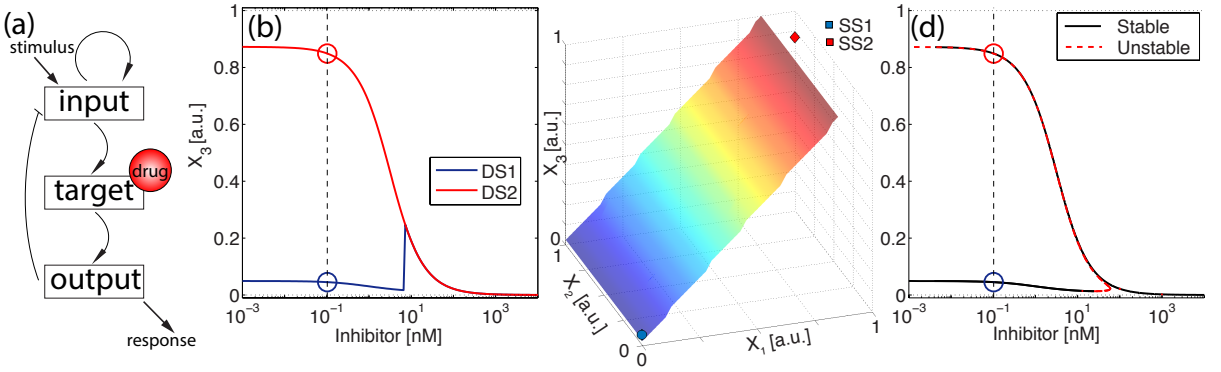

Supplementary Figure 6: The network architecture can induce inverse irreversible hysteresis. (a) Example of a network architecture that induces inverse hysteresis with one of the dose-response curves insensitive to treatment. (b) Dose-response curves DS_{low} (blue) and DS_{high} red for initial conditions IC_{low} and IC_{high}, respectively. The rest of parameter values are the same between the two curves. Blue and red circles SS_{low} and SS_{high} represent the steady state solutions for a given concentration of inhibitor. Panel (c) represents the three-dimensional phase plane and the separatrix between the two basins of attraction. (d) Bifurcation diagram of X_3. Black curves are the stable branches and the dash red curve is the unstable branch.

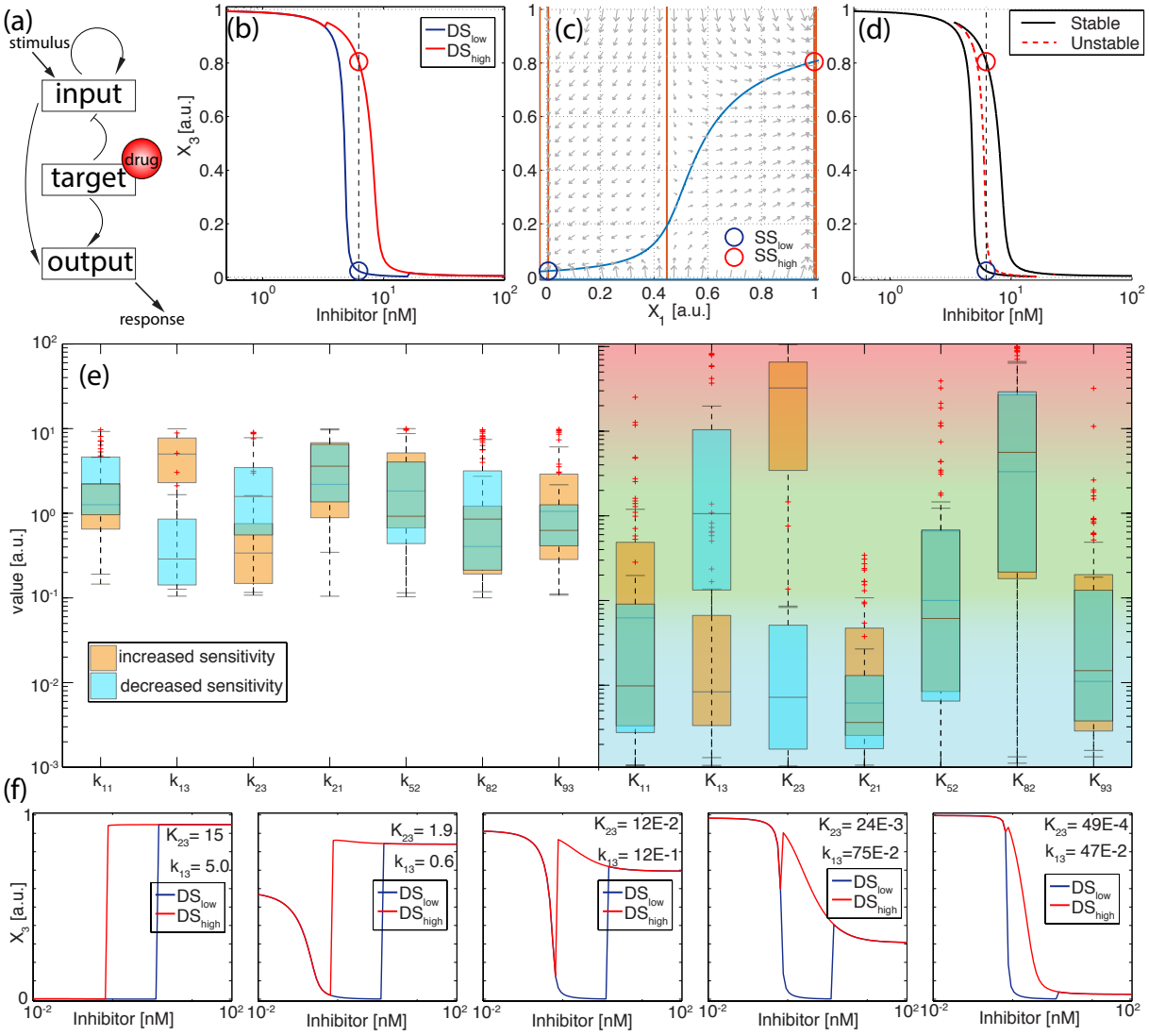

Supplementary Figure 7: The network architecture can induce inverse hysteresis. (a) Example of a network architecture that induces inverse hysteresis. (b) Dose-response curves DS_{low} (blue) and DS_{high} red for initial conditions IC_{low} and IC_{high}, respectively. The rest of parameter values are the same between the two curves. Blue and red circles SS_{low} and SS_{high} show the steady state solutions for a given concentration of inhibitor. (c) Phase plane with vector field and nullclines (nullclines for X_1 in orange, nullcline for X_3 in blue), representing the two steady states SS_{low} (blue) and SS_{high} (red) respectively. (d) Bifurcation diagram of X_3. Black curves are the stable branches and the red dash curve is the unstable branch. (e) Box plot for all parameter sets that show normal and inverse hysteresis. Blue, green and red background represents the saturated, unconstrained and linear regimes of the Michaelis-Menten kinetics, respectively. (f) Changes in the dose-response curve when two parameters are changed from normal to inverse hysteresis conditions.

References

[1] **Albeck, J., Mills, G. and Brugge, J.** (2013). Frequency-Modulated Pulses of ERK Activity Transmit Quantitative Proliferation Signals. *Molecular Cell* **49**, 249–261. ISSN 10972765.

[2] **Alon, U.** (2007). Network motifs: theory and experimental approaches. *Nature Reviews Genetics* **8**, 450–461. ISSN 1471-0056.

[3] **Altan-Bonnet, G., Germain, R. N., Germain, R., Oltz, E. and Stewart, V.** (2005). Modeling T Cell Antigen Discrimination Based on Feedback Control of Digital ERK Responses. *PLoS Biology* **3**, e356. ISSN 1545-7885.

[4] **Arkin, M. R., Tang, Y. and Wells, J. A.** (2014). Small-molecule inhibitors of protein-protein interactions: Progressing toward the reality.

[5] **Arkin, M. R. and Wells, J. a.** (2004). Small-molecule inhibitors of protein-protein interactions: progressing towards the dream. *Nature reviews. Drug discovery* **3**, 301–317. ISSN 1474-1776.

[6] **Burrill, D. R., Inniss, M. C., Boyle, P. M. and Silver, P. A.** (2012). Synthetic memory circuits for tracking human cell fate. *Genes & development* **26**, 1486–97. ISSN 1549-5477.

[7] **Chen, W. W., Niepel, M. and Sorger, P. K.** (2010). Classic and contemporary approaches to modeling biochemical reactions. *Genes & development* **24**, 1861–75. ISSN 1549-5477.

[8] **Collins, J. J., Gardner, T. S. and Cantor, C. R.** (2000). Construction of a genetic toggle switch in Escherichia coli. *Nature* **403**, 339–342. ISSN 00280836.

[9] **Cotterell, J. and Sharpe, J.** (2010). An atlas of gene regulatory networks reveals multiple three-gene mechanisms for interpreting morphogen gradients. *Molecular Systems Biology* **6**, 425. ISSN 1744-4292.

[10] **Doldán-Martelli, V., Guantes, R. and Míguez, D. G.** (2013). A mathematical model for the rational design of chimeric ligands in selective drug therapies. *CPT: pharmacometrics & systems pharmacology* **2**, e26. ISSN 2163-8306.

[11] **Doldán-Martelli, V. and Míguez, D. G.** (2015). Synergistic interaction between selective drugs in cell populations models. *PloS one* **10**, e0117558. ISSN 1932-6203.

[12] **Elf, J., Nilsson, K., Tenson, T. and Ehrenberg, M.** (2006). Bistable Bacterial Growth Rate in Response to Antibiotics with Low Membrane Permeability. *Physical Review Letters* **97**, 258104. ISSN 0031-9007.

[13] **Fabian, M. A., Biggs, W. H., Treiber, D. K., Atteridge, C. E., Azimioara, M. D., Benedetti, M. G., Carter, T. A., Ciceri, P., Edeen, P. T., Floyd, M., Ford, J. M., Galvin, M., Gerlach, J. L., Grotzfeld, R. M., Herrgard, S., Insko, D. E., Insko, M. A., Lai, A. G., Lélias, J.-M., Mehta, S. A., Milanov, Z. V., Velasco, A. M., Wodicka, L. M., Patel, H. K., Zarrinkar, P. P. and Lockhart, D. J.** (2005). A small molecule-kinase interaction map for clinical kinase inhibitors. *Nature biotechnology* **23**, 329–36. ISSN 1087-0156.

[14] **Fehmann, H. C., Habener, J. F. and Fehmann, H. C.** (1991). Homologous desensitization of the insulinotropic glucagon-like peptide-i(7-37) receptor on insulinoma (hit-t15) cells. *Endocrinology* **128**, 2880–2888. ISSN 19457170.

[15] **Ferrell, J. E., Pomerening, J. R., Kim, S. Y., Trunnell, N. B., Xiong, W., Huang, C.-Y. F. and Machleder, E. M.** (2009). Simple, realistic models of complex biological processes: Positive feedback and bistability in a cell fate switch and a cell cycle oscillator. *FEBS Letters* **583**, 3999–4005. ISSN 00145793.

[16] **Freedman, N. J. and Lefkowitz, R. J.** (1996). Desensitization of G protein-coupled receptors. *Recent progress in hormone research* **51**, 319–51; discussion 352–3. ISSN 0079-9963.

[17] **Gainetdinov, R. R., Premont, R. T., Bohn, L. M., Lefkowitz, R. J. and Caron, M. G.** (2004). Desensitization of G protein Coupled Receptors and neuronal Functions. *Annu. Rev. Neurosci* **27**, 107–44. ISSN 0147-006X.

[18] **Karaman, M. W., Herrgard, S., Treiber, D. K., Gallant, P., Atteridge, C. E., Campbell, B. T., Chan, K. W., Ciceri, P., Davis, M. I., Edeen, P. T., Faraoni, R., Floyd, M., Hunt, J. P., Lockhart, D. J., Milanov, Z. V., Morrison, M. J., Pallares, G., Patel, H. K., Pritchard, S., Wodicka, L. M. and Zarrinkar, P. P.** (2008). A quantitative analysis of kinase inhibitor selectivity. *Nature Biotechnology* **26**, 127–132. ISSN 1546-1696.

[19] **Karslake, J., Maltas, J., Brumm, P. and Wood, K. B.** (2016). Population Density Modulates Drug Inhibition and Gives Rise to Potential Bistability of Treatment Outcomes for Bacterial Infections. *PLOS Computational Biology* **12**, e1005098. ISSN 1553-7358.

[20] **Ma, W., Trusina, A., El-Samad, H., Lim, W. A. and Tang, C.** (2009). Defining network topologies that can achieve biochemical adaptation. *Cell* **138**, 760–73. ISSN 1097-4172.

[21] **Míguez, D. G.** (2013). Network nonlinearities in drug treatment. *Interdisciplinary Sciences: Computational Life Sciences* **5**, 85–94. ISSN 1913-2751.

[22] **Míguez, D. G., Vanag, V. K. and Epstein, I. R.** (2007). Fronts and pulses in an enzymatic reaction catalyzed by glucose oxidase. *Proceedings of the National Academy of Sciences of the United States of America* **104**, 6992–7. ISSN 0027-8424.

[23] **Milo, R., Shen-Orr, S., Itzkovitz, S., Kashtan, N., Chklovskii, D. and Alon, U.** (2002). Network Motifs: Simple Building Blocks of Complex Networks. *Science* **298**, 824–827. ISSN 00368075.

[24] **Perlman, Z. E., Slack, M. D., Feng, Y., Mitchison, T. J., Wu, L. F. and Altschuler, S. J.** (2004). Multidimensional drug profiling by automated microscopy. *Science (New York, N.Y.)* **306**, 1194–8. ISSN 1095-9203.

[25] **Rodrik-Outmezguine, V. S., Chandarlapaty, S., Pagano, N. C., Poulikakos, P. I., Scaltriti, M., Moskatel, E., Baselga, J., Guichard, S. and Rosen, N.** (2011). mTOR Kinase Inhibition Causes Feedback-dependent Biphasic Regulation of AKT Signaling. *Cancer Discovery* .

[26] **Ruiz-Herrero, T., Estrada, J., Guantes, R. and Miguez, D. G.** (2013). A Tunable Coarse-Grained Model for Ligand-Receptor Interaction. *PLoS Computational Biology* **9**. ISSN 1553734X.

[27] **Shah, N. A. and Sarkar, C. A.** (2011). Robust Network Topologies for Generating Switch-Like Cellular Responses. *PLoS Computational Biology* **7**, e1002085. ISSN 1553-7358.

[28] **Shokat, K. M.** (2014). *Methods in enzymology. Volume 584, Protein kinase inhibitors in research and medicine*. 1st editio edition. ISBN 9780123984623.

[29] **Sun, Y., Olson, R., Horning, M., Armstrong, N., Mayer, M. and Gouaux, E.** (2002). Mechanism of glutamate receptor desensitization. *Nature* **417**, 245–253. ISSN 0028-0836.

[30] **Thurmond, R. L., Wadsworth, S. A., Schafer, P. H., Zivin, R. A. and Siekierka, J. J.** (2001). Kinetics of small molecule inhibitor binding to p38 kinase. *European journal of biochemistry* **268**, 5747–54. ISSN 0014-2956.

[31] **Tyson, J. J., Chen, K. C. and Novak, B.** (2003). Sniffers, buzzers, toggles and blinkers: dynamics of regulatory and signaling pathways in the cell. *Current Opinion in Cell Biology* **15**, 221–231. ISSN 09550674.

[32] **Vanag, V. K., Míguez, D. G. and Epstein, I. R.** (2006). Designing an enzymatic oscillator: bistability and feedback controlled oscillations with glucose oxidase in a continuous flow stirred tank reactor. *The Journal of chemical physics* **125**, 194515. ISSN 0021-9606.

[33] **Vogel, R. M., Erez, A. and Altan-Bonnet, G.** (2016). Dichotomy of cellular inhibition by small-molecule inhibitors revealed by single-cell analysis. *Nature communications* **7**, 12428. ISSN 2041-1723.

[34] **Wan, X., Harkavy, B., Shen, N., Grohar, P. and Helman, L. J.** (2007). Rapamycin induces feedback activation of Akt signaling through an IGF-1R-dependent mechanism. *Oncogene* **26**, 1932–1940. ISSN 0950-9232.

[35] **Wolf, D. M. and Arkin, A. P.** (2003). Motifs, modules and games in bacteria.

[36] **Wu, P., Nielsen, T. E. and Clausen, M. H.** (2016). Small-molecule kinase inhibitors: An analysis of FDA-approved drugs.

4 Discussion

This thesis combines computational tools with experimental data to unveil the mechanism of action of different therapeutic ligands and which factors may have an impact on their physiological effect.

The first contribution of this thesis (see 'Results', section 3.1) uses a computational approach to understand the mechanisms of action of asymmetric ligands such as the growth hormone (GH) and the erythropoietin (EPO).

To this end, the publication explores different versions of a mathematical model that gradually includes more and more relevant characteristics of GH and EPO systems (see 'Introduction' section 1.2). The initial model incorporates only a few aspects of the active complex assembly, using a 1:1 ligand-receptor interaction scheme, while the last version of the model considers a 1:2 ligand-receptor interaction scheme which is asymmetric and sequential. This final model reveals that key aspects of GH and EPO signaling are induced by this particular ligand-receptor configuration. A more detailed mathematical approach that includes the effect of intracellular processes, such as receptors recycling, degradation and down-regulation by endocytosis, can be found in [80]. Furthermore, the model unveils the distinct roles that each of the binding sites on the ligand is playing in the process of the active complex formation. The assembly of the active complex occurs in a sequential manner and the strong binding is necessary to increase the local concentration of ligand on the cell surface to facilitate the interaction with the receptor through the weak binding site. The weak binding site is the one tightly controlling the signal strength and the amount of active signaling complexes. This regulatory role is also evident when homodimers of the ligand — with two strong affinity binding sites — interact with the receptors, the homodimers exhibit a strong increase in activity, when compared to the endogenous ligand stimulation. Here, the model supports the experimental data, predicting a strong increase in activity when compared to the ligand-monomeric case. Moreover, the strong binding site determines the self-antagonistic effect at high ligand concentrations and the optimal ligand concentration which induces maximum activity of the complex.

This theoretical approach does not consider the conformational change after the first binding event, which would affect the dissociation constant of the second binding event, as suggested by several authors. According to crystallographic measurements, the nuclear magnetic resonance structures of free EPO and EPO inside the active complex show very high similarities [81], so the model assumes identical dissociation constant before and after binding. Regarding the structure of unstimulated EPO and GH receptors, the classical hypothesis of free monomeric receptors diffusing on the cell membrane (receptor monomer hypothesis) implies that the active complex assembly is modulated by the diffusion rate of the receptors. The alternative hypothesis claims that receptors exist in dimeric form prior to ligand binding (receptor dimer hypothesis)[75, 82, 83]; in this case, the active complex formation would not be modulated by receptors diffusion.

The model predicts that the receptor dimer hypothesis doubles the number of active complexes predicted by the receptor monomer hypothesis, which is consistent with the fact that receptors diffusion is slowing down the formation of the complex by modulating the binding rate of complex formation. Unfortunately, the addition of diffusion to the model does not change the system dynamics, which prevents from discriminating between the two approaches by direct comparison with experimental data. More measurements of the absolute values of active complex concentration would be helpful to distinguish between both hypotheses.

Nevertheless, the model predicts that self-antagonism and ligand homodimer effect are incompatible with the dimer receptor hypothesis, unless the receptor dimer is capable of housing accommodating two ligands, resulting in a 2:2 ligand-receptor configuration. Different studies propose that the GHR extracellular domain is flexible enough to productively accommodate GH dimers [84, 85]. On the other hand, the self-antagonistic effect at high ligand concentrations requires that two unbound ligands fail in inducing the conformational change required for complex activation. A third hypothesis considers that two receptors can have a weak interaction between the inter-membrane domains of two free unstimulated receptors [86].

In summary, the mathematical models of the first publication of this thesis show that the interaction scheme of GH-GHR and EPO-EPOR strongly determines their dynamics and regulation, and that 1:2 ligand-receptor configuration combined with the sequential ligand binding and the asymmetric nature of the ligand dictate fundamental aspects of the system. These mathematical approaches can be used to predict the effect of mutations varying the binding sites affinities on the signaling of the ligands. A better understanding of active complex assembly for GH and EPO systems will permit to develop more efficient drugs to overcome many GH- and EPO-related diseases.

The asymmetric and sequential ligand-receptor binding constitutes the basis for the design of some targeted delivery drugs like the chimeric ligands. The second publication ('Results', section 3.2) introduces a theoretical model to simulate the dynamics and binding kinetics of chimeric ligands as an alternative to conventional empirical design.

Many chimeric constructs have been developed synthetically to target specific cell types (see [57, 87–90]) and most of them belong to the so-called *cancer targeted therapy* (see 'Introduction', section 1.4), allowing high activity at very low drug concentration and therefore reducing side effects. This model provides an *in silico* tool to design and test the efficiency of new synthetic compounds with chimeric nature, and also to optimize those available ones by testing variants with improved selective potential.

The presented model is able to quantitatively reproduce the experimental results of the different chimeric constructs used in [77] in terms of pathway activation and cytotoxic potential. Those synthetic compounds are monomeric and chimeric variations of a specific *chimera* formed by an activity element, the interferon IFN$\alpha 2a$, a linker, and a targeting element, the epidermal growth factor (EGF). The model was informed with experimental parameter values from the literature.

In this publication the model is confined to interactions at the cell membrane level. The calibration of downstream events was performed using the experimental dose-response curve for the wild type IFN$\alpha 2a$ monomer. A more detailed model including all involved downstream molecular interactions (signaling networks) that ultimately trigger cytotoxic response will reduce the generality and simplicity of the model, so this approach is far from the scope of this contribution.

The modeling framework does not consider the dimeric nature of both EGF and IFN$\alpha 2a$ active complexes [91, 92] assuming a *1:1 ligand-receptor configuration*. Given the accuracy of the 1:1 model reproducing the experimental results, it is hypothesized that receptor homo-dimerization is not playing a significant role in the dynamics of the system.

The internalization of the active complex is calculated as the sum of the internalization constants of both intermediate complexes, assuming that they are independent. However, the proximity of both complexes in the active complex configuration may induce dependence on the internalization of proximal active receptors linked to the same chimeric molecule.

The diffusion of free receptors and complexes is assumed to be uniform, although the plasma membrane is highly heterogeneous, including lipid rafts, protein domains or shape fluctuations [93], which may influence the diffusion of components on the membrane.

In addition, the model does not consider paracrine interaction of chimeric ligands, which has

been observed experimentally, cross-linking receptors of nearby cells [87].

The model also assumes a dynamic equilibrium in the concentration of unstimulated free receptors and do not include synthesis and degradation of free receptors. It also simplifies all possible downstream regulation in receptor expression after activation. In addition, it is considered that the activity triggered by the ligand-receptor interaction is proportional to the amount of maximum active complexes formed, although another potential values such as the total value of active complexes at a given time also produce equivalent results. Finally, the pro-survival signals of the targeting element EGF [94, 95] may antagonize the anti-proliferative and pro-death effects of the cytotoxic subunit. This EGF interaction is also considered in the scientific paper where the chimeric ligand was constructed and analyzed, but experimental data monitoring differences in cell cycle length for Daudi versus Daudi-EGFR are not available [96].

Altogether, this model makes a series of necessary assumptions regarding the nature of the ligands, complexes and receptors, including simplifications in their conformation, internalization, diffusion or signaling mechanisms. Despite all the simplifications, the model is able to reproduce the experimental data quantitatively [77] for all compounds and all tested cell types. Although this scientific paper works only with the specific IFN$\alpha 2a$-EGF chimeric ligand, the generality of the model facilitates a straightforward customization to simulate other chimeric constructs, using different combinations of activity and targeting elements to design selective compounds, with improved therapeutic efficacy against specific cells.

The model implemented in this publication constitutes a reliable and systematic method to design chimeric ligands allowing us to determine optimal configurations prior to synthesis and *in vivo* tests at the single cell level.

The contribution in 'Results', section 3.3 generalizes the chimeric ligand-receptor model for single cells (previously discussed) to explore new strategies to facilitate the design of therapeutic treatments with higher selectivity but reduced drug concentrations, from a *prior-to-bench* theoretical perspective.

The previous publication predicted the optimal values for the kinetic parameters of both activity and targeting elements to achieve chimeric ligands with higher selectivity, but the affinity and dissociation rates in a given ligand-receptor interaction cannot be modulated gradually since single mutations in the ligand change those parameters abruptly.

This newer publication proposes the combination of two distinct chimeric ligands as a means to improve the selective potential of a treatment; highly efficient chimeras could affect those cells

with elevated number of target receptors (EGF receptors) while less potent but more selective ligands could discriminate between healthy and unhealthy cells. Furthermore, the model considers the effect of cell-to-cell phenotypic variability, applying the original ligand-receptor equations (see 'Results' chapter, section 3.2) to populations of cells with heterogeneous receptor expression.

The model uses two approaches to simulate the combination of chimeras, with equivalent results: an explicit model of two drugs and a simplified model where the two drugs are assumed to interact additively, based on the Loewe additivity model [97]. Using the second approach, it was developed a 'performance map' where selectivity was computed for any given concentration of the combined drugs. Interestingly, the model revealed that chimeric drugs show *synergism* in their selective potential (the combination of two selective drugs is more efficient than each agent separately), despite the assumption of *additivity* interaction between chimeric ligands.

The basic ligand-receptor assumptions made by this mathematical framework are equivalent to those presented in the original ligand-receptor model, i.e., those regarding the nature of the ligands, complexes and receptors. Additionally, it is assumed that all cells proliferate at the same rate, independently of the amount of EGFR receptors. As we have already mentioned, EGFR stimulation is correlated with the activation of proliferative signals, but the differences in cell cycle between Daudi and Daudi- EGFR cells used to inform the model have not been experimentally measured and consequently, they can not be included in the model.

Some simulations include phenotypic heritability in the number of receptors for each cell of the population. In this case, the expression of the receptors depends on the amount of cell surface receptors expressed by the progenitors. Although there are other more realistic scenarios to capture the effect of mutations in the regulation of the expression of receptors, those scenarios were discarded as they would result in more free parameters and assumptions.

In addition, it was presumed that the effect of heritability would be more significant in simulations at higher times, i.e., when more generations of cells are allowed to develop. Unfortunately, experimental data were only available at the time point of t = 60h, corresponding to an average of 2.2 generations, insufficient to observe the selective pressure effect induced by the drug treatment.

To mimic cell-to-cell variability in number of receptors and cell cycle length the model uses the gamma distribution. Other distributions were also tested (gaussian, lognormal) with no significant difference in the results [98–101]. In order to compare the different combinatorial treatments, a threshold was established in terms of the *potential selectivity* of the treatment towards the different cell types (expressing different concentrations of the target proteins): A treatment was considered

as *selective* if 80% of the healthy cell population survived while the number of unhealthy cells was maintained (or diminished). Other potential threshold values defined also evidenced the reported synergism when combining two chimeric ligands, but at different drug concentrations.

In summary, the third scientific publication of this thesis shows that the combination of chimeric drugs can selectively affect a given cell population at reduced concentrations compared to single drug treatment. This publication constitutes the first computational study on the combination of targeted delivery drugs by generalizing the previous results of single cell treatments with chimeras (see 'Results', section 3.2) to explore the effect of chimeric drug combinations in cell population models.

The last contribution of this thesis (see 'Results', section 3.4) presents the first global analysis of the impact of network topology in the cellular response to a given drug treatment, focusing on three-node networks treated with inhibitory treatments. The three interacting nodes have different roles: the input node X_1 receives a constant stimulus, the target node X_2 is the one interacting with the inhibitor, and the output node X_3 serves as a readout of the network activity.

To characterize the effect of the network architecture on the response to inhibition, the manuscript compares two dose-response curves resulted from applying a range of inhibitor concentrations to the same network but with two different initial conditions.

The results reveal that most of the three-node network topologies exhibit a response to the treatment that depends on the initial state of the network (i.e., the initial concentration of the three nodes). This dependence is translated into dual dose-response curves and changes in the $EC50$ of the inhibitor as well as in the overall effect of the inhibitor.

The simulations were restricted to networks where the target node does not self-regulate since, under these conditions, the effect of the inhibitor cannot be simplified as an effective concentration of active target at equilibrium. In these topologies, the effect of the inhibitor has to be modeled explicitly as a sequestering interaction will probably give rise to other interesting dose-response scenarios. Unfortunately, the analysis of motifs with direct auto-regulation of the target would not permit to use the same automated script to run and screen all possible simulations for all topologies tested, and it has not been performed.

The analysis is constrained to small networks in an attempt to identify the minimal motifs that induce *dual dose-response curves*. Since linear protein-protein interactions can be reduced to smaller networks with equivalent dynamics without reducing the spectrum of behaviors reported [24, 45, 102], it is assumed that those results can also apply to much larger networks with an

increasing number of nodes that interact linearly. Furthermore, if the number of nodes increases, the computational cost will increase exponentially and will not be easily manageable. The sacrifice in the network size allows to perform a detailed search of the architecture space, where many studies focus on just a selection of network topologies and explore a tiny fraction of the overall space of topologies.

The minimal network motif for a pair of dose-response curves showing a shift in the $EC50$ (dual dose-response) is a direct or indirect positive feedback loop in the network. This positive feedback, under specific parameter conditions, induces a bistable regime in a region of the parameter space, and the inhibitor has to be able to switch between the two stable branches of the system. These dual response may occur in a narrow range of inhibitor concentration, mainly depending on the topology, and the values of the catalytic and Michaelis-Menten constants.

Interestingly, there are some topologies that show a particular type of dual dose-response. Instead of a classical bistable response, these networks present an inversion in the sensitivity of the treatment between the two dose-response curves, or 'inverse bistability'. The basic ingredients for 'inverse bistability' are more complex to summarize, since several apparently unrelated topologies show this behavior. Although inverse bistability occurs more often when the number of network interactions increases, all the highly connected topologies which show inverse bistability can be traced back to 24 minimal architectures with 4 interactions between nodes.
For all these 4-link topologies, there are at least two interactions: one positive and one negative.This is presumably because this behavior requires a positive feedback to generate the bistable regime, and a negative or a combination of negative interactions to 'invert' the bistability. In addition, these minimal topologies do not present any negative direct auto-regulatory interaction. These 4-link circuits are grouped in three main overlapping families (where a given topology can belong to more than one family). On the other hand, the 24 topologies include the 11 minimal architectures able to induce inverse hysteresis. There are two ways of achieving inverse bistability: The first one implies that, due to the relationship between the values for the two fixed initial conditions (IC_{low} and IC_{high}) and the conformation of the basins of attraction, the separatrix forces the trajectories (starting from those ICs) to travel toward the steady state that is farther in the direction of the X_3 axis, creating an "inversion" between the two dose-response curves. The second option is the result of the combination of the network topology and the kinetic parameters, giving rise to a bifurcation diagram with an unusual profile and consequently, to this singular dose-response curve.

It is important to notice that while some topologies showing inverse bistability can induce this

behavior via each of the alternatives explained above, other topologies only show one of the two ways of acquiring inverse bistability. The relationship between these two possibilities and the comparison of parameter regimes where the two occur in the same topology is far from the scope of this publication.

From the point of view of drug development, the fact that some network topologies induce a different response to inhibition depending on the initial state of activation of the network nodes is important when establishing the optimal target, the optimal dose or the optimal schedule or treatment. The fact that the majority of topologies present different dose-response curves suggests that the effect of the initial conditions in the efficiency of a given treatment is widespread and may be impacting reproducibility of drug treatments, since the same concentration of inhibitor can result in different outcomes.

The concept of inverse bistability is here used to illustrate the situation of initial conditions preferring to transit to the furthest steady state, instead of the closest one in the phase space. When comparing dose-response curves corresponding to the low and high initial conditions, normal bistability results in an increase of the sensitivity (reduced $EC50$), while inverse bistability results in a reduction (higher $EC50$) of the effect of the inhibitor. This reduction of the sensitivity after a first treatment is very different from the well-known homologous or heterologous *desensitization* after repeated or prolonged receptor stimulation [103, 104]. Receptor desensitization is achieved mainly by reducing the number or the efficiency of receptors on the cell surface, after a first stimulation. This is translated into a initial strong transient activation of the targets downstream with a much lower response after a second stimulus application. This type of desensitization serves as mechanism for attenuation of the signal, mediated mainly by a direct or indirect negative feedback loop [105, 106].

While the *receptor desensitization* refers to transient activation, the inverse bistability reported here refers to steady state of the network, and requires an interplay between positive and negative feedback loops interactions between its elements.

This last contribution highlights that the efficiency of treatments targeting a regulatory signaling network is highly influenced by the wiring of the network and consequently, the initial state of the interconnected members (such as level of phosphorylation or concentration); all these factors must be considered for an accurate prediction of the cell response when designing or optimizing a treatment.

In conclusion, this thesis combines computational and experimental methods to understand the

behavior of asymmetric ligands and targeted delivery drugs. On the other hand, it explores new factors that may affect the outcome of drug treatments such as the initial conditions or the topology of the system. The models here presented provide novel tools to design and optimize drug treatments, contributing to the progress of the Biomedicine and Pharmacology fields.

5 Conclusions

- A mathematical framework has been developed to understand the dynamics and regulation of the interaction between EGF or EPO ligands and their receptors. The asymmetric and sequential 1:2 ligand receptor mode is able to reproduce the main key features of the system dynamics.

- The model unveils the different roles of the two binding sites of GH and EPO ligands: While the weak binding site controls the signal strength and the amount of active complexes formed, the strong binding site regulates the self-antagonist effect at high ligand concentrations. These roles are essential in the regulation of the signaling.

- A second mathematical model was designed to study and optimize the selectivity of chimeric ligands toward tumoral cells, being the first mathematical framework focused on synthetic chimeric drugs.

- The model quantitatively reproduces the experimental results of the different chimeric compounds in terms of pathway activation and cytotoxic potential and provides a systematic *in silico* tool to design and test the efficiency and selectivity of chimeric compounds at the single-cell level in order to determine optimal chimeric configurations prior to synthesis and *in vivo* tests.

- The previous theoretical framework was generalized for combination therapies applied to heterogeneous cell populations as a means to improve the selective potential of chimeric drugs and to study the effect that phenotypic variability and heritability has on the output of these treatments.

- The model reveals that chimeric drugs show synergism in terms of their selective potential,

i.e., that the combination of two chimeras is more selective than each agent separately and predicts that synergism of these selective drugs is robust to variability in receptors expression and phenotypic heritability.

- The author presents the first global analysis of how the network nonlinearities can influence the cellular response to a given drug treatment by creating a high-throughput framework to study the response to molecular inhibition (using small molecule inhibitors) of all possible 3-node generic signaling pathways with different regulatory motifs.
- The results from the analysis illustrate that the efficiency of drug treatments is highly influenced by the wiring of the targeted signaling network and by the initial state of activation of the members; all these factors must be considered for an accurate prediction of the cell response in drug studies and clinical trials.

- Se ha desarrollado un modelo matemático con el objetivo de comprender la dinámica y regulación de la interacción entre ligandos asimétricos como la hormona del crecimiento o la eritropoyetina con sus receptores. El modelo 1:2 ligando-receptor de interacción asimétrica y secuencial es capaz de reproducir los rasgos más distintivos de la dinámica de estos sistemas.

- Dicho modelo desvela los diferentes roles de cada uno de los sitios de unión de GH y EPO: mientras el sitio de unión más débil controla la fuerza de la señalización y el número de complejos activos que se forman, el sitio de unión fuerte regula el efecto auto-antagonista que poseen estos ligandos altas concentraciones. Ambos roles son esenciales para la regulación de la señalización de ambas moléculas.

- Un segundo modelo fue diseñado para estudiar y optimizar la selectividad de las quimeras hacia las células tumorales, y constituye el primer marco teórico centrado en las drogas quiméricas.

- El modelo reproduce cuantitativamente los resultados experimentales para diferentes compuestos quiméricos en términos de activación de la ruta y de potencial citotóxico de la droga, aportando una herramienta sistemática *in silico* para el diseño y evaluación de la eficacia y selectividad de compuestos quiméricos a nivel celular, con el objetivo de determinar las configuraciones quiméricas óptimas previamente a su síntesis y a ensayos *in vivo*.

- A partir del marco teórico anterior se creó un nuevo modelo aplicado terapias con combinaciones de quimeras actuando en poblaciones celulares heterogéneas con el objetivo de mejorar el potencial selectivo de los tratamientos con quimeras y estudiar el efecto de la variabilidad intracelular y la herencia fenotípica en la respuesta a los tratamientos combinatorios.

- El modelo desvela que las quimeras son sinérgicas en términos de potencial selectivo, es decir que la combinación de dos compuestos quiméricos es más selectiva que cada uno de los agentes por separado, y predice que dicha sinergia es robusta a la variabilidad en la expresión de receptores y a la herencia fenotípica.

- Por último, en esta tesis se presenta el primer análisis global de cómo las no-linealidades en las redes de señalización pueden influenciar la respuesta celular a tratamientos farma-

cológicos, a través de la creación de una plataforma teórica donde estudiar la respuesta a inhibición molecular en redes de señalización genéricas de tres nodos con diferentes interacciones no lineales.

- Los resultados de este análisis desvelan que la eficacia de los tratamientos farmacológicos está enormemente influenciada por la topología de la red y por el estado inicial de activación de sus componentes; todos estos factores podrían afectar a la reproducibilidad de los tratamientos y deberían ser considerados para una predicción más precisa de la respuesta celular en estudios farmacológicos y ensayos clínicos.

Bibliography

[1] K. I. Kaitin and J. A. DiMasi. Pharmaceutical innovation in the 21st century: new drug approvals in the first decade, 2000-2009. Clinical Pharmacology and Therapeutics **89**, 183 (2011). (cited on p. 1)

[2] S. M. Paul, D. S. Mytelka, C. T. Dunwiddie, C. C. Persinger, B. H. Munos, S. R. Lindborg, and A. L. Schacht. How to improve R&D productivity: the pharmaceutical industry's grand challenge. Nature Reviews Drug Discovery **9**, 203 (2010). (cited on p. 1)

[3] P. K. Sorger, S. R. Allerheiligen, D. R. Abernethy, R. B. Altman, K. L. Brouwer, A. Califano, D. Z. D'Argenio, R. Iyengar, W. J. Jusko, R. Lalonde, *et al*. Quantitative and systems pharmacology in the post-genomic era: new approaches to discovering drugs and understanding therapeutic mechanisms. In *An NIH white paper by the QSP workshop group*, volume 48 (NIH Bethesda, 2011). (cited on pages 1, 3, 16, and 137)

[4] J. Kotz. Phenotypic screening, take two. SciBX: Science-Business eXchange **5** (2012). (cited on p. 2)

[5] D. Noble. Claude Bernard, the first systems biologist, and the future of physiology. Experimental Physiology **93**, 16 (2008). (cited on p. 2)

[6] D. Noble. Biophysics and systems biology. Philosophical Transactions of the Royal Society of London A: Mathematical, Physical and Engineering Sciences **368**, 1125 (2010). (cited on p. 2)

[7] A. L. Hodgkin and A. F. Huxley. A quantitative description of membrane current and its application to conduction and excitation in nerve. The Journal of Physiology **117**, 500 (1952). (cited on p. 2)

[8] D. Noble. Cardiac Action and Pacemaker Potentials based on the Hodgkin-Huxley Equations. Nature **188**, 495 (1960). (cited on p. 2)

[9] H. Kitano. Systems Biology: A Brief Overview. Science **295**, 1662 (2002). (cited on p. 2)

[10] P. Kohl and D. Noble. Systems biology and the virtual physiological human. Molecular Systems Biology **5**, 292 (2009). (cited on p. 3)

[11] P. Vicini and P. H. van der Graaf. Systems pharmacology for drug discovery and development: paradigm shift or flash in the pan? Clinical Pharmacology and Therapeutics **93**, 379 (2013). (cited on p. 3)

[12] B. Alberts, A. Johnson, J. Lewis, M. Raff, K. Roberts, and P. Walter. *Molecular Biology of the Cell* (Garland Science, 2002), 4th edition. (cited on p. 4)

[13] J. Cai, M. Sun, X. Ge, and Y. Sun. EGFR tyrosine kinase inhibitors differentially affect autophagy in head and neck squamous cell carcinoma. Biochemical and Biophysical Research Communications (2017). (cited on p. 5)

[14] H. S. Park, M. H. Jang, E. J. Kim, H. J. Kim, H. J. Lee, Y. J. Kim, J. H. Kim, E. Kang, S.-W. Kim, I. A. Kim, and S. Y. Park. High EGFR gene copy number predicts poor outcome in triple-negative breast cancer. Modern Pathology: An Official Journal of the United States and Canadian Academy of Pathology, Inc **27**, 1212 (2014). (cited on p. 5)

[15] C.-P. Schneider, D. Heigener, K. Schott-von Römer, S. Gütz, E. Laack, W. Digel, W.-R. Guschall, A. Franke, H. Bodenstein, C. Schmidtgen, and M. Reck. Epidermal Growth Factor Receptor-Related Tumor Markers and Clinical Outcomes with Erlotinib in Non-small Cell Lung Cancer: An Analysis of Patients from German Centers in the TRUST Study. Journal of Thoracic Oncology **3**, 1446 (2008). (cited on p. 5)

[16] G. M. Cooper. *The Cell* (Sinauer Associates, 2000), 2nd edition. (cited on p. 5)

[17] B. Zhang, B. Gao, S. Dong, Y. Zhang, and Y. Wu. Anti-tumor efficacy and pre-clinical immunogenicity of IFN2a-NGR. Regulatory Toxicology and Pharmacology **60**, 73 (2011). (cited on pages 5 and 15)

[18] V. Rijckborst and H. L. A. Janssen. The Role of Interferon in Hepatitis B Therapy. Current Hepatitis Reports **9**, 231 (2010). (cited on p. 5)

[19] S. Juul and U. Felderhoff-Mueser. Epo and other hematopoietic factors. Seminars in fetal & neonatal medicine **12**, 250 (2007). (cited on p. 6)

[20] P. C. Hindmarsh and M. T. Dattani. Use of growth hormone in children. Nature Reviews Endocrinology **2**, 260 (2006). (cited on p. 6)

[21] D. K. Morrison. MAP Kinase Pathways. Cold Spring Harbor Perspectives in Biology **4** (2012). (cited on p. 6)

[22] E. U. Azeloglu and R. Iyengar. Signaling Networks: Information Flow, Computation, and Decision Making. Cold Spring Harbor Perspectives in Biology **7**, a005934 (2015). (cited on p. 6)

[23] J. Monod and F. Jacob. General Conclusions: Teleonomic Mechanisms in Cellular Metabolism, Growth, and Differentiation. Cold Spring Harbor Symposia on Quantitative Biology **26**, 389 (1961). (cited on pages 7 and 8)

[24] U. Alon. Network motifs: theory and experimental approaches. Nature Reviews Genetics **8**, 450 (2007). (cited on pages 7 and 118)

[25] S. H. Strogatz. *Nonlinear Dynamics and Chaos: With Applications to Physics, Biology, Chemistry, and Engineering* (Avalon Publishing, 1994). Google-Books-ID: FIYHiBLWCJMC. (cited on pages 7 and 10)

[26] J. J. Tyson and B. Novák. Functional Motifs in Biochemical Reaction Networks. Annual review of physical chemistry **61**, 219 (2010). (cited on p. 7)

[27] J. E. Ferrell Jr. Self-perpetuating states in signal transduction: positive feedback, double-negative feedback and bistability. Current Opinion in Cell Biology **14**, 140 (2002). (cited on p. 8)

[28] A. Becskei and L. Serrano. Engineering stability in gene networks by autoregulation. Nature **405**, 590 (2000). (cited on p. 8)

[29] M. B. Elowitz and S. Leibler. A synthetic oscillatory network of transcriptional regulators. Nature **403**, 335 (2000). (cited on p. 8)

[30] J. J. Tyson, K. C. Chen, and B. Novak. Sniffers, buzzers, toggles and blinkers: dynamics of regulatory and signaling pathways in the cell. Current Opinion in Cell Biology **15**, 221 (2003). (cited on p. 9)

[31] Y. Schaerli, A. Munteanu, M. Gili, J. Cotterell, J. Sharpe, and M. Isalan. A unified design space of synthetic stripe-forming networks. Nature Communications **5**, 4905 (2014). (cited on p. 9)

[32] B. Ghosh, R. Karmakar, and I. Bose. Noise characteristics of feed forward loops. Physical Biology **2**, 36 (2005). (cited on p. 9)

[33] W. Ma, A. Trusina, H. El-Samad, W. A. Lim, and C. Tang. Defining Network Topologies that Can Achieve Biochemical Adaptation. Cell **138**, 760 (2009). (cited on p. 9)

[34] H. C. Berg and D. A. Brown. Chemotaxis in Escherichia coli analysed by Three-dimensional Tracking. Nature **239**, 500 (1972). (cited on p. 9)

[35] A. Levchenko and P. A. Iglesias. Models of eukaryotic gradient sensing: application to chemotaxis of amoebae and neutrophils. Biophysical Journal **82**, 50 (2002). (cited on p. 9)

[36] H. El-Samad, J. P. Goff, and M. Khammash. Calcium homeostasis and parturient hypocalcemia: an

integral feedback perspective. Journal of Theoretical Biology **214**, 17 (2002). (cited on p. 9)

[37] A. Goldbeter and D. E. Koshland. An amplified sensitivity arising from covalent modification in biological systems. Proceedings of the National Academy of Sciences of the United States of America **78**, 6840 (1981). (cited on p. 9)

[38] J. E. Ferrell and S. H. Ha. Ultrasensitivity part I: Michaelian responses and zero-order ultrasensitivity. Trends in Biochemical Sciences **39**, 496 (2014). (cited on p. 9)

[39] Q. Yang and J. E. Ferrell. The Cdk1-APC/C cell cycle oscillator circuit functions as a time-delayed, ultrasensitive switch. Nature Cell Biology **15**, 519 (2013). (cited on p. 9)

[40] S. Y. Kim and J. E. Ferrell. Substrate competition as a source of ultrasensitivity in the inactivation of Wee1. Cell **128**, 1133 (2007). (cited on p. 9)

[41] S. L. Harvey, G. Enciso, N. Dephoure, S. P. Gygi, J. Gunawardena, and D. R. Kellogg. A phosphatase threshold sets the level of Cdk1 activity in early mitosis in budding yeast. Molecular Biology of the Cell **22**, 3595 (2011). (cited on p. 9)

[42] Q. Zhang, S. Bhattacharya, and M. E. Andersen. Ultrasensitive response motifs: basic amplifiers in molecular signalling networks. Open Biology **3**, 130031 (2013). (cited on p. 9)

[43] J. E. Ferrell and W. Xiong. Bistability in cell signaling: How to make continuous processes discontinuous, and reversible processes irreversible. Chaos (Woodbury, N.Y.) **11**, 227 (2001). (cited on p. 10)

[44] D. Hanahan and R. A. Weinberg. Hallmarks of Cancer: The Next Generation. Cell **144**, 646 (2011). (cited on pages 11, 12, and 138)

[45] D. G. Míguez. Network nonlinearities in drug treatment. Interdisciplinary Sciences, Computational Life Sciences **5**, 85 (2013). (cited on pages 13, 14, 88, 118, and 138)

[46] A. Carracedo and P. P. Pandolfi. The PTEN–PI3k pathway: of feedbacks and cross-talks. Oncogene **27**, 5527 (2008). (cited on pages 13 and 14)

[47] B. T. Hennessy, D. L. Smith, P. T. Ram, Y. Lu, and G. B. Mills. Exploiting the PI3k/AKT pathway for cancer drug discovery. Nature Reviews. Drug Discovery **4**, 988 (2005). (cited on p. 13)

[48] F. Vazquez and W. R. Sellers. The PTEN tumor suppressor protein: an antagonist of phosphoinositide 3-kinase signaling. Biochimica Et Biophysica Acta **1470**, M21 (2000). (cited on p. 13)

[49] B.-H. Jiang and L.-Z. Liu. PI3k/PTEN signaling in angiogenesis and tumorigenesis. Advances in Cancer Research **102**, 19 (2009). (cited on p. 14)

[50] S. Chandarlapaty. Negative feedback and adaptive resistance to the targeted therapy of cancer. Cancer Discovery **2**, 311 (2012). (cited on p. 14)

[51] P. Gual, Y. Le Marchand-Brustel, and J.-F. Tanti. Positive and negative regulation of insulin signaling through IRS-1 phosphorylation. Biochimie **87**, 99 (2005). (cited on p. 14)

[52] M. Onsum and C. V. Rao. A Mathematical Model for Neutrophil Gradient Sensing and Polarization. PLOS Computational Biology **3**, e36 (2007). (cited on p. 14)

[53] S. Misra, S. Ghatak, and B. P. Toole. Regulation of MDR1 expression and drug resistance by a positive feedback loop involving hyaluronan, phosphoinositide 3-kinase, and ErbB2. The Journal of Biological Chemistry **280**, 20310 (2005). (cited on p. 14)

[54] H. Q. Wang, D. A. Altomare, K. L. Skele, P. I. Poulikakos, F. P. Kuhajda, A. Di Cristofano, and J. R. Testa. Positive feedback regulation between AKT activation and fatty acid synthase expression in ovarian carcinoma cells. Oncogene **24**, 3574 (2005). (cited on p. 14)

[55] M. S. Kinch. An analysis of FDA-approved drugs for oncology. Drug Discovery Today **19**, 1831 (2014). (cited on p. 14)

[56] P. Wu, T. E. Nielsen, and M. H. Clausen. Small-molecule kinase inhibitors: an analysis of FDA-approved drugs. Drug Discovery Today **21**, 5 (2016). (cited on p. 14)

[57] K. Kawakami, B. B. Aggarwal, and R. K. Puri (editors) *Cytotoxins and Immunotoxins for Cancer Therapy: Clinical Applications* (CRC Press, 2004), 1 edition. (cited on pages 15 and 115)

[58] F. Turturro. Denileukin diftitox: a biotherapeutic paradigm shift in the treatment of lymphoid-derived disorders. Expert Review of Anticancer Therapy **7**, 11 (2007). (cited on p. 15)

[59] R. J. Kreitman, W. H. Wilson, J. D. White, M. Stetler-Stevenson, E. S. Jaffe, S. Giardina, T. A. Waldmann, and I. Pastan. Phase I trial of recombinant immunotoxin anti-Tac(Fv)-PE38 (LMB-2) in patients with hematologic malignancies. Journal of Clinical Oncology: Official Journal of the American Society of Clinical Oncology **18**, 1622 (2000). (cited on p. 15)

[60] M. Kioi, S. R. Husain, D. Croteau, S. Kunwar, and R. K. Puri. Convection-enhanced delivery of interleukin-13 receptor-directed cytotoxin for malignant glioma therapy. Technology in Cancer Research & Treatment **5**, 239 (2006). (cited on p. 15)

[61] C. Xuan, K. K. Steward, J. M. Timmerman, and S. L. Morrison. Targeted delivery of interferon-alpha

via fusion to anti-CD20 results in potent antitumor activity against B-cell lymphoma. Blood **115**, 2864 (2010). (cited on p. 15)

[62] S. Yuan, F. Wang, G. Chen, H. Zhang, L. Feng, L. Wang, H. Colman, M. J. Keating, X. Li, and R.-H. . H. Xu. Effective elimination of cancer stem cells by a novel drug combination strategy. Stem Cells **31**, 23 (2013). (cited on p. 15)

[63] I. Bozic, J. G. Reiter, B. Allen, T. Antal, K. Chatterjee, P. Shah, Y. S. Moon, A. Yaqubie, N. Kelly, and D. T. Le. Evolutionary dynamics of cancer in response to targeted combination therapy. Elife **2** (2013). (cited on p. 15)

[64] X. Tan, L. Hu, L. J. Luquette III, G. Gao, Y. Liu, H. Qu, R. Xi, Z. J. Lu, P. J. Park, and S. J. Elledge. Systematic identification of synergistic drug pairs targeting hiv. Nature biotechnology **30**, 1125 (2012). (cited on p. 15)

[65] J. Jia, F. Zhu, X. Ma, Z. W. Cao, Y. X. Li, and Y. Z. Chen. Mechanisms of drug combinations: interaction and network perspectives. Nature reviews Drug discovery **8**, 111 (2009). (cited on p. 15)

[66] M. C. Berenbaum. Synergy, additivism and antagonism in immunosuppression. a critical review. Clinical and experimental immunology **28**, 1 (1977). (cited on p. 16)

[67] A. A. Borisy, P. J. Elliott, N. W. Hurst, M. S. Lee, J. Lehár, E. R. Price, G. Serbedzija, G. R. Zimmermann, M. A. Foley, B. R. Stockwell, and C. T. Keith. Systematic discovery of multicomponent therapeutics. Proceedings of the National Academy of Sciences **100**, 7977 (2003). (cited on p. 16)

[68] J. Gunawardena. Models in biology: 'accurate descriptions of our pathetic thinking'. BMC Biology **12**, 29 (2014). (cited on p. 16)

[69] P. Waage and C. M. Guldberg. Studies concerning affinity. Journal of Chemical Education **63**, 1044 (1986). (cited on p. 16)

[70] D. A. Lauffenburger and J. Linderman. *Receptors: Models for Binding, Trafficking, and Signaling* (Oxford University Press, USA, 1996). (cited on p. 17)

[71] J. Keener and J. Sneyd. *Mathematical Physiology* (Springer Science & Business Media, 2006). Google-Books-ID: fIfhBwAAQBAJ. (cited on p. 17)

[72] L. Michaelis, M. L. Menten, K. A. Johnson, and R. S. Goody. The original Michaelis constant: translation of the 1913 Michaelis-Menten paper. Biochemistry **50**, 8264 (2011). (cited on p. 17)

[73] G. E. Briggs and J. B. S. Haldane. A Note on the Kinetics of Enzyme Action. Biochemical Journal **19**, 338 (1925). (cited on p. 18)

[74] D. G. Miguez. The role of asymmetric binding in ligand-receptor systems with 1:2 interaction ratio. Biophys. Chem. **148**, 74 (2010). (cited on p. 23)

[75] J. S. Philo, K. H. Aoki, T. Arakawa, L. O. Narhi, and J. Wen. Dimerization of the extracellular domain of the erythropoietin (EPO) receptor by EPO: one high-affinity and one low-affinity interaction. Biochemistry **35**, 1681 (1996). (cited on pages 23 and 114)

[76] G. Fuh, B. C. Cunningham, R. Fukunaga, S. Nagata, D. V. Goeddel, and J. A. Wells. Rational design of potent antagonists to the human growth hormone receptor. Science **256**, 1677 (1992). (cited on p. 23)

[77] P. Cironi, I. A. Swinburne, and P. A. Silver. Enhancement of Cell Type Specificity by Quantitative Modulation of a Chimeric Ligand. Journal of Biological Chemistry **283**, 8469 (2008). (cited on pages 52, 62, 115, and 116)

[78] P. Silver, P. Cironi, and D. Míguez. Chimeric activators: quantitatively designed protein therapeutics and uses thereof (2011). US Patent App. 12/594,747. (cited on p. 52)

[79] P. Gregorio-Godoy and D. G. Míguez. Synthetic approaches to study transcriptional networks and noise in mammalian systems. IET Systems Biology **7**, 11 (2013). (cited on p. 88)

[80] D. G. Míguez. The role of asymmetric binding in ligand-receptor systems with 1:2 interaction ratio. Biophysical Chemistry **148**, 74 (2010). (cited on p. 113)

[81] J. C. Cheetham, D. M. Smith, K. H. Aoki, J. L. Stevenson, T. J. Hoeffel, R. S. Syed, J. Egrie, and T. S. Harvey. NMR structure of human erythropoietin and a comparison with its receptor bound conformation. Nat. Struct. Biol. **5**, 861 (1998). (cited on p. 114)

[82] O. Livnah, E. A. Stura, S. A. Middleton, D. L. Johnson, L. K. Jolliffe, and I. A. Wilson. Crystallographic evidence for preformed dimers of erythropoietin receptor before ligand activation. Science **283**, 987 (1999). (cited on p. 114)

[83] S. N. Constantinescu, T. Keren, M. Socolovsky, H. Nam, Y. I. Henis, and H. F. Lodish. Ligand-independent oligomerization of cell-surface erythropoietin receptor is mediated by the transmembrane domain. Proc. Natl. Acad. Sci. U.S.A. **98**, 4379 (2001). (cited on p. 114)

[84] J. W. Mockridge, R. Aston, D. J. Morrell, and A. T. Holder. Cross-linked growth hormone dimers have enhanced biological activity. Eur. J. Endocrinol. **138**, 449 (1998). (cited on p. 114)

[85] N. Yang, J. F. Langenheim, X. Wang, J. Jiang, W. Y. Chen, and S. J. Frank. Activation of growth hormone receptors by growth hormone and growth hormone antagonist dimers: insights into

receptor triggering. Mol. Endocrinol. **22**, 978 (2008). (cited on p. 114)

[86] S. J. Frank. Receptor dimerization in GH and erythropoietin action–it takes two to tango, but how? Endocrinology **143**, 2 (2002). (cited on p. 114)

[87] E. Bremer, D. F. Samplonius, L. van Genne, M. H. Dijkstra, B. J. Kroesen, L. F. M. H. de Leij, and W. Helfrich. Simultaneous inhibition of epidermal growth factor receptor (EGFR) signaling and enhanced activation of tumor necrosis factor-related apoptosis-inducing ligand (TRAIL) receptor-mediated apoptosis induction by an scFv:sTRAIL fusion protein with specificity for human EGFR. The Journal of Biological Chemistry **280**, 10025 (2005). (cited on pages 115 and 116)

[88] E. Bremer, B. ten Cate, D. F. Samplonius, L. F. M. H. de Leij, and W. Helfrich. CD7-restricted activation of Fas-mediated apoptosis: a novel therapeutic approach for acute T-cell leukemia. Blood **107**, 2863 (2006). (cited on p. 115)

[89] E. Ruoslahti, S. Bhatia, and M. Sailor. Targeting of drugs and nanoparticles to tumors. The Journal of cell biology **188**, 759 (2010). (cited on p. 115)

[90] C. Xuan, K. K. Steward, J. M. Timmerman, and S. L. Morrison. Targeted delivery of interferon-alpha via fusion to anti-CD20 results in potent antitumor activity against B-cell lymphoma. Blood **115**, 2864 (2010). (cited on p. 115)

[91] Y. Yarden and J. Schlessinger. Self-phosphorylation of epidermal growth factor receptor: evidence for a model of intermolecular allosteric activation. Biochemistry **26**, 1434 (1987). (cited on p. 115)

[92] R. N. Harris. Guidebook to cytokines and their receptors: Edited by N A Nicola. pp 261. Oxford University Press. ISBN 0-19-859946-3. Biochemical Education **23**, 226 (1995). (cited on p. 115)

[93] S. Semrau and T. Schmidt. Membrane heterogeneity: from lipid domains to curvature effects. Soft Matter **5**, 3174 (2009). (cited on p. 115)

[94] M. Caraglia, A. Abbruzzese, A. Leardi, S. Pepe, A. Budillon, G. Baldassare, C. Selleri, S. D. Lorenzo, A. Fabbrocini, G. Giuberti, G. Vitale, G. Lupoli, A. R. Bianco, and P. Tagliaferri. Interferon-alpha induces apoptosis in human KB cells through a stress-dependent mitogen activated protein kinase pathway that is antagonized by epidermal growth factor. Cell death and differentiation **6**, 773 (1999). PMID: 10467351. (cited on p. 116)

[95] K. Oda, Y. Matsuoka, A. Funahashi, and H. Kitano. A comprehensive pathway map of epidermal growth factor receptor signaling. Molecular systems biology **1** (2005). (cited on p. 116)

[96] P. Cironi, I. A. Swinburne, and P. A. Silver. Enhancement of cell type specificity by quantitative

modulation of a chimeric ligand. Journal of biological chemistry **283**, 8469 (2008). (cited on p. 116)

[97] M. C. Berenbaum. Synergy, additivism and antagonism in immunosuppression. A critical review. Clinical and Experimental Immunology **28**, 1 (1977). (cited on p. 117)

[98] J. C. Weddell and P. I. Imoukhuede. Quantitative characterization of cellular membrane-receptor heterogeneity through statistical and computational modeling. PloS one **9**, e97271 (2014). (cited on p. 117)

[99] M. Bengtsson, A. Stahlberg, P. Rorsman, and M. Kubista. Gene expression profiling in single cells from the pancreatic islets of langerhans reveals lognormal distribution of mrna levels. Genome research **15**, 1388 (2005). (cited on p. 117)

[100] M. R. Dowling, D. Milutinović, and P. D. Hodgkin. Modelling cell lifespan and proliferation: is likelihood to die or to divide independent of age? Journal of The Royal Society Interface **2**, 517 (2005). (cited on p. 117)

[101] N. Friedman, L. Cai, and X. S. Xie. Linking stochastic dynamics to population distribution: An analytical framework of gene expression. Phys. Rev. Lett. **97**, 168302 (2006). (cited on p. 117)

[102] D. M. Wolf and A. P. Arkin. Motifs, modules and games in bacteria (2003). (cited on p. 118)

[103] H. C. Fehmann, J. F. Habener, and H. C. Fehmann. Homologous desensitization of the insulinotropic glucagon-like peptide-i(7-37) receptor on insulinoma (hit-t15) cells. Endocrinology **128**, 2880 (1991). (cited on p. 120)

[104] Y. Sun, R. Olson, M. Horning, N. Armstrong, M. Mayer, and E. Gouaux. Mechanism of glutamate receptor desensitization. Nature **417**, 245 (2002). (cited on p. 120)

[105] N. J. Freedman and R. J. Lefkowitz. Desensitization of G protein-coupled receptors. Recent progress in hormone research **51**, 319 (1996). (cited on p. 120)

[106] R. R. Gainetdinov, R. T. Premont, L. M. Bohn, R. J. Lefkowitz, and M. G. Caron. Desensitization of G protein coupled receptors and neuronal function. Annu. Rev. Neurosci **27**, 107 (2004). (cited on p. 120)

List of Figures

List of publications

Publications included in 'Results':

- **Doldán-Martelli, V. and Míguez, D. G.** (2012). Theoretical Approaches to Growth Hormone Signaling, in 'Growth Hormones: Synthesis, Regulation and Health Implications'. Eds. A. Andersdtr and J. Anderssen. ISBN 9781619426818. In 'Results' section 3.1
- **Doldán-Martelli, V., Guantes, R. and Míguez, D. G.** (2013). A mathematical model for the rational design of chimeric ligands in selective drug therapies. *CPT: pharmacometrics & systems pharmacology* 2, e26. ISSN 2163-8306. In 'Results' section 3.2
- **Doldán-Martelli, V. and Míguez, D. G.** (2015). Synergistic interaction between selective drugs in cell populations models. *PloS one* 10, e0117558. In 'Results' section 3.3.
- **Doldán-Martelli, V. and Míguez, D. G.** The influence of network topologies in drug treatments. *In preparation*. In 'Results' section 3.4